The Dissertation Committee for Chang Min Park certifies that this is the approved version of the following dissertation:

Mercury Speciation During Thermal Remediation and in Post-Treatment Environments

Committee:

Lynn E. Katz, Co-Supervisor

Howard M. Liljestrand, Co-Supervisor

Desmond F. Lawler

Danny D. Reible

Gary A. Pope

Mercury Speciation During Thermal Remediation and in Post-Treatment Environments

by

Chang Min Park, B.S.; M.S.

Dissertation

Presented to the Faculty of the Graduate School of

The University of Texas at Austin

in Partial Fulfillment

of the Requirements

for the Degree of

Doctor of Philosophy

The University of Texas at Austin

December 2011

Dedication

…to my parents and brother, whose love and dedicated support have been an invaluable asset to me

…and to her who has provided trust and encouragement to continue my journey towards a Ph.D. staying by my side every step of the way

Acknowledgments

Acknowledgments are due to my supervisors, Drs. Lynn Katz and Howard Liljestrand for their encouragement, support, and guidance over the past three years. I also appreciate the assistance of my committee members, Professors Desmond Lawler, Danny Reible, and Gary Pope. Special thanks are due to EWRE students (past and present), Lynn Katz group (Amanda Epps, Celina Dozier, Ellison Carter, Fernando Alma, Katherine Alfredo, Lee Blaney), and EWRE Korean connection (Jinyong Choi, Ijung Kim, and Yeonjeong Ha) and especially to Jeremiah Mangold for the initial help with surface complexation modeling. I wish to acknowledge the Center for Petroleum and Geosystems Engineering (CPGE) and the Department of Energy – Basic Energy Sciences for their financial support of this research.

Mercury Speciation During Thermal Remediation and in Post-Treatment Environments

Chang Min Park, Ph.D.

The University of Texas at Austin, 2011

Supervisors: Lynn E. Katz and Howard M. Liljestrand

Mercury is a toxic metal that has been released to the environment through numerous industrial activities. It can exist in various solid, aqueous, and gaseous forms. Volatile Hg(0) is frequently present at the source of a spill where it behaves as a dense non-aqueous phase liquid (DNAPL) contaminant that can change oxidation state and speciation via chemical or biological reactions. Mercury speciation is a key factor determining the mobility, bioavailability, and toxicity of Hg in the environment.

Previous research has demonstrated that *In Situ* Thermal Desorption (ISTD) can be used in various modes to treat soil contaminants including Hg(0). The application of ISTD and other remediation processes must incorporate potential speciation during remediation and assess mobility of any mercury remaining in the soil post-remediation. However, research examining the impact of mercury speciation on ISTD processes is limited. The goals of this research are to investigate the fate and transport of mercury in

soils from the source where concentrations are expected to be high to dilute solutions associated with down gradient groundwater, lakes, and rivers.

For high concentrations of mercury, equilibrium speciation has been investigated to identify potential transformations at high temperatures consistent with those applied in ISTD processes. A model has been developed that describes mercury speciation over a range of environmental conditions. At low mercury concentrations, competitive Hg(II) adsorption on the soil minerals, goethite and gibbsite, has been evaluated over a range of experimental conditions. Models describing Hg(II) adsorption and aqueous speciation have been developed to provide a tool for predicting the fate and transport of residual mercury after thermal remediation applications.

The results of these studies demonstrate that ISTD is feasible, but the off-gas speciation will depend on both the applied temperatures and the soil composition and redox conditions of the site. Pure phase mercury was predicted to be vaporized at temperatures well within the range of typical ISTD processes. The adsorption of trace levels of Hg(II) remaining after ISTD was successfully modeled on goethite and gibbsite using the 1-p*K* CD-MUSIC model.

Table of Contents

TABLE OF CONTENTS VIII

LIST OF TABLES XI

LIST OF FIGURES XIII

CHAPTER 1: INTRODUCTION 1

1.1 Research Objectives 3

1.2 Specific Objectives 5

1.3 Dissertation Outline 6

CHAPTER 2: LITERATURE REVIEW 7

2.1 Properties affecting the Fate and Transport of Mercury 7

2.1.1 Chemical Properties of Mercury 7

2.1.2 Fate and Transport of Mercury 9

2.2 Remediation of Mercury 10

2.2.1 General Remediation 10

2.2.2 In Situ Thermal Desorption (ISTD) Remediation 12

2.3 Speciation at High Concentration of Mercury 14

2.3.1 Ambient Temperature Speciation 14

2.3.2 High Temperature Speciation 16

2.4 Aqueous Speciation at Dilute Mercury Concentration 20

2.4.1 Aqueous Mercury Species 20

2.4.2 Adsorption to Soils 22

2.4.3 Adsorption to Metal (hydr)oxides 24

2.4.4 Surface Complexation Models (SCMs) 27

2.4.4.1 General SCMs Tenets 27

2.4.4.2 Charge Distribution and Multi Site Complexation Model (CD-MUSIC) 38
2.5 Summary 46
CHAPTER 3: SPECIATION OF HIGH CONCENTRATIONS OF HG AT HIGH TEMPERATURE 48
3.1 Introduction 48
3.2 Modeling Approach 50
3.3 Results and Discussion 52
3.3.1 Mercury Speciation at Ambient Temperature 52
3.3.2 Mercury Speciation at Higher Temperature 54
3.3.3 Impact of Soil Components on Mercury Removal 58
3.4 Summary 65
CHAPTER 4: MERCURY(II) ADSORPTION ON GOETHITE (A-FEOOH) 66
4.1 Introduction 66
4.2 Materials and Methods 69
4.3 Modeling Approach 71
4.4 Results and Discussion 82
4.4.1 Dissolved Mercury Speciation 82
4.4.2 Carbonate Species on Goethite 85
4.4.3 Calibration of Mercury(II) Adsorption on Goethite 89
4.5 Summary 101
CHAPTER 5. MERCURY(II) ADSORPTION ON GIBBSITE (A-AL(OH)$_3$) 103
5.1 Introduction 103
5.2 Materials and Methods 105
5.3 Modeling Approach 106
5.4 Results and Discussion 110

5.4.1 Aqueous Mercury Speciation 110
5.4.2 Potentiometric Titration of Gibbsite 113
5.4.3 Calibration of Hg(II) Adsorption on Gibbsite 115
5.4.4 Model Verification 122
5.5 Summary 126
CHAPTER 6. CONCLUSIONS AND RECOMMENDATIONS 128
6.1 Summary and Conclusions 128
6.1.1 Thermodynamic Speciation Modeling 128
6.1.2 CD-MUSIC Modeling for Hg(II) Adsorption 129
6.2 Engineering Implications 131
6.3 Recommendations for Future Work 132
6.3.1 Experimental Approach for Thermodynamic Mercury Speciation 132
6.3.2 Temperature Effects on Hg(II) Sorption 134
REFERENCES 135
VITA 154

List of Tables

Table 2. 1 Chemical properties of various mercury species (Chemfinder.com, 2004; EPA, 2007; Hempel and Thoeming, 1999; Lide, 2007, 2008; Mason *et al.*, 1996). 8

Table 2. 2 Pure phase speciation of mercury and thermodynamic formation constants used in speciation modeling. 16

Table 2. 3 Example chemical equilibria that consists of aqueous reactions, surface acidity, ion-pair formation and surface complexation reactions formulated in the 1-p*K* CD-MUSIC model. 45

Table 3. 1 Aqueous mercury complexes and solid form of mercury with formation constants used in the speciation modeling (MINEQL+ 4.5 database, Schecher (2001)).....52

Table 3. 2 Thermodynamic phase transition reactions and decomposition of mercury solid and carbonate components in soil. 56

Table 3. 3 Soil conditions used in model calculations for phase transition of mercury solid. 58

Table 3. 4 Thermodynamic equilibrium constants and Gibbs free energy of the reaction, $2HgO_{(g)} \rightarrow 2Hg_{(g)} + O_{2(g)}$ (Chase, 1998). 62

Table 4. 1 The physico-chemical parameters and suspension properties used in model simulations with the 1-p*K* CD-MUSIC approach. 80

Table 4. 2 Bond valence analysis of various Hg(II) sorption complexes on the surface of Fe (hydr)oxides (Kim *et al.*, 2004a).....81

Table 4. 3 The intrinsic solution equilibrium constants of various Hg(II) species used in the 1-p*K* CD-MUSIC model calculation (Schecher, 2001). 82

Table 4. 4 Surface complexation reactions, and intrinsic equilibrium constants used in the 1-p*K* CD-MUSIC modeling of Hg(II) adsorption on goethite.....92

Table 5. 1 The physico-chemical parameters and suspension properties used in model simulations with the 1-p*K* CD-MUSIC approach. 106

Table 5. 2 Bond valence analysis of various Hg(II) sorption complexes on the surface of Al (hydr)oxides (Kim *et al.,* 2004a).....109

Table 5. 3 The intrinsic solution equilibrium constants of various Hg(II) species used in the 1-p*K* CD-MUSIC model calculation (Schecher, 2001). 110

Table 5. 4 Surface complexation reactions, and intrinsic equilibrium constants used in the 1-p*K* CD-MUSIC modeling of Hg(II) adsorption on gibbsite. 116

List of Figures

Figure 2. 1 Mercury cycle in the subsurface soil, Adapted from Kunkel, 2004.....9

Figure 2. 2 ISTD thermal blanket (left) and thermal well (right) processes. Source: TerraTherm 2004. 13

Figure 2. 3 Hg(II) aqueous speciation diagram with initial concentration of 5 μM as a function of pH. 21

Figure 2. 4 Hg(II) aqueous speciation diagrams with initial concentration of 5 μM in the presence of Cl ($[Cl^-_{TOT}]$ = 5 mM). 22

Figure 2. 5 Major building blocks of natural substrates: (a) Goethite (α-FeOOH) crystal and (b) Gibbsite (α-$Al(OH)_3$) crystal. 25

Figure 2. 6 Effect of pH on Cd adsorption isotherms on a peat humic acid at 0.1M KNO_3. Adapted from Sposito, 2004. 30

Figure 2. 7 Schematic of the Constant Capacitance Model (CCM). Source: Hayes *et al.*, 1991.....34

Figure 2. 8 Schematic of the diffuse layer model (DLM). Source: Hayes *et al.*, 1991.....35

Figure 2. 9 Schematic of the classic 2-p*K* triple layer model (extended stern layer model). Source: Hayes *et al.*, 1991. 36

Figure 2. 10 Schematic of a water dipole adsorbed at a surface site in the TLM. Source: Sverjensky and Fukushi, 2006. 37

Figure 2. 11 Schematic presentation of surface protonation for the 1-p*K* and 2-p*K* approach in TLM. ψ denotes electrical potential and δ charge located in planes. Adapted from Piasecki, 2006. 38

Figure 2. 12 Competitive adsorption of Cd(II) on goethite with 0.5 mM P (closed symbols) and without phosphate (open symbols) in the system at 0.1 M $NaNO_3$. (a) $[Cd^{2+}{}_{TOT}]$ = 0.25 mM and (b) $[Cd^{2+}{}_{TOT}]$ = 0.5 mM. The solid and dashed lines represent the model calculations with and without carbonate species respectively. Adapted from Venema *et al.*, 1997. 42

Figure 2. 13 Example of the 2-p*K* triple layer model of Hg(II) adsorption by gibbsite (3.3 g L^{-1}) as a function of solution chemistry: (a) 0.1 *M* $NaNO_3$; (b) 0.1 *M* $NaNO_3$ + 0.01 *M* NaCl; (c) 0.1 *M* $NaNO_3$ + 0.01 *M* Na_2SO_4. Adapted from Sarkar *et al.*, 1999. 44

Figure 3. 1 Distribution of aqueous mercury species as a function of pH, (a) $[Hg^{2+}]$ = 2.4 M, $[Hg_2{}^{2+}]$ = 9e-7 M, $[Cl^-]$ = 0.1 M, $[HS^-]$ = 1e-33 M, and $[SO_4{}^{2-}]$ = 1e-18 M, (b) $[Hg^{2+}]$ = 2.4 M, $[Hg_2{}^{2+}]$ = 1e-8 M, $[Cl^-]$ = 8.9 M, $[HS^-]$ = 1e-33 M, and $[SO_4{}^{2-}]$ = 1e-18 M, and (c) $[Hg^{2+}]$ = 2.4 M, $[Hg_2{}^{2+}]$ = 1e-8 M, $[Cl^-]$ = 1e-18 M, $[HS^-]$ = 1e-3 M, and $[SO_4{}^{2-}]$ = 1e-18 M at 20 °C and pe = 0. The model lines were calculated using MINEQL+ 4.5 (Schecher and McAvoy, 2003). 54

Figure 3. 2 Model simulation of phase transition of mercury, (a) Hg^0 (liquid), (b) HgS (solid), and (c) $HgCl_2$ (solid) as temperature increases. 57

Figure 3. 3 Vaporization of mercury solid and soil components including soil pore water and carbonate at (a) reducing and (b) oxidizing conditions. 64

Figure 4. 1 Crystal structure of goethite. Source: Cudennec and Lecerf, 2005. 77

Figure 4. 2 Distribution of aqueous mercury species as a function of pH, (a) $[Hg_{TOT}]$ = 5 μM and (b) $[Hg_{TOT}]$ = 5 μM and $[Cl_{TOT}]$ = 5000 μM. The model lines were calculated using MINEQL+ 4.5 (Schecher and McAvoy, 2003). Solid line indicates the total dissolved mercury concentration. 84

Figure 4. 3 Optimization of surface acidity constants, ion-pair formation, and carbonate surface reactions. (a) Proton surface charge profile of carbonate-free goethite (closed system) in 0.1 M (closed squares) and 0.015 M (closed triangles) $NaNO_3$. (b) Calibration of carbonate species with the adsorption of carbonate on goethite in open CO_2 system in 0.1 M (open squares) and 0.01 M (open triangles) $NaNO_3$. (c) Surface charge profile of goethite in open system in 0.1 M (open squares), 0.01 M (open triangles), and 0.001 M (open circles) of $NaNO_3$. 85

Figure 4. 4 CD-MUSIC modeling of adsorption pH-edge data collected for total Hg(II) loadings of 5, 10, 25, and 50 μM on goethite (76 m^2/g) in the absence of Cl. The model lines were calculated using innersphere surface species described by reactions in Table 4.4 and assuming an open CO_2 system. 94

Figure 4. 5 The surface speciation of Hg(II) on goethite (76 m^2/g) for the model simulation of the adsorption pH edge data collected at a total Hg(II) loading of 25 µM in the absence of Cl. The solid line represents the total Hg(II) adsorbed and the dashed and dotted lines represent the surface species used in the 1-p*K* CD-MUSIC model. 95

Figure 4. 6 CD-MUSIC modeling for adsorption pH-edges for experiments conducted at a total Hg(II) loading of 10 μM and $[Cl_{TOT}]$ = 0, 5, 50, 500, and 5000 μM on goethite (76 m^2/g). The model lines were calculated assuming innersphere surface species and an open system. 97

Figure 4. 7 Surface speciation of Hg(II) on goethite (76 m^2/g) in a model simulation of adsorption pH edge for a total Hg(II) loading of 10 µM and total Cl^- loading of 500 µM. The solid model line indicates the total Hg(II) adsorbed and the

dashed and dotted lines represent the surface species used in the 1-p*K* CD-MUSIC model. 98

Figure 4. 8 The dissolved Hg(II) speciation in model simulation of adsorption pH edges on goethite (76 m^2/g). The total Hg(II) loading for these simulations was 10 µM and total Cl loading was (a) 0 µM, (b) 50 µM, and (c) 5000 µM. The model lines were calculated using the 1-p*K* CD-MUSIC model. 99

Figure 4. 9 Model verification of Hg(II) adsorption on goethite with data from Bonnissel-Gissinger *et al.,* (1999). The estimated parameters (i.e. the consistent innersphere surface species and the intrinsic affinity constants previously determined) were used and an open system was assumed. The solid model lines indicate the total Hg(II) adsorbed and the dashed and dotted lines represent individual surface or dissolved species of Hg(II) used in the 1-p*K* CD-MUSIC model. (a, b) $[Hg_{TOT}]$ = 12.4 μM and $[Cl_{TOT}]$ = 20 μM; (c, d) $[Hg_{TOT}]$ = 12.4 μM and $[Cl_{TOT}]$ = 100 mM. 101

Figure 5. 1 Distribution of aqueous mercury species as a function of pH, (a) $[Hg_{TOT}]$ = 0.1 µM and (b) $[Hg_{TOT}]$ = 0.1 µM and $[Cl_{TOT}]$ = 0.1 M. The model lines were calculated using MINEQL+ 4.5 (Schecher and McAvoy, 2003). Solid line indicates the total dissolved mercury concentration. 112

Figure 5. 2 Proton surface charge profile of carbonate-free gibbsite in 0.1 M (closed squares), 0.01 M (closed triangles), and 0.001 M (closed circles) of (a) $NaNO_3$ and (b) NaCl. The solid lines were calculated using the 1-p*K* CD-MUSIC model.....114

Figure 5. 3 CD-MUSIC modeling for adsorption pH-edges for experiments conducted at a total Hg(II) loading of 0.1 μM on gibbsite (13 m^2/g) in closed system. The

model lines were calculated using innersphere surface species described by reactions in Table 5.4 in 0.1 M (closed squares), 0.01 M (closed triangles), and 0.001 M of (a) $NaNO_3$ and (b) NaCl. 118

Figure 5. 4 Speciation of (a) Hg(II) adsorbed on gibbsite (13 m^2/g) in 0.01 M of $NaNO_3$ and (b) dissolved Hg(II) species in 0.01 M of $NaNO_3$ for the model simulation of the adsorption pH-edge data collected at a total Hg(II) loading of 0.1 μM. The model lines were calculated using the 1-p*K* CD-MUSIC model. 120

Figure 5. 5 Speciation of (a) Hg(II) adsorbed on gibbsite (13 m^2/g) in 0.01 M NaCl and dissolved Hg(II) species in (b) 0.01 M and (c) 0.001 M of NaCl for the model simulation of the adsorption pH-edges data collected at a total Hg(II) loading of 0.1 μM. The model lines were calculated using the 1-p*K* CD-MUSIC model.....122

Figure 5. 6 Model verification of Hg(II) adsorption on gibbsite with other data set from Sarkar *et al.* (1999). The estimated parameters (i.e. the consistent innersphere surface species and the intrinsic affinity constants previously determined) were used and an open system was assumed. The solid model lines indicate the total Hg(II) adsorbed and the dotted and dashed lines represent individual surface or dissolved species of Hg(II) used in the 1-p*K* CD-MUSIC model. The total loadings of Hg(II) was 0.6 μM in (a) 0.1 M $NaNO_3$ and (b) 0.1 M $NaNO_3$ and 0.01 M NaCl. 125

Chapter 1: Introduction

Mercury is one of the most common metals identified at contaminated sites (U.S. EPA, 1997 and Evanko and Dzombak, 1997). Mercury contamination has occurred extensively in many industries from historical uses associated with the paper industry, cosmetics, and pharmaceutics to modern uses in chlor alkali plants (45 percent of all domestic mercury emissions), writing devices and switches, lighting, and dental work (U.S. EPA, 2006). Quantities as large as 700,000 pounds of mercury may have been released during nuclear weapons production in the 1950s and 1960s at the Y-12 Plant in Oak Ridge, and 1.3 million pounds remain unaccounted for (DOE News, 2002). Between the two common forms of mercury ions, Hg_2^{2+} and Hg^{2+} in aqueous solution, Hg^{2+} is more stable in natural, brackish, and seawater systems. However, elemental mercury (Hg^0) is frequently present at the source of a spill. Elemental mercury spilled in soil behaves as a dense non-aqueous phase liquid (DNAPL) and can contaminate groundwater. In this environment, the mercury can interact with the soil media and the water. It can be oxidized to Hg(I) and Hg(II) ions in oxic water. The oxidized mercury may undergo complexation with strong complexing ligands, precipitation, and/or sorption onto the soil matrix. When inorganic mercury is transported into lakes or streams, bacteria (e.g., sulfate reducing bacteria) can methylate the mercury to produce species that are hydrophobic and can bioaccumulate. Numerous studies have demonstrated the risks associated with consumption of fish containing methylated mercury. Thus, it is essential to investigate the fate and transport of mercury in soils incorporating speciation

from the source where concentrations are expected to be high to dilute solutions associated with down gradient groundwaters, lakes and rivers.

Mercury speciation is extremely complicated because mercury is present in various oxidation states in the environment and reacts with inorganic ligands (e.g., sulfide and chloride) and organic ligands (Wuana and Okieimen, 2011). Recent studies have addressed mercury speciation emitted from coal combustion and gasification systems. However, in-depth mercury speciation during thermal treatment in soil has not been studied extensively. Gas phase speciation (both equilibrium and kinetics) at high concentrations has implications with regard to both the efficacy of treatment scenarios that rely on transfer from the soil, liquid or pure phase to the gas phase, as well as the potential for Hg capture during post-treatment of the gas phase.

No remediation scenario will be completely successful at removing all of the Hg that has contaminated a particular site. In many cases, the quantity of mercury remaining after remediation could still be significant and impact downgradient water supplies. Adsorption of inorganic mercury to soil minerals is the primary process controlling the fate and transport of mercury present at low concentrations, and the underlying mechanisms are similar to other transition metals such as Cd, Zn, Cu, and Pb. The fate of Hg(II) in soil/water environments is also controlled by its adsorption behavior on mobile particles (Schuster, 1991). Among the most common inorganic adsorbents, metal (hydr)oxides have the highest affinity for inorganic ions in solution due to their high specific surface area, favorable surface charge, and reactive surface sites (MacNaughton and James, 1974). To date, the adsorption behavior of Hg(II) on metal (hydr)oxides has

not been extensively studied in the presence of inorganic ligands, even though mercury is known to form strong aqueous complexes with ligands such as chloride.

1.1 Research Objectives

The primary objective of this study is to predict mercury speciation during and subsequent to thermal remediation processes. To this end, two sub-objectives are defined that address the two unique environmental concentration ranges that occur in these systems. Because thermal remediation is typically applied at sites in which high concentrations of mercury are present, the first sub-objective addresses speciation modeling at high concentration. However, upon completion of the remediation and down gradient of the initial spill, low concentrations of mercury prevail. Therefore, speciation under these conditions is addressed in the second sub-objective. Thermodynamic modeling is used to determine mercury speciation throughout the concentration range, from dilute solutions of Hg(I) and Hg(II) to pure phase elemental mercury and solid phase species, because remediation strategies must address removal of bulk mercury phases as well as residual concentrations. At high concentrations, speciation of inorganic mercury is evaluated for assessing potential transformation reactions during thermal treatment since speciation at high concentrations (pure phase mercury species) is highly temperature dependent. At dilute concentrations, Hg(II) adsorption is evaluated with the essential building blocks of geological substrates such as goethite (iron oxide) and gibbsite (aluminum oxide) that are both ubiquitous and highly reactive in soil systems with divalent metal ions and oxyanions.

The purpose of the first phase of the study is to model mercury speciation for a range of biogeochemical conditions and over a range of temperatures to predict its distribution and environmental impact at near source environments where pure phase Hg species are present. This information is of importance for all potential remediation processes especially thermal processes. For example, *In Situ* Thermal Desorption (ISTD) is a viable technique to remediate volatile and semi-volatile contaminants in soil. The design and application of ISTD processes requires knowledge of mercury speciation for developing cost-effective design and monitoring remediation strategies. Major goals of this phase of study are to identify phase transitions that occur at high temperature based on equilibrium calculations using chemical equilibrium software and to examine the impact of soil conditions on mercury speciation and remediation strategies of soil. Soil conditions include soil composition, temperature, solution pH, and redox potential.

The goal of the second phase of the study is to describe Hg(II) adsorption onto goethite (α-FeO(OH)) in the presence of inorganic ligands in open systems. Goethite was chosen since it is a common and thermodynamically stable iron (hydr)oxide in aqueous environments at low temperature and its surface properties are well characterized (Schwertmann and Taylor, 1997; Macalady *et al.*, 1990). Macroscopic experimental data from previous research were used to calibrate a surface complexation model (SCM) that incorporates the aqueous mercury speciation, surface acidity of goethite, and competitive metal ion binding as a function of solution chemistry. The 1-p*K* approach has been used for charge distribution and multi-site (CD-MUSIC) modeling to quantify proton and Hg(II) adsorption on goethite based on bond valence theory.

The objective of the last phase of the study is to model Hg(II) sorption onto gibbsite (α-$Al(OH)_3$), a representative aluminum (hydr)oxide mineral, in the presence of inorganic ligands. Gibbsite was selected due to its abundance in soils (Dissanayake and Vitanage, 1977). A number of macroscopic investigations have been conducted with different models for Hg(II) adsorption by gibbsite (Sarkar *et al.*, 1999; Weerasooriya *et al.*, 2007), and these studies provide the data for model development. In this phase of the study, the surface chemical equilibria on the surface of thoroughly characterized gibbsite particles were investigated in the 1-p*K* CD-MUSIC surface model on the basis of molecular scale data that account for the adsorptive mechanisms on $Al(O,OH)_6$ octahedra.

1.2 Specific Objectives

In summary, the specific objectives of this work are:

- Identify phase transitions that occur at high temperature and examine the impact of soil conditions on mercury speciation that will affect remediation strategies of soil.
- Describe Hg(II) adsorption onto goethite, α-FeO(OH), incorporating inorganic ligands and carbonate species in an open carbon dioxide system.
- Model Hg(II) adsorption onto gibbsite, α-$Al(OH)_3$, in the presence of inorganic ligands and carbonate species.

1.3 Dissertation Outline

This dissertation consists of six chapters. The introduction presented in Chapter 1, general literature review presented in Chapter 2, and the conclusions presented in Chapter 6 give an overview and summarize the objectives, background and results of this research. Chapters 3, 4, and 5 are presented in a format that is consistent with requirements for submission in scientific, peer-reviewed journals. Each of these chapters focuses on one of the three specific objectives of the research.

Chapter 2: Literature Review

2.1 Properties affecting the Fate and Transport of Mercury

2.1.1 Chemical Properties of Mercury

Mercury (Hg), also known as quicksilver or hydragyrum, is a common metal found in the environment in various forms, including inorganic, and organic mercury. Despite its usefulness in various electrical applications and a broad range of industries from medicine and cosmetics to chlor-alkali plants, elemental mercury and its compounds can be extremely detrimental to human health and to the environment. Both acute and chronic effects of mercury depend on its speciation and can occur through exposure by inhalation or ingestion. Elemental mercury is volatile so that exposure through inhalation can lead to neurological effects because mercury vapor can pass the blood brain barrier (Boening, 2000).

The chemical properties of various stable mercury species, such as elemental mercury (Hg^0), mercuric chloride ($HgCl_2$), mercuric sulfide (HgS), methyl mercury chloride (CH_3HgCl), phenyl mercury chloride (C_6H_5HgCl), and dimethyl mercury ($(CH_3)_2Hg$), are listed in Table 2.1. Elemental mercury can be oxidized under environmentally relevant redox conditions, resulting in the most prevalent oxidation states of mercury, Hg^+ (mercurous) and Hg^{2+} (mercuric, the more stable form in oxic environments) ions. In addition, inorganic and organic mercury form complexes with ligands (S^{2-}, Cl^-, and O^{2-}) that are ubiquitous in soil. Because elemental mercury has an exceptionally low melting temperature and high surface tension, it forms small spherical droplets which increase its surface area to volume ratio. Moreover, its relatively high

vapor pressure, as shown in Table 2.1, compared to other metals can cause evaporation easily at ambient temperature. Thus, adverse health effects are expected when elemental mercury is inhaled and absorbed through the lungs (MADEP, 1996; Taube *et al.*, 2008). The solubility of the different mercury phases as provided in Table 2.1 demonstrates the variability in solubility from the low solubility of Hg^0 and HgS to higher values of $HgCl_2$.

Table 2. 1 Chemical properties of various mercury species (Chemfinder.com, 2004; EPA, 2007; Hempel and Thoeming, 1999; Lide, 2007, 2008; Mason *et al.*, 1996).

Chemical Properties	Elemental Mercury	Mercuric Chloride	Mercuric Sulfide	Methyl Mercury Chloride	Dimethyl Mercury
Molecular Formula	Hg	$HgCl_2$	HgS	CH_3HgCl	$(CH_3)_2Hg$
M.W [g/mol]	200.59	271.50	232.65	251.08	230.66
Melting Point [°C]	-38.87	276	583.5	170	–
Boiling Point [°C]	356.9	302	–	–	93
Density at 20°C [g/mL]	13.546	5.44 (25°C)	7.73 – 8.10	4.06 (20°C)	3.07
Vapor Pressure [μmHg]	1220 (20°C)	834000 (25°C)	–	4700 (20°C)	58.6 (23.7°C)
Solubility in H_2O [g/L]	5.6×10^{-5} (25°C)	69 (20°C)	10^{-5} (18°C)	0.1 (21°C)	1 (21°C)
K_{OW}	4.15	3.33	–	1.7	182

2.1.2 Fate and Transport of Mercury

The mercury cycle in subsurface soil is illustrated in Figure 2.1. Once elemental mercury (Hg^0) is spilled in soil, it can migrate downward due to its high density, volatilize due to its high vapor pressure or remain trapped within the soil matrix. Within each of these environments, Hg^0 reacts with the air, soil, and aqueous media; however, it can also remain in the elemental form for extended time periods.

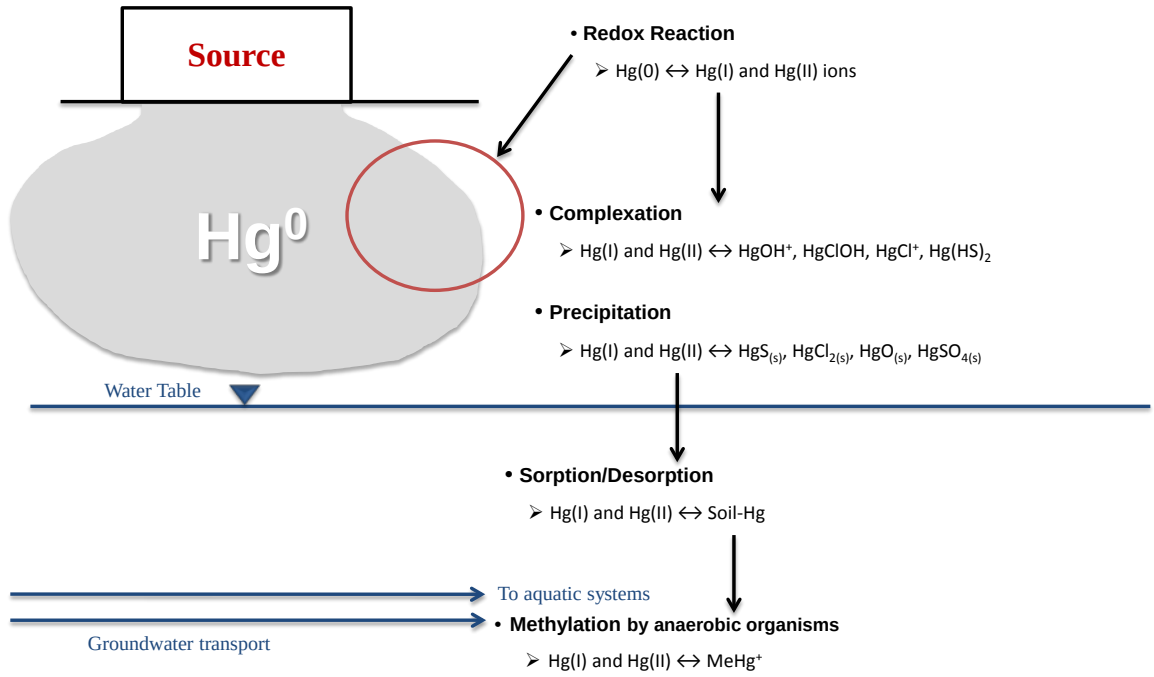

Figure 2. 1 Mercury cycle in the subsurface soil, Adapted from Kunkel, 2004

2.2 Remediation of Mercury

2.2.1 General Remediation

The most challenging aspect associated with remediation of metals is that it is not possible to convert a metal ion into a non-hazardous species. As a result, transformation processes may alter speciation of the metal to a less toxic or less mobile form, but will not eliminate the metal from the environment. Selection of the appropriate technology for remediation of metals in soil is largely influenced by physicochemical properties and the level of contamination at a particular site. Several technologies including isolation, immobilization, toxicity reduction, physical separation, and extraction have been employed. They can be used independently or in combinations of one or more of those techniques to achieve cost effective treatment (Evanko and Dzomback, 1997).

Isolation technologies used to prevent the spread of contamination in soil by isolating the contaminated area are typically employed when other treatment attempts are not feasible. Capping or subsurface barriers are an example of contaminant isolation processes that reduce release of contaminants, control contaminant migration, and improve aesthetics.

Immobilization techniques are designed to use chemical reagents or thermal treatment to physically restrict contact between the contaminant and surroundings or chemically alter the contaminant to be more stable. Solidification and stabilization (S/S) immobilization technologies are frequently used for remediation at metal contaminated sites (Conner, 1990). S/S processes include mixing or injecting inorganic binders such as cement, fly ash, or blast furnace slag and organic binders such as bitumen to the

contaminated soils. The long-term stability of soil or waste treated with S/S is not known even if it has been used to meet regulatory levels without further effort before disposal (EPA, 2007). Furthermore, costs for S/S are considered to be high relative to other remediation strategies.

Chemical treatment by oxidation, reduction, and neutralization reactions or biological processes involving certain plants and microorganisms can be used for toxicity and/or mobility reduction. This technique has been employed for conversion of Cr(VI) to Cr(III) and U(VI) to U(IV) because these metals ions are less soluble in the reduced state (Lovely, 1993).

Physical separation is an *ex situ* method used to separate the contaminants from the soil matrix. It includes screening, classification, gravity concentration, magnetic separation and froth flotation. Extraction techniques can be used to extract the contaminant fraction from soil either via *in situ* or *ex situ* processes. Effective remediation has been achieved using extracting agents (soil washing and *in situ* soil flushing) or by electrokinetic processes (Alshawabkeh, *et al.*, 1999; Evanko and Dzomback, 1997; Khodadoust, *et al.*, 2005; Reddy *et al.*, 2001).

In situ thermal treatment has been explored as an alternative that meets the needs of a broad range of sites and contaminants such as volatile organic compounds (VOCs) and semi-volatile organic compounds (SVOCs), PCBs, petroleum aromatic hydrocarbons (PAHs), and volatile metals contained in the soil matrix. Application of thermal treatment to mercury contaminated sites has not been as extensive as it has for other contaminants even though thermal processes appear to have potential. Three remediation techniques,

including thermal treatment were evaluated for two soil samples (sand and clay) by the Gas Research Institute to identify the most effective approach for mercury remediation. The processes included a pilot-scale portable thermal treatment process (PTT), a bench-scale oxidative chemical leaching process, and a pilot-scale physical separation process followed by chlorine leaching. Among these three processes, the thermal treatment process was found to be most effective in that total mercury content in sand was reduced from 12,720 mg/kg to 0.07 mg/kg (99.9994 % removal) and in clay from 1090 mg/kg to 0.12 mg/kg (99.9890 % removal) (Stepan *et al.,* 1995).

2.2.2 In Situ Thermal Desorption (ISTD) Remediation

In Situ thermal desorption (ISTD) applies both heat and vacuum simultaneously to the soil to remediate mercury contaminated soil. In ISTD, thermal blankets, thermal wells, or combinations of heater-only wells and heater-vacuum wells are used to remediate contaminants in soil. The use of thermal blankets and thermal wells at a site is illustrated in Figure 2.2. The heater-vacuum wells are used to draw contaminant gases driven by high temperature heating. The wells are placed within the target treatment zone at depths greater than 3 feet where heating by the surface thermal blankets is not effective. Thermal wells heat the soil up to 1400 to 1600 F (760 to 871 °C) using electrical resistance elements. The heating temperature is typically higher than the boiling point of water so that the soil is easily desiccated yielding higher gas permeability, especially in clay. This increased permeability improves the transport of vaporized

contaminants in clay or mixtures of silt and clay, since the conduction of heating is very uniform in vertical or horizontal sweep (TerraTerm, 2002).

Figure 2. 2 ISTD thermal blanket (left) and thermal well (right) processes. Source: TerraTherm 2004.

The temperature history of the soil during thermal processes contains three stages: heating, boiling of water, and superheating. The soil pore water and the soil minerals are heated from ambient temperature to the boiling point of water during the first stage. The soil heats quickly due to the low heat capacity of many minerals. Then, the temperature stays at the boiling point of water where all the soil pore water is vaporized during the boiling stage. The boiling time is highly dependent on the amount of pore water that exists in soil considering groundwater inflow. After all the pore water is boiled off, the

dry soil is superheated during the third stage; the soil temperature rapidly increases since no pore water is left in the soil and only soil minerals are heated.

As the temperature increases in the soil, volatile organic compounds (VOCs) and semi-volatile organic compounds (SVOCs) can be destroyed and/or vaporized by several mechanisms including evaporation, boiling of water and VOCs, steam distillation at temperatures below 100ºC and boiling of SVOCs, oxidation, and pyrolysis above 100 ºC within the "superheated" region.

During thermal desorption from soils, impermeable covers have to be placed over the remediation site in order to prevent gas phase contaminants from being emitted into the atmosphere (Stegemeier and Vinegar, 2001). Investigation of both mercury speciation and potential transformations of mercury at elevated temperature is of importance to better understand the potential environmental impact of thermal treatment on soil solutions. In addition, the fate and transport of residual mercury must be understood after removal of mercury vapors during the ISTD processes.

2.3 Speciation at High Concentration of Mercury

2.3.1 Ambient Temperature Speciation

Knowledge of mercury speciation in soil facilitates predictions of mobility and toxicity which are essential for assessing the potential environmental risk of contaminant sites and proposed remediation strategies. Elemental mercury and mercury compounds in soil are problematic once transported to groundwater or to the atmospheric environment, since the various mercury species exhibit unique toxicological and physicochemical

properties. Therefore, the investigation of mercury fate and transport at ambient temperature is of significance for human and ecological health (Boening, 2000).

An investigation of mercury speciation is typically conducted by solving the series of mass balance and mass action equations associated with potential reactions involving mercury and associated ligands. At the Oak Ridge, Tennessee (East Fork Poplar Creek) site, the mercury distribution is 91% inorganic of which 85% is in the form of insoluble $HgS_{(s)}$ due to metabolism of sulfate-reducing bacteria, and 6% is present as elemental liquid mercury (Revis *et al.*, 1989). While only 0.01% of the mercury is present as MeHg, the toxicity of this form of mercury drives most remediation goals. The soft Lewis acid, Hg^{2+} ion and MeHg (methylmercury) have a very high affinity for reduced sulfur groups (R-SH and R-SS-R) under conditions typical of soil rich in natural organic matter and inorganic sulfides and decreased redox potential (Benes and Haylik, 1979; Dyrssen and Wedborg, 1991; Hudson *et al.*, 2004; Hesterberg *et al.*, 2001; Skyllberg *et al.*, 2003). HgS persists in soils even at increasing redox potential with slow weatherization (Barnett *et al.*, 1997). In contrast, inorganic mercury salts, $HgCl_{2(s)}$, $HgO_{(s),}$ and $HgSO_{4(s)}$ are dominant in oxidizing conditions, and $Hg^{0}_{(l)}$ is the dominant pure phase in reducing environments in soil with limited availability of organic matter. The formation reactions of metallic and inorganic salts of mercury are shown in Table 2.2.

Table 2. 2 Pure phase speciation of mercury and thermodynamic formation constants used in speciation modeling.

	Solid phase reaction	Log *K*	ΔH_f (kcal/mol)
1	$Hg^{2+} + 2e^- = \mathbf{Hg_{(l)}}$	28.851	-16.666
2	$Hg^{2+} + H_2O = \mathbf{HgO_{(s)}} + 2H^+$	-2.554	20.172
3	$Hg^{2+} + SO_4^{2-} = \mathbf{HgSO_{4(s)}}$	3.225	7.365
4	$Hg^{2+} + 2Cl^- = \mathbf{HgCl_{2(s)}}$	15.068	-14.895
5	$Hg^{2+} + HS^- = \mathbf{HgS_{(s)}} + H^+$	39.500	-49.775

Geochemical models that incorporate aqueous chemical speciation can be used to predict equilibrium concentrations of mercury in solution and to predict the dominant pure phases at a particular site. Among the available software packages for chemical speciation modeling, WHAM 6 and MINEQL+ 4.5 are the two most cited in the literature. Cloutier-Hurteau *et al.* (2007) extensively evaluated the reliability of these two modeling packages with Cu^{2+} and determined that MINEQL+ 4.5 better incorporates inorganic ligand complexation than does WHAM 6. While other geochemical codes are also capable of determining equilibrium compositions, the user-friendly interface and prevalence in the field of MINEQL+ 4.5 suggest that this is a suitable package to evaluate dissolved mercury speciation as a function of pH and to identify the predominant forms of mercury in different types of soil environments such as those rich in chloride or sulfur.

2.3.2 High Temperature Speciation

Taube *et al.* (2008) investigated the thermodynamic mercury speciation using FactSage 5.2, a computer software program that is solved through minimization of the

total Gibb's free energy (Bale *et al. 2002*). In their study to evaluate thermal treatment of mercury, various soil compositions were considered to identify both mercury speciation and phase transitions of mercury. In their modeling, calculations of thermodynamically favorable equilibrium reactions were performed for cases with different availability of O, S, and Cl. For a system with low oxygen availability, Hg^0 or $HgS_{(s)}$ was predicted to form at 20°C depending on the availability of chloride and sulfur. These predominant forms were expected to be released to the gas phase at 90°C and 140°C, respectively, upon thermal heating. In contrast, a system with high oxygen availability, $HgCl_{2(g)}$ and $HgO_{(g)}$ were predicted to dominate in the vapor at 90°C and 350°C respectively. Finally, for a system with high sulfur availability, $Hg_{(g)}$ and $HgO_{(g)}$ were predicted to be vaporized from $HgO_{(s)}$ at 140°C to a minor extent and 230°C to a maximum, respectively. They also observed that $HgSO_{4(s)}$ started to decompose to Hg^0 and $HgO_{(g)}$ at approximately 270°C. Two separate steps of mercury volatilization were observed, the initial elemental vaporization and the subsequent volatilization of the oxide or sulfate phase at higher temperatures (>230°C). In addition, these researchers concluded that it is possible to remove more than 95% of the mercury present at a site by thermal treatment in heavily contaminated soil (up to 2,400 ppm) at 300°C within minutes, and removals of more than 99% of mercury were achievable at 470°C in just over 20 minutes of heating to these temperatures (Taube *et al.*, 2008). The detailed explanation of these phase transitions of mercury not only allows the prediction of mercury speciation at given temperatures and soil conditions but also helps determine removal strategies for mercury contaminated sites. Unfortunately, vague model parameters (i.e. high or low availability of inorganic

ligands in soil rather than molar ratios) were used in the equilibrium calculations of Taube *et al.* (2008). Application of these results to field scenarios requires that operating parameters such as temperature be optimized for the specific site. This requires a parameterized model that can be used to simulate mercury phase transitions for potential inorganic mercury species at relatively low temperatures. In addition, the impacts on vapor pressures generated from gas phase mercury species and the decomposition of soil components during thermal remediation should be determined for the particular redox conditions to evaluate the effect of soil components on mercury gas displacement.

Vapor pressures of carbon dioxide generated from a total carbonate concentration and soil pore-water can be predicted in soil systems. These calculation include the slight decomposition to $CO_{(g)}$ and $½O_{2(g)}$ during thermal treatment (CHERIC; Stern, 2001). The partial pressure of carbon dioxide varies from 0.39 matm (atmospheric) to 10-50 matm due to plant respiration and microbial decomposition of natural organic matter in various natural aqueous settings (Bolt and Bruggenwert, 1978; Buyanovsky, 1983; Sposito, 1989), within 0.1-0.2 atm in certain groundwater systems (Hem, 1970; Bulter, 1982, Langmuir, 1997), or between 0.002 and 130 bar in confined aquifers of sedimentary basins and 10^{-6} to 50 bar in geothermal fields with magmatic rocks at higher temperature (Coudrain-Ribstein *et al.*, 1998). Typically, a value of 1-2 mM for the average total carbonate concentration including the amount of organic carbon (approximately 58% of organic matter that is present typically between about 1 and 10 % in mineral soils) is assumed to be present in a soil matrix. In addition, decomposition of $HgO_{(s)}$ and $HgSO_{4(s)}$ to Hg^0 and HgO gas are expected at approximately 140°C and 270°C, respectively, under

oxidizing conditions in which $HgCl_{2(g)}$ can be vaporized with temperature increase (Chase, 1998; Cox *et al.*, 1989; NIST; Stumm and Morgan, 1996; Taube *et al.*, 2008; Wagman *et al.*, 1969). The decomposition of $HgO_{(g)}$ to $Hg_{(g)}$ and $O_{2(g)}$ at 523.15K is considered to account for the increasing proportion of $Hg_{(g)}$ in the vapor pressure calculation. Inorganic carbonate minerals occur in many common soils, and their influence on soil is significant due to its relatively high solubility and pH buffering properties (Loeppert and Suarez, 1996). Calcite is typically the dominant form in active pedogenic environments, but a few occurrences of aragonite ($CaCO_3$) and vaterite ($CaCO_3$) are also reported in soils (Doner and Lynn, 1977; Nelson, 1982). The carbonate minerals decompose to oxide or basic carbonates (e.g., $PbO{\cdot}PbCO_3$) with evolution of carbon dioxide. The thermal stability of group 2 alkaline earth metal compounds tends to be higher than transition metal or d-block group compounds because of the smaller cationic charge and lower polarizing power. The thermal decomposition orders for these groups are as follows: $BaCO_3 > SrCO_3 > CaCO_3 > MgCO_3 > ZnCO_3 > CdCO_3 > Ag_2CO_3$ (L'vov, 2002). Kaolinite is a clay mineral that can undergo endothermic dehydration which begins at 550-600°C to form disordered metakaolin, $Al_2Si_2O_7$, and a series of further phase transformations during thermal treatment (Bellotto *et al.*, 1995). Of the carbonate solids above, only $Ag_2CO_{3(s)}$ and $CdCO_{3(s)}$ (initial temperature of decomposition of 371 and 442°C, respectively) are expected to decompose to release carbon dioxide below 500°C, the temperature at which 99% of mercury can be removed (Stern, 2001). The calcination reaction for limestone to form lime and carbon dioxide at

1 atmosphere pressure occurs above 800°C and for carbon dioxide at a partial pressure of 0.35 mbar occurs above 500°C.

2.4 Aqueous Speciation at Dilute Mercury Concentration

2.4.1 Aqueous Mercury Species

The toxicity and acute pollution associated with dilute concentrations of mercury remaining after remediation is largely affected by the physico-chemical properties (chemical redox speciation) of mercury and other species in the system. A thorough understanding of aqueous and surface chemistry in these environments is of significance for the investigation of mode and stability of mercury. Mercury exists in three oxidation states, 0 (Hg^0), I (Hg^+), and II (Hg^{2+}) in natural waters. Among these oxidation states, Hg(II) is the most stable form, one that has strong complexing ability towards S-derived ligands and halides (Stein *et al.*, 1996; Stumm and Morgan, 1996). Speciation analyses in Figure 2.3 have shown that hydrolysis reactions are dominant for aqueous Hg(II) in the absence of strong complexing ligands. At low pH, the hexaqua ion $Hg(H_2O)_6^{2+}$ is coordinated octahedrally by water molecules. As pH increases, the importance of stable $HgOH^+$ and $Hg(OH)_2$ aqueous species formed through hydrolysis increases (Kim *et al.*, 2004a). When in the presence of chloride which is ubiquitous in marine systems, the stable nonsorbing $HgCl_{2(aq)}$ species becomes dominant at pH 6 and below when chloride ion is more than 10^{-3} M as shown in Figure 2.4 (Kim *et al.*, 2004b).

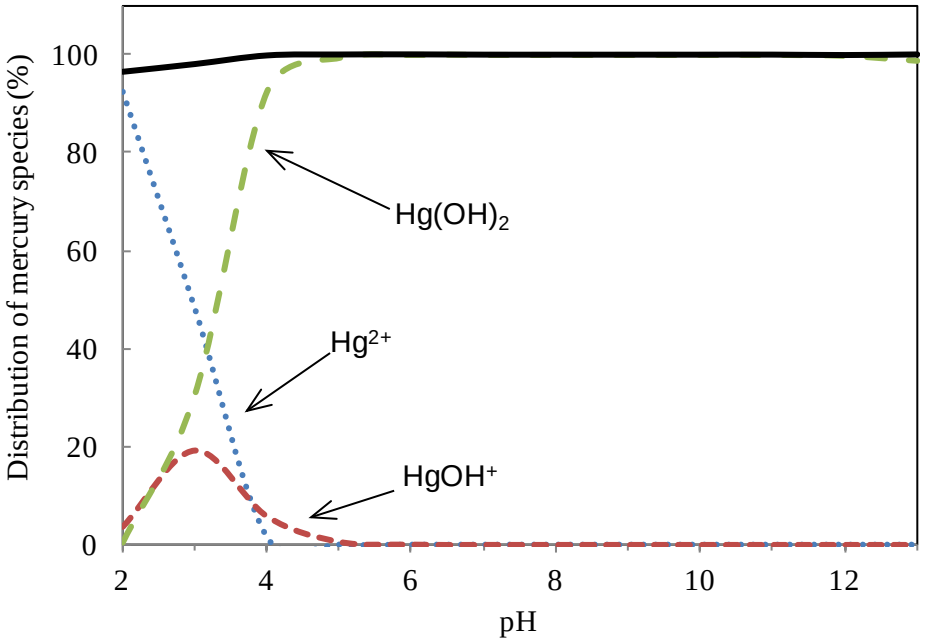

Figure 2. 3 Hg(II) aqueous speciation diagram with initial concentration of 5 μM as a function of pH.

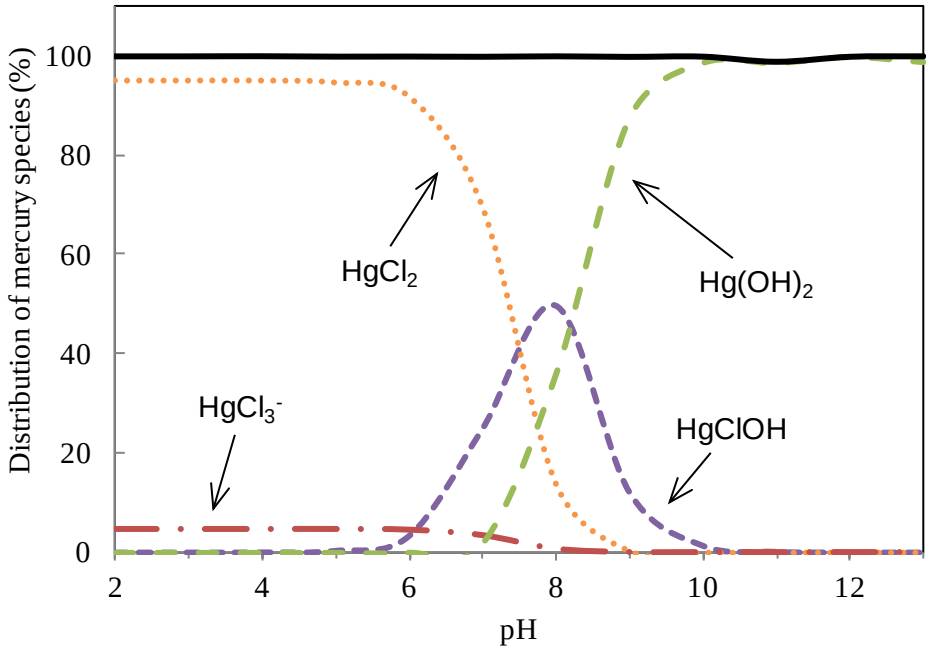

Figure 2. 4 Hg(II) aqueous speciation diagrams with initial concentration of 5 μM in the presence of Cl ($[Cl^-_{TOT}]$ = 5 mM).

2.4.2 Adsorption to Soils

Aqueous/soil interface chemistry is of importance for predicting the fate and transport of all metal ions. The mobility, toxicity, and removal of trace metal ions in aquifers and natural waters are determined by chemical processes including sorption/desorption on geological substrates such as soils, sediments or aquifer materials. The sorption/desorption behavior of trace metal ions on particle surfaces is complicated because it is often dictated by inorganic ligands (carbonate, chloride, phosphate, sulfate, and sulfide in fresh and seawater) and organic ligands (amino, carboxylic, fulvic, and humic acids in natural water) (Stumm and Morgan, 1996). The extent of sorption is

highly dependent on both solution phase conditions as well as the mineralogy of the sorbent.

Several studies have documented the influence of pH and the presence of chloride and sulfate on the Hg(II) adsorption by various mineral surfaces. As is typical of most metal cations, adsorption to a mineral oxides (e.g., goethite and gibbsite) increases with increasing pH. The formation of stable, nonsorbing aqueous complexes with inorganic ligands or competitive ligand sorption can lower Hg(II) sorption to soil minerals by blocking the reactive surface sites. The direct sorption or accumulation of sulfate ions reduces the electrostatic repulsion of metal cations towards the positive mineral surface charge, thereby enhancing Hg(II) uptake to soil substrates (Kim *et al.,* 2004). Additionally, the reduction in the extent of adsorption at all pH values that has been observed when chloride ion has been attributed to the presence of chloride inhibiting Hg(II) adsorption (Newton *et al.*, 1976; Kinniburgh and Jackson, 1978; Farrah and Pickering, 1978; Thanabalasingam and Pickering, 1985; Barrow and Cox, 1992a, 1992b; Yin *et al.*, 1996).

Liao *et al.* (2009) investigated the kinetics of mercury sorption to quantify the extent of retention or release in different surface soils including the Ap horizon (0-10 cm) of Olivier loam (fine-silty, mixed, thermic Aquic Fragiudalf), Sharkey clay (very fine, montmorillonitic, nonacid, thermic, Vertic Haplaquept), Windsor sand (mixed, mesic Typic Dipsamment), and washed sea sand for a reference without no clay and organic matter. They found that mercury adsorption was rapid (more than 93% of mercury retained within 24 h), and the sorption capacities followed the sequence of Sharkey clay

> Olivier loam > Windsor sand. These results correlated with the surface area largely due to the different particle size distributions of the three soils. The finest particles with the largest surface areas exhibited the highest sorption affinity of mercury (Babiarz *et al.*, 2001; Gabriel and Williamson, 2004; Ramamoorthy and Rust, 1978).

Moreover, the presence of soil organic matter influenced the amount of Hg adsorption on the three soils. They reported that mercury adsorption capacity decreased adsorption capacity of those soils significantly decreased after removal of soil organic matter. These results are consistent with other studies that highlighted the affinity of mercury for soil organic matter (Yin *et al.*, 1996, 1997b). Compared to other heavy metals such as Cd, Zn, Cu, and Pb, Hg has a higher complexing affinity to organic matter due to the covalent bonds that can be found between Hg and humic matter (Kernorff and Schnitzer, 1980; Gabriel and Williamson, 2004). Therefore, different Hg adsorption/desorption behavior is expected for soil samples with different mineralogy, surface area and organic matter content and composition.

2.4.3 Adsorption to Metal (hydr)oxides

The fate of Hg(II) in the environment is controlled to a large extent by sorption to fixed or mobile adsorbents (Schindler, 1967). Potential inorganic and organic sorbents for Hg include clay minerals; amorphous oxides; hydroxides; oxyhydroxides of Fe, Mn, and Al (such as FeOOH); amorphous FeS (under reducing conditions); and dissolved/particulate organic substances (Lockwood and Chen, 1973). Of these substances, Fe and Al (hydr)oxides and silica are most abundant in many aquatic systems

and particularly reactive (high capacities of Hg adsorption) in the soil environment as well as organic matter such as humic material (Gabriel and Williamson, 2004; Kim *et al.*, 2004a). Goethite (α-FeOOH) that consists of Fe(III) ions coordinated by six O(H) ligands to form Fe(O,OH)6 octahedra or gibbsite (α-Al(OH)3) that is composed of Al ions in hexacoordination with OH groups are considered as major building blocks of natural substrates as shown in Figure 2.5.

(a) (b)

Figure 2. 5 Major building blocks of natural substrates: (a) Goethite (α-FeOOH) crystal and (b) Gibbsite (α-$Al(OH)_3$) crystal.

Many batch experiments for Hg adsorption on these minerals have been reported (Kinniburgh and Jackson, 1978; Lockwood and Chen, 1974; MacNaughton, 1973). However, the silica has low surface area in general, and Hg sorption data on silica are rarer. Tiffreau *et al.* (1995) reported that adsorption of the free cation Hg^{2+} on α-SiO_2 was not important, and differences in magnitude of sorption building constants were

consistent with the conclusion that iron oxides are more important that SiO_2 surfaces. Using a surface complexation model (see description in Section 2.4.4), constants for HFO ternary surface species ($K^{int}_{\equiv SOHgOH}$ = -0.9 ± 0.2 and $K^{int}_{\equiv SOHgCl}$ = 9.8 ± 0.4) were two orders of magnitude higher than those for α-SiO_2 ($K^{int}_{\equiv SOHgOH}$ = -3.2 ± 0.1 and $K^{int}_{\equiv SOHgCl}$ = 7.0 ± 0.1). In the experimental data from MacNaughton (1973), 90% of Hg(II) was sorbed to HFO when the total Hg loadings were 0.184 µM, and solid content was 80 mg HFO/liter in 0.1 M of $HClO_4$ and NaOH, while 70% of Hg(II) was sorbed to α-SiO_2 when the total Hg loadings were 0.184 µM, and solid content was 40 g α-SiO_2/liter in 0.1 M of NaOH. Bonnissel-gissinger *et al.* (1999) found that for equivalent surface site numbers, 40 times more Hg(II) was sorbed to goethite (Bayferrox) than amorphous silica (Aerosil 200). These studies highlight differences in affinity of Hg for different mineral surfaces and suggest that it is important to distinguish adsorption to different types of minerals when assessing the fate and transport of mercury in soils. The rationale employed in the modeling study described in this dissertation is to calibrate the physicochemical interfacial processes of discrete minerals which are dominant in soil. Future research can then expand the gathered information to model Hg sorption behavior on the complex soil system. To this end, it is essential to incorporate an understanding of the surface chemistry of mineral oxides and relevant soil components into predictive models. Metal hydroxides contain what is termed a variable charge surface in which the surface charge (e.g., zeta potential) varies as a function of pH and the chemical composition of reactive surfaces. The degree and mechanism of Hg(II) adsorption to these variable charge surfaces is dependent upon the acidity of the reactive surface site

groups (i.e. surface hydroxyl sites), reactive surface site densities, and presence of competing sorbates. Models that incorporate this variable charge behavior offer considerable advantage for predicting metal ion speciation over a range of conditions expected in the environment.

2.4.4 Surface Complexation Models (SCMs)

2.4.4.1 General SCMs Tenets

Adsorption of cations and anions through particulate-solution interactions is of importance in a broad range of environmental applications. Various experimental and theoretical studies of adsorption on particle surfaces have been performed and their data were used to calibrate either adsorption isotherms or surface complexation models (SCMs).

An adsorption isotherm describes the macroscopic relationship between the equilibrium concentration of the adsorbent (e.g., goethite surface) and the amount of adsorbate (e.g., Hg^{2+}) bound to the surface at constant temperature. Metal ion adsorption is frequently modeled in soils using either a linear, Langmuir, or Freundlich model. The Langmuir model,

$$q = KCb/(1 + KC) \qquad (2.1)$$

where q is the amount of adsorption (adsorbate per unit mass of adsorbent) in mol kg^{-1}, b is the maximum adsorption capacity, and C is the equilibrium concentration of the

adsorbate, assumes that there are a finite number of uniform sites for adsorption which yields a plateau in the isotherm at high concentration corresponding to site saturation as shown by the adsorption of cadmium on Anderson sandy clay loam at pH 6.2 and 298 K in I = 0.02 M (Figure 2.6 from Sposito (2004)). This model can be derived using these assumptions and the adsorption reaction:

$$S + A = SA \qquad K = [SA]/([S][A]) \tag{2.2}$$

in which S represents an unoccupied surface site, A is the adsorbate and SA an occupied adsorption site. Combining this mass action expression with the mass balance on surface sites.

$$S_T = S + SA \tag{2.3}$$

yields:

$$[SA] = K[A]S_T/(1+K[A]) \tag{2.4}$$

which is analogous to the Langmuir model presented in equation (2.1).

The Freundlich model:

$$q = K_f C^{1/n} \quad (2.5)$$

where K_f is the Freundlich adsorption capacity coefficient and $1/n$ reflects the degree of non-linearity associated with the isotherm, has also been employed to describe metal ion adsorption. In many cases, it provides a better prediction of metal ion adsorption because it empirically incorporates mineral and site heterogeneity within a soil (Sparks, 2003). The linear model represents a simplification of both of these models in which the Freundlich exponent is equal to one or the equilibrium concentration is low in the Langmuir model. However, none of these models are capable of accounting for the impact of pH or ionic strength on metal ion adsorption shown in Figure 2.6 without changing the values of the capacity terms, K, K_f or the linear sorption coefficient K_d.

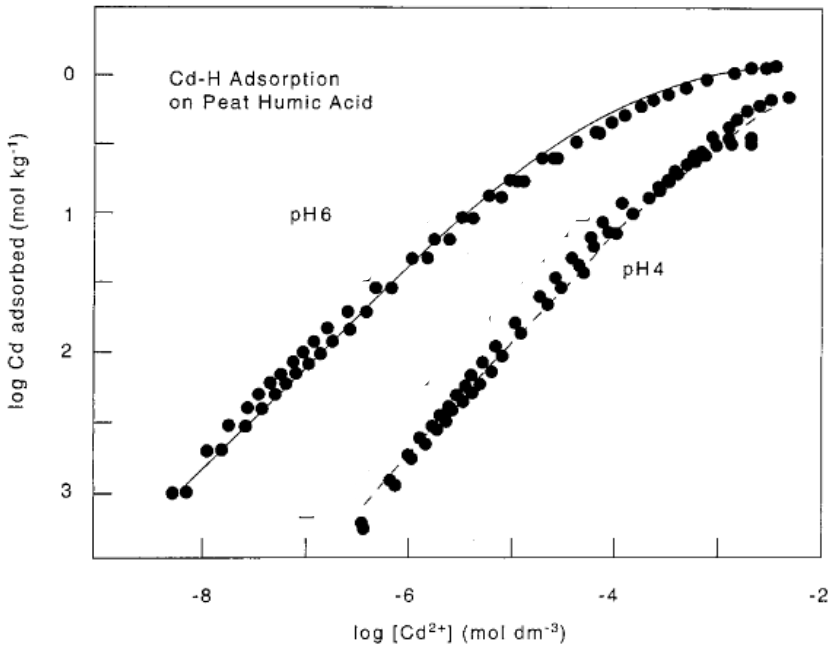

Figure 2. 6 Effect of pH on Cd adsorption isotherms on a peat humic acid at 0.1M KNO_3. Adapted from Sposito, 2004.

Surface complexation models were developed as a means of incorporating the impact of pH (Davis and Leckie, 1978). In many ways, they are an extension of the Langmuir model as they share many of the same assumptions in the adsorption process between an adsorbate, A, vacant surface sites, S, and occupied surface sites, SA except that the reaction involves release or consumption of a proton:

$$SOH + A \Leftrightarrow SOA + H^{+} \quad (2.6)$$

$$S_T = SOH + SOA \quad (2.7)$$

Thus, surface complexation models are an extension of the Langmuir model in which protons are incorporated into the adsorption reaction. The surface sites are typically represented by >MeOH in which the > denotes that the bulk mineral. These sites are often treated as diprotic acids that can be described in the classic 2-p*K* approach as follows (s denotes surface and K_i^0 is intrinsic acidity constants):

$$>MeOH + H_s^+ \rightarrow >MeOH_2^+ \qquad K_1^0 \qquad (2.8)$$

$$>MeOH \rightarrow >MeO^- + H_s^+ \qquad K_2^0 \qquad (2.9)$$

The development of surface charge that is apparent in the products of these reactions is responsible for the formation of an electrical double layer. Surface complexation models must also describe the relationship between surface charge and potential. A range of descriptions of this interfacial region have evolved to incorporate surface charge and ionic strength dependency as a function of pH, reactive surface area, and adsorbate loadings. Description of the surface sites as proton reactive functional groups located on the surface planes of crystal faces of the mineral has followed either the 1-p*K* or 2-p*K* approach (Hiemstra *et al.*, 1996; Lutzenkirchen, 1998; Westall and Hohl, 1980). The sorption of metal ions are defined by complexation reactions with the surface functional groups in which the metal ions are located at various distances from the surface based on their affinity for the surface and electrostatic interactions with the functional groups. Different surface complexation models employ different representations of the

relationship between surface charge and potential and the location of sorbing species relative to the surface.

The Constant Capacitance Model was developed by Schindler's research group, and the Diffuse Layer Model developed by Stumm's group (~1970) are early versions of SCMs. The classic 2-p*K* triple layer model (TLM) first proposed by Davis and Leckie (1978 and 1980) is considered to be a generalized mechanistic model that provides a reasonable description of the electrical double layer by incorporating an inner Helmholtz surface plane (0-plane), an outer Helmholtz plane (β-plane) and a classical diffuse plane. The TLM can be simplified for either low or high surface potential. The constant capacitance model (CCM), which incorporates only a single plane, the diffuse layer model (DLM), in which ions behave as point charges and only innersphere complexes are accounted for, and the Stern layer model (SLM), in which ions have finite size that can be placed on two planes as shown in Figures 2.7-2.9 (Hiemstra and Van Riemsdijk, 1996), can be derived as simplifications of the more descriptive TLM. These models work within limited regions of surface potential but are typically applied well beyond the limits of their assumptions.

In all of the SCMs mentioned above, the outermost layer is regarded as the diffuse layer and is described using the classic Gouy-Chapman theory (Westall and Hohl, 1980). They share a number of inherent assumptions: (a) All adsorbing ions as point charges; (b) Homogeneous binding sites, but in reality these sites are inherently heterogeneous; and (c) Planar adsorbing surfaces in the formulation of DDL theory as shown in Figure 2.7-2.9.

The TLM revised by Hayes and Leckie (1987) accounts for ionic strength effects by allowing adsorbates to form either inner- or outersphere surface complexes at the solid-water interface. The formation of inner- and outersphere surface complexes depends on whether a water molecule is intercalated between the reactive mineral surface and its adsorbed ions (i.e., whether the sorbing ion retains its waters of hydration). If at least one molecule of water resides between the sorbing metal ion and the surface metal ion, it is termed an outer-sphere complex (Manning *et al.,* 1998; Sposito, 1984). Sverjensky and Fukushi (2006) applied a water dipole modification to the TLM for anion adsorption using a ligand-exchange mechanism. The electrostatic work which is associated with desorption of water from 0-plane by proton adsorption is illustrated in Figure 2.10.

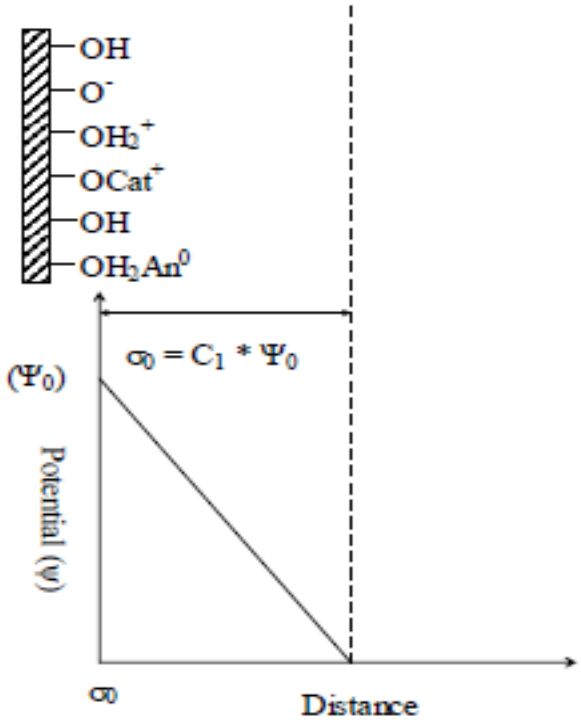

Figure 2. 7 Schematic of the Constant Capacitance Model (CCM). Source: Hayes *et al.*, 1991.

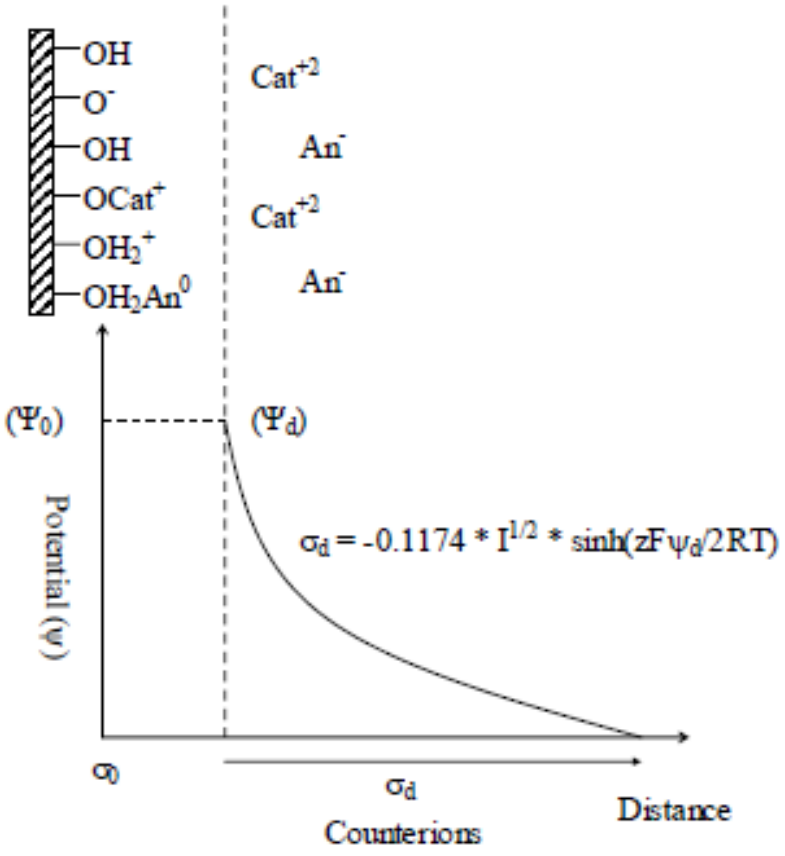

Figure 2. 8 Schematic of the diffuse layer model (DLM). Source: Hayes *et al.*, 1991.

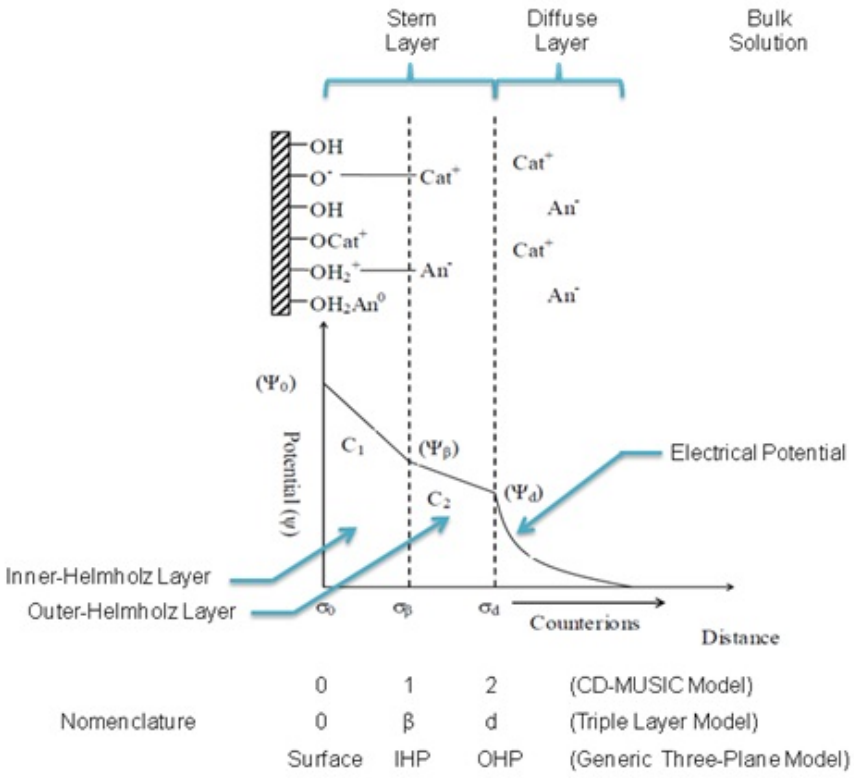

Figure 2. 9 Schematic of the classic 2-p*K* triple layer model (extended stern layer model). Source: Hayes *et al.*, 1991.

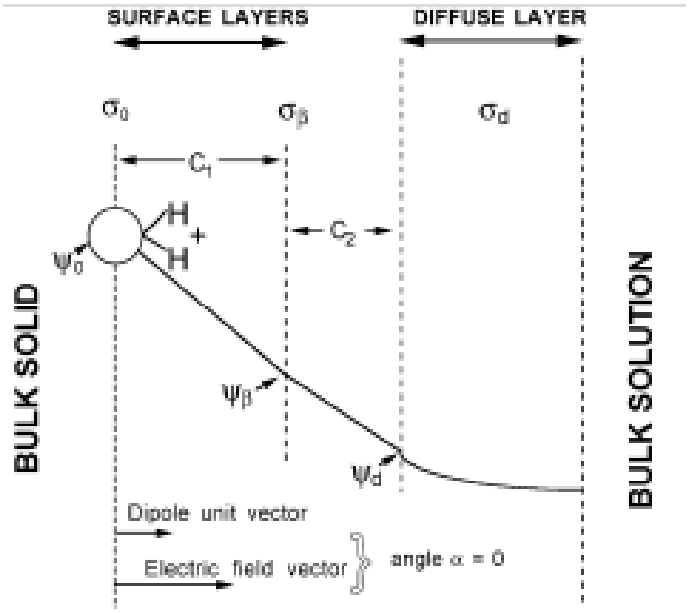

Figure 2. 10 Schematic of a water dipole adsorbed at a surface site in the TLM. Source: Sverjensky and Fukushi, 2006.

Both the 2-p*K* TLM and Stern layer models require estimation of seven parameters (acidity constants (K_{a1}, K_{a2}), electrolyte binding constants (K_{anion} and K_{cation}), Helmholtz capacitance (C_1 and C_2), and surface site density (N_s)) from a limited set of experimental data (Koopal *et al.,* 1987). Moreover, the classic 2-p*K* models assume one unit charge per bond, leading to MeO^-, $MeOH^0$, and $MeOH_2$ in Figure 2.11 which has been disputed based on bond valence theory (Hiemstra *et al.,* 1996).

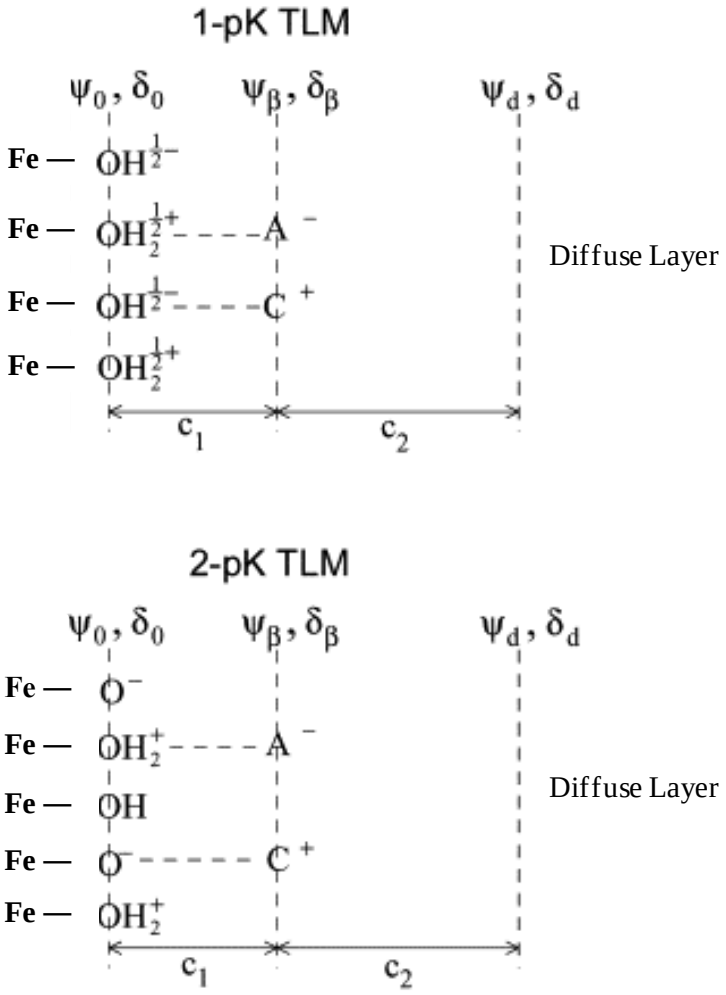

Figure 2. 11 Schematic presentation of surface protonation for the 1-p*K* and 2-p*K* approach in TLM. ψ denotes electrical potential and δ charge located in planes. Adapted from Piasecki, 2006.

2.4.4.2 Charge Distribution and Multi Site Complexation Model (CD-MUSIC)

The charge distribution multi-site complexation (CD-MUSIC) has been developed to incorporate the finite size of adsorbing ions and multisite heterogeneity based on documented crystallography data (Hiemstra *et al.,* 1996; Venema *et al.,* 1996). The CD-MUSIC model accounts for the finite size of adsorbing ions and site heterogeneity based

on the crystal surfaces. In contrast to the 2-p*K* model which requires estimation of seven parameters for model calculations, the 1-p*K* approach requires only six adjustable parameters. The acidity constants for the 2-p*K* approach largely depend on electrostatic models used, but such a limitation does not exist in the 1-p*K* modeling approach. Those constants can be simply derived from the pH_{zpc} of the solid. Additionally, inner- and outersphere complexes are distinctly placed in two different planes as with the TLM.

The following two consecutive reaction scheme represents the surface acidity as shown in Figure 2.11.

$$\equiv Me_nO^{-2+nv} + H^+ \rightarrow \equiv Me_nOH^{-1+nv} + H^+ \rightarrow \equiv Me_nOH_2^{nv} \qquad (2.10)$$

where v and n are Pauling's bond valence [1] and valence number, respectively. The Boltzmann factors related to the electrostatic energy change of species are used for electrostatic 0-, 1-, 2-planes. For those specifically adsorbed ions (SAIs, innersphere by ligand exchange), the change of charge (Δz) on 0- and 1-planes can be obtained as

$$\Delta z_0 = \Delta n_H z_H + f z_{Me} \qquad (2.11)$$

and

[1] Pauling's 2nd rule: The bond valence sum of each ion should equal its oxidation state. In organic chemistry, each bond has a valence of 1. Pauling took this concept and extended it to inorganic compounds, including extended ionic lattices. The valence of a bond, s_{ij}, could be non-integer, and the sum of the bond valences around each atom, should equal its oxidation state. If there are n equivalent bonds around a central atom with valence m, valence of each bond is equal to $s_{ij} = m/n$.

$$\Delta z_1 = (1 - f)\, z_{Me} + \sum m_j z_j \qquad (2.12)$$

where n_H is the net change in protons on the 0-plane, z_H is the charge of the proton, f is is the CD factor, z_{Me} is the charge of the central metal ion in the adsorbed species, m_j is the number of ligands adsorbed in the 1-plane, and z_j is the charge of adsorbed ligands m_j in the 1-plane. A certain fraction f of the central metal ion represents the charge neutralization of ligands placed in the 0-plane if symmetrically distributed. The remaining portion (1 - f) is attributed to ligands in the 1-plane. It is also possible that non symmetrical charge neutralization occurs in the 0-plane due to a shift in electron density in the adsorbed species. A larger neutralization (i.e. higher f value) on the solution side may take place in the process of adsorption, since former surface ligands can be buried to become a more significant part of the solid, and vice versa (Hiemstra and Van Riemsdijk, 1996).

The Gibbs free energy change of adsorption on charged surfaces is divided into the standard Gibbs free energy ΔG_r^o and a composition dependent Gibbs free energy change. The standard Gibbs free energy term can be connected to the intrinsic and electrostatic Gibbs free energy and $RT\ln Q$, in which Q is the reaction quotient variable depending on the composition of the system.

$$\Delta G_{adsorption} = \Delta G_{intrinsic} + \Delta G_{electrostatic} + RT \ln Q \qquad (2.13)$$

where

$$\Delta G_{\text{intrinsic}} = -RT \ln K_{\text{int}}^{s} \quad (2.14)$$

and

$$\Delta G_{\text{elec}} = \sum \Delta z_i F \Psi_i \quad (2.15)$$

in which Δz_i is the net change of charge on the surface, Ψ_i is the surface potential at position i, and F is the Faraday's constant. The intrinsic component reflects the energy change due to adsorption on surface functional groups, while the electrostatic energy term represents the energy required to move ions from bulk solution to the surface. The electrostatic energy is determined by the electrostatic potential, ψ. From the equations above, the apparent equilibrium constant can be simplified at the equilibrium condition.

$$K_{\text{app}}^{s} = K_{\text{int}}^{s} \exp^{-\frac{\Delta z_i F \Psi_i}{RT}} \quad (2.16)$$

where the exponential term represents the Boltzmann factor that describes the effect of surface potential on ion adsorption.

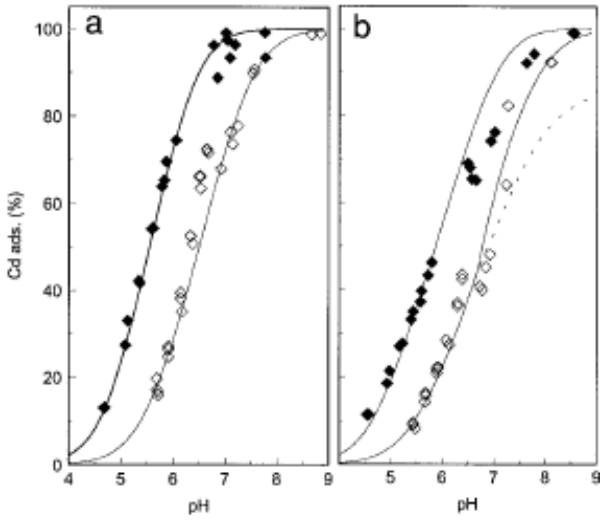

Figure 2. 12 Competitive adsorption of Cd(II) on goethite with 0.5 mM P (closed symbols) and without phosphate (open symbols) in the system at 0.1 M $NaNO_3$. (a) $[Cd^{2+}_{TOT}]$ = 0.25 mM and (b) $[Cd^{2+}_{TOT}]$ = 0.5 mM. The solid and dashed lines represent the model calculations with and without carbonate species respectively. Adapted from Venema *et al.*, 1997.

The 1-p*K* CD-MUSIC model has been used to describe adsorption of toxic heavy metals such as Cd which exhibits a low melting point similar to Hg. Data from Venema *et al.* (1997) shows Cd adsorption on goethite in multi-component systems (Figure 2.12). The data in Figure 2.12 were derived by calculating the percent of metal ion removed from the aqueous phase of a series of batch reactors to which identical total amounts of metal ion and sorbent had been added, and the pH varied. These adsorption edges reflect the importance of pH on metal ion adsorption.

Simulations of competitive Cd adsorption in the presence of PO_4 were consistent with parameters from the single-solute Cd and PO_4^{2-} systems. The success of this modeling effort was attributed to the fundamentally different protonation approach that

utilizes modified Pauling's bond valence theory in contrast to the the 2-p*K* approach which assumes one unit charge per bond, inherent heterogeneity, and spatial distribution of charges at the oxide-water interface (Hiemstra *et al.,* 1996; Lützenkirchen, 1998; Venema *et al.,* 1996, 1997). The parameters used in the adsorption modeling of Cd and PO_4^{2-} are consistent with molecular scale spectroscopic analyses such as EXAFS for Cd(II) and CIR-FTIR for PO_4 (Hiemstra *et al.,* 1999).

A number of researchers have attempted to model Hg(II) adsorption on oxide surfaces in single and multicomponent systems (Barrow and Cox, 1992; Bonnissel-Gissinger *et al.,* 1999; Davis and Leckie, 1978; Gunneriusson and Sjöberg, 1993; Sarkar *et al.,* 1999; Tiffreau *et al.,* 1995; Weerasooriya *et al.,* 2000, 2001, 2003, 2007). Most researchers have adequately described the single component adsorption behavior using various SCMs which suggests that fitting single solute adsorption data is not a valid test of the robustness of an SCM. Indeed, modeling Hg(II) adsorption in the presence of other competing or complexing ligands has met with limited success. Sarkar *et al.* (1999) was incapable of modeling Hg(II) adsorption by gibbsite using the classic 2-p*K* TLM, as shown in Figure 2.13. The failure of the adsorption model using the 2-p*K* approach may be due to incorrect assignment of charge to the primary surface groups, the assumption of adsorbing ions as point charges, inaccurate surface site densities and their distribution on the mineral face, incorrect surface species that were not consistent with molecular scale analysis, or the use of intrinsic constants that are dependent upon the electrostatic planes used especially in the 2-p*K* approach.

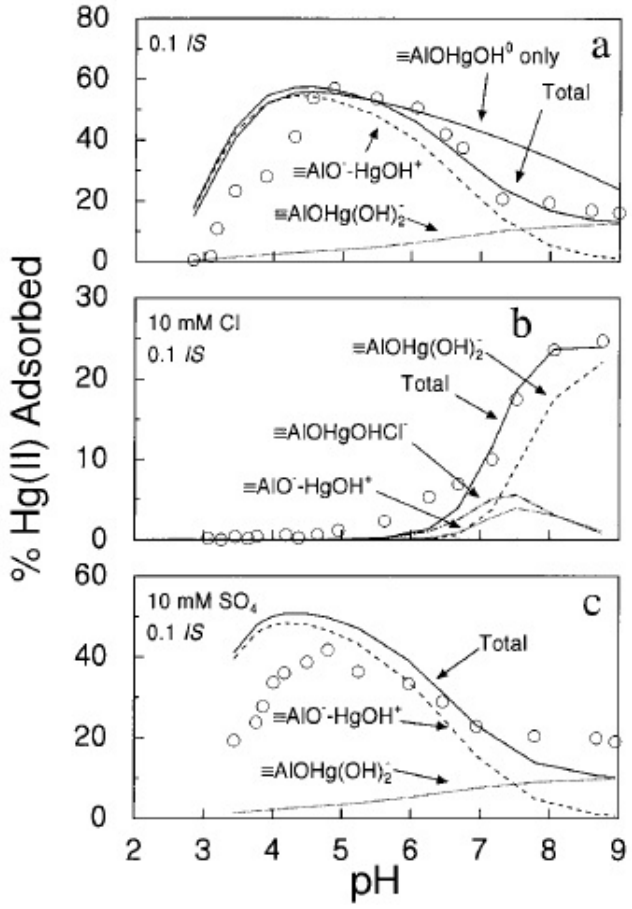

Figure 2. 13 Example of the 2-p*K* triple layer model of Hg(II) adsorption by gibbsite (3.3 g L^{-1}) as a function of solution chemistry: (a) 0.1 *M* $NaNO_3$; (b) 0.1 *M* $NaNO_3$ + 0.01 *M* NaCl; (c) 0.1 *M* $NaNO_3$ + 0.01 *M* Na_2SO_4. Adapted from Sarkar *et al.*, 1999.

Application of the CD-MUSIC model to Hg adsorption has been more successful. Various aqueous and surface chemical equilibria for the 1-p*K* CD-MUSIC model (e.g., Table 2.3) can be formulated into equilibrium adsorption computer codes such as ECOSAT (Keizer and Van Riemsdijk, 1991) or FITEQLC (an equilibrium adsorption computer code that combines a nonlinear least squares fitting routine with a chemical

model that describes aqueous speciation and adsorption) to yield the optimum fit to experimental adsorption data (Gustafsson, 2003).

Table 2. 3 Example chemical equilibria that consists of aqueous reactions, surface acidity, ion-pair formation and surface complexation reactions formulated in the 1-p*K* CD-MUSIC model.

Chemical Equilibria
Aqueous reactions
$Hg^{2+} + H_2O = HgOH^+ + H^+$
$Hg^{2+} + 2H_2O = Hg(OH)_2 + 2H^+$
$Hg^{2+} + 3H_2O = Hg(OH)_3^- + 3H^+$
Surface acidity
$\equiv FeOH^{1/2-} + H^+ = \equiv FeOH_2^{1/2}$
Ion-pair formation
$\equiv FeOH^{1/2-} + H^+ + NO_3^{2-} = \equiv FeOH_2NO_3^{1/2-}$
$\equiv FeOH^{1/2-} + Na^+ = \equiv FeOHNa^{1/2}$
Carbonate surface complexation
$\equiv FeOH^{1/2-} + CO_3^{2-} + H^+ = \equiv FeOCOO^{3/2-} + H_2O$
$\equiv FeOH^{1/2-} + CO_3^{2-} + 2H^+ = \equiv FeOCOOH^{1/2-} + H_2O$
$\equiv FeOH^{1/2-} + CO_3^{2-} + Na^+ + H^+ = \equiv FeOCOONa^{1/2-} + H_2O$

In the pre-processor of the existing framework of FITEQL 4.0 (Herbelin and Westall, 1999) in which a series of mass-action constraints can be included, a set of species are defined as the product of thermodynamic reactions with a set of components, and then an

iterative strategy is used for the solution to the chemical equilibrium problems using a Newton-Raphson method. The intrinsic equilibrium constants are calculated by the sequential optimization approach in FITEQLC (Westall and Hohl, 1980). These constants are regarded as non-adjustable parameters (once the model has been calibrated to proton adsorption and a limited set of metal ion adsorption data) to describe metal ions at the oxide-water interface over a range of pH, ionic strength, and competing metal ions and ligands.

2.5 Summary

Mercury exists in various forms including elemental, inorganic, and organic in the environment. Hg^0 is frequently present at the source of a spill and can interact with the soil media and the water to undergo oxidation, complexation with strong complexing ligands, precipitation, and/or sorption onto the soil matrix. All forms of mercury at even trace levels are extremely detrimental to humans and the environment. *In situ* thermal treatment that applies both heat and vacuum simultaneously meets the needs of a broad range of sites and contaminants including volatile metals in the soil matrix. Gas phase speciation of mercury at near source has implications with regard to the efficacy of treatment scenarios and Hg gas capture.

Taube *et al.* (2008) studied thermodynamic Hg speciation and phase transitions in various soil compositions during thermal treatment. However, vague model parameters limit the use of these results to design remediation processes or predict mercury speciation at given temperatures and soil conditions. Thus, mercury speciation over a

range of biogeochemical conditions and temperatures should be modeled to identify Hg distribution at elevated temperature, and the impact of soil compositions and Hg vapor pressures. Hg speciation must be examined at particular redox conditions to optimize removal strategies at near source environments.

Both mobility and toxicity of trace Hg remaining after remediation is largely controlled by sorption/desorption processes on geological substrates (e.g., soils, sediments or aquifer materials). However, it is complicated to predict the sorption/desorption behavior on particle surfaces because it is often dictated by the presence of inorganic/organic ligands and the mineralogy of the sorbent. Two dominant and reactive substrates in soil are iron and aluminum oxides. Surface complexation models that predict adsorption of Hg(II) onto these surfaces have shown promise, but more research is required to develop a model that predicts adsorption in multicomponent systems. Of the different models employed in the literature, the CD-MUSIC model appears to show the most promise for predicting adsorption in well-defined complex systems.

Chapter 3: Speciation of High Concentrations of Hg at High Temperature

3.1 Introduction

Mercury is highly mobile and among the most highly bioconcentrated metal contaminants in the environment (Kloke *et al.*, 1994; WHO, 1990). It can be found in various forms including elemental (metallic), inorganic, and organic in the environment. Elemental mercury (Hg^0) is sparingly soluble in water (5.6×10^{-5} g L^{-1} at 25 ºC), but its high vapor pressure allows long-range transport in the air (Carpi, 1997). Despite its usefulness in a broad range of industries, elemental mercury and its compounds are extremely detrimental to human health and to the environment at even trace levels. Once the elemental mercury is spilled on soil, it migrates downward to create a plume in the vadose zone with infiltration due to its high density. It can also be transported in water-soluble mercury forms such as monovalent and divalent mercury via chemical redox reactions. The divalent mercury (Hg(II)) is more stable than monovalent mercury (Hg(I)) and common in the environment, and may undergo complexation, precipitation with inorganic ligands, and sorption onto the soil matrix. Recently, the impact of mercury emitted from coal combustion sources or municipal solid waste (MSW) gasification systems on the atmosphere has been investigated with the speciation studies in many literature (Carpi, 1997; Galbreath and Zygarlicke, 1996; Lindberg and Stratton, 1998). However, knowledge of mercury speciation during thermal remediation of soil is not well

known, even though it is crucial to not only identify potential mercury species, but also understand the fate and transport of mercury.

In Situ Thermal Desorption (ISTD) is one of the soil remediation processes in which both heat and vacuum are simultaneously applied to the subsurface soil with high displacement efficiency (Stegemeier and Vinegar, 2001). In ISTD, surface heating with thermal blankets and subsurface heating with an array of vertical heater/vacuum wells placed to virtually any depth are used for contaminant removal in soil. Contaminants in soil are vaporized during the thermal remediation by several mechanisms. Large amounts of water vapor are also produced during the remediation process, so that vapor phase contaminants can be preferably removed by steam distillation in the vapor stream. The heating temperature is typically higher than the boiling point of water, so that the soil is easily desiccated to yield a matrix with a higher gas permeability as a result of drying and shrinking of the soil. The increased permeability provides uniform vapor flow patterns in clay or mixtures of silt and clay (TerraTerm, 2002). Several contaminated sites have been treated using ISTD by TerraTherm Environmental Services, Inc. (TESI), and the operations were successful with the residuals well below the remediation goals.

Thermodynamic mercury speciation and phase change of mercury were investigated by Taube *et al.* (2008) to evaluate the thermal treatment of mercury using FactSage 5.2, a computer software based on minimization of Gibb's free energy, for the equilibrium calculations (Bale *et al.* 2002). Equilibrium calculations for thermodynamically favorable reactions were performed in various soil conditions including different availability of O, S and Cl, in general terms of high or low initial

availability. In their modeling, two separate steps of mercury volatilization were observed, initial elemental vaporization and subsequent volatilization of oxide or sulfate phase at higher temperatures (>230°C). They showed that more than 95% of mercury in heavily contaminated soil (up to 2,400 ppm) can be possibly removed within minutes by thermal treatment at 300°C, and more than 99% of mercury removal can be achieved in 20 min at 470°C (Taube *et al.*, 2008). However, model development is required to identify model parameters in more detail, describe the mercury and all gas removal mechanisms, and thus determine removal strategies at mercury contaminated sites.

In this study, equilibrium calculations were conducted to identify dissolved mercury species and solids over a range of environmental conditions at ambient temperature and its phase changes at higher temperature for thermal remediation of mercury. The impact of soil compositions on mercury removal was also examined by vaporization mechanisms with temperature increase, since other substances in soil can also be vaporized and contribute mass to the recovered vapor stream.

3.2 Modeling Approach

Mercury equilibrium reactions and their enthalpy data were collected to investigate mercury speciation at elevated temperature. The model calculations were performed incorporating mono- and divalent mercury (Hg(I) and Hg(II)) in the environmental conditions that can be expected at contaminated sites. All possible aqueous equilibria were formulated in MINEQL+ 4.5, a chemical equilibrium model software, to calculate mercury speciation due to complex reactions participating in the

soil-solution environment. Among other available software for chemical speciation modeling, WHAM 6 and MINEQL+ 4.5 are the most cited in the literature. Cloutier-Hurteau *et al.* (2007) extensively evaluated the reliability of those modeling software with Cu(II). MINEQL+ 4.5 incorporates mass balance, thermodynamic reactions, and complexation reactions of inorganic ligands with an extensive thermodynamic database. The main reactions are presented in Table 3.1. In model calculations, an open system was used to describe the associated with ISTD in which 0.02 bar of vacuum is typically applied to the target treatment zone (Kunkel *et al.*, 2006).

Table 3. 1 Aqueous mercury complexes and solid form of mercury with formation constants used in the speciation modeling (MINEQL+ 4.5 database, Schecher (2001)).

no.	Complexation reaction	log K_1	ΔH_1^0 (kcal mol^{-1})
1	$0.5Hg_2^{2+} + e^- = Hg_{(aq)}$	6.567	-10.931
2	$2Hg(OH)_2 + 2e^- + 4H^+ = Hg_2^{2+} + 4H_2O$	43.185	-15.198
3	$0.5Hg_2^{2+} + e^- = Hg_{(g)}$	7.873	-5.27
4	$Hg(OH)_2 + 2H^+ = Hg^{2+} + 2H_2O$	6.194	-10.875
5	$Hg(OH)_2 + H^+ = HgOH^+ + H_2O$	2.797	-4.515
6	$Hg(OH)_2 + H_2O = Hg(OH)_3^- + H^+$	-14.897	9.051
7	$0.50Hg_2^{2+} + Cl^- = (Hg_2)_{0.5}Cl$	-19.497	38.74
8	$Hg(OH)_2 + H^+ + Cl^- = HgClOH_{(aq)} + H_2O$	10.444	-10.210
9	$Hg(OH)_2 + 2H^+ + Cl^- = HgCl^+ + 2H_2O$	13.494	-14.991
10	$Hg(OH)_2 + 2H^+ + 2Cl^- = HgCl_{2(aq)} + 2H_2O$	20.194	-22.089
11	$Hg(OH)_2 + 2H^+ + 3Cl^- = HgCl_3^- + 2H_2O$	21.194	-22.512
12	$Hg(OH)_2 + 2H^+ + 4Cl^- = HgCl_4^{2-} + 2H_2O$	21.794	-24.073
13	$Hg_2^{2+} + SO_4^{2-} = Hg_2SO_4$	6.13	-1.29
	Mercury solid formation	**log K_s**	**ΔH_s^0 (kcal mol^{-1})**
14	$Hg^{2+} + 2e^- = Hg_{(l)}$	28.851	-16.666
15	$Hg^{2+} + H_2O = HgO_{(s)} + 2H^+$	-2.554	20.172
16	$Hg^{2+} + SO_4^{2-} = HgSO_{4(s)}$	3.225	7.365
17	$Hg^{2+} + 2Cl^- = HgCl_{2(s)}$	15.068	-14.895
18	$Hg^{2+} + HS^- = HgS_{(s)} + H^+$	39.500	-49.775

3.3 Results and Discussion

3.3.1 Mercury Speciation at Ambient Temperature

In natural waters, concentration range of inorganic ligands varies for $Cl(-I)_T$ from 10^{-5} to 10^{-3}, $HS^{-1}/S(-II)_T$ (anoxic conditions) from 10^{-6} to 10^{-3}, and SO_4^{2-} from 10^{-5} to 10^{-3}

(Stumm and Morgan, 1996). Based on soil compositions in natural aqueous settings, the three model concentrations for inorganic soil ligands of Cl, HS^-, and SO_4^{2-} as well as redox potential have been determined in the simulation of mercury distribution and phase changes that can be occurred during the thermal processes. Each model condition, low $Cl(-I)_T$ and $S(-II)_T$, high $Cl(-I)_T$ and low $S(-II)_T$, and low $Cl(-I)_T$ and high $S(-II)_T$ concentrations were used to determine distribution of aqueous mercury species and solid formation of mercury for an electron activity set at pe = 0.

MINEQL+ 4.5 provided predictions of the predominant and trace mercury species as a function of pH in different soil conditions. The dissolved mercury species for concentrations greater than 10^{-24} M are shown in Figure 3.1. For low Cl and low reduced S (HS^-) or low Cl and high reduced S concentrations, the aqueous Hg^0 species was predominant over a range of pH considered, while the aqueous $Hg(OH)_3^-$ species increased in importance with higher pH in Figure 3.1a and 3.1c. For a system of high Cl and low reduced S concentrations, $HgCl_2$, $HgCl_3^-$, and $HgCl_4^{2-}$ were dominant as shown in Figure 3.1b. The pure phase forms of mercury, $Hg_{(l)}$ and $HgS_{(s)}$ at reducing conditions, and $HgCl_{2(s)}$, ,$HgSO_{4(s)}$, and $HgO_{(s)}$ at oxidizing soil conditions were predicted to form at ambient temperature in closed systems (pe = 0) by the reactions in Table 3.1.

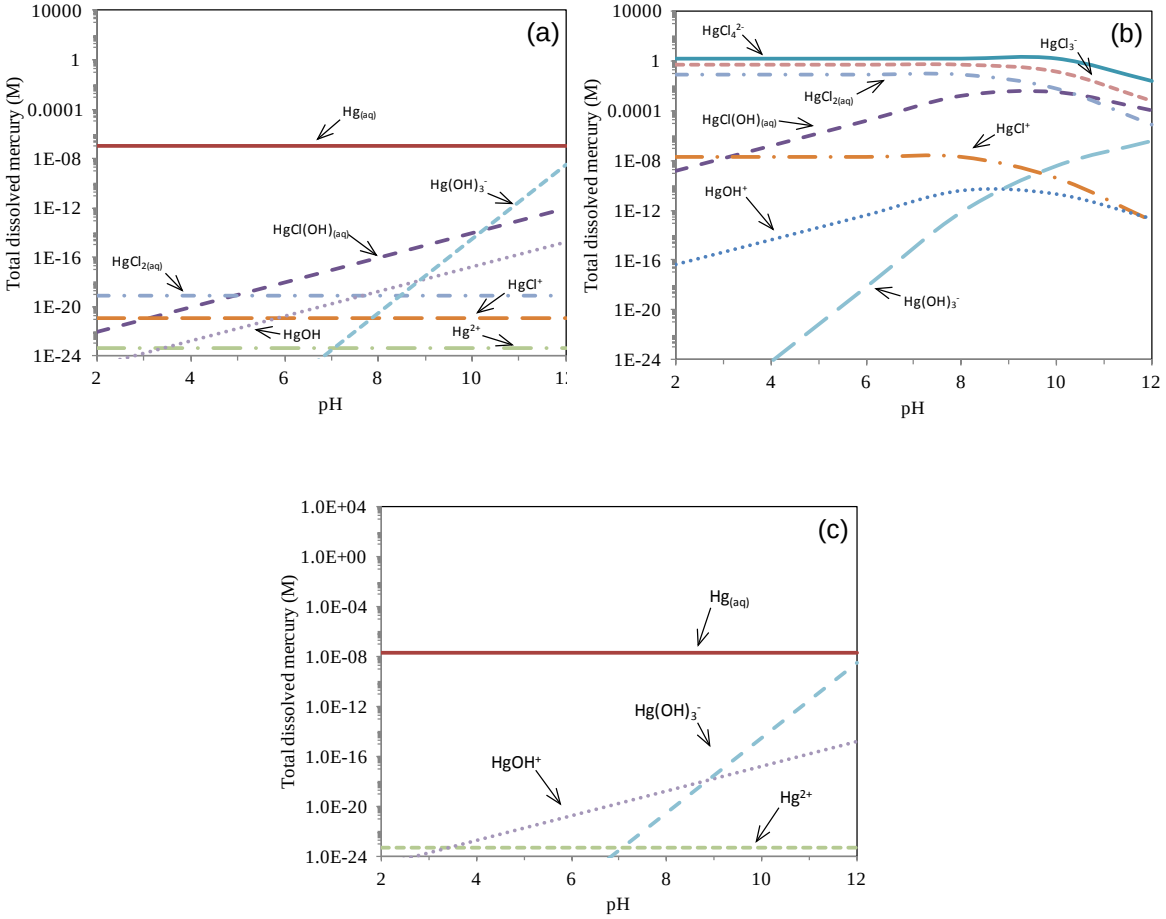

Figure 3. 1 Distribution of aqueous mercury species as a function of pH, (a) $[Hg^{2+}]$ = 2.4 M, $[Hg_2^{2+}]$ = 9e-7 M, $[Cl^-]$ = 0.1 M, $[HS^-]$ = 1e-33 M, and $[SO_4^{2-}]$ = 1e-18 M, (b) $[Hg^{2+}]$ = 2.4 M, $[Hg_2^{2+}]$ = 1e-8 M, $[Cl^-]$ = 8.9 M, $[HS^-]$ = 1e-33 M, and $[SO_4^{2-}]$ = 1e-18 M, and (c) $[Hg^{2+}]$ = 2.4 M, $[Hg_2^{2+}]$ = 1e-8 M, $[Cl^-]$ = 1e-18 M, $[HS^-]$ = 1e-3 M, and $[SO_4^{2-}]$ = 1e-18 M at 20 °C and pe = 0. The model lines were calculated using MINEQL+ 4.5 (Schecher and McAvoy, 2003).

3.3.2 Mercury Speciation at Higher Temperature

Elemental mercury can be formed by reaction no. 18 in Table 3.1 at ambient temperature, when low concentrations of Cl and S ($[Cl^-] < 10^{-1}$ M, $[HS^-] < 10^{-33}$ M, $[SO_4^{2-}] < 10^{-18}$ M as described in Table 3.3) are present in soil at suboxic conditions (pe < 4.4).

Taube *et al.* (2008) modeled formation of Hg^0 ($Hg_{(l)}$) and $HgS_{(s)}$ at 20°C according to the availability of Cl and S for a low oxygen system, and these phases are expected to release mercury to the gas phase at 90°C and 140°C, respectively. During thermal remediation, elemental mercury formed from oxidized mercury or Hg^0 spill in soil can be vaporized as elemental mercury gas by reaction no. 1 in Table 3.2 at elevated temperature (Cox *et al.*, 1989; Stumm and Morgan, 1996). Speciation of Hg^0 with complexation reactions and their thermodynamic constants defined in Table 3.1 was simulated using MINEQL+ 4.5 in an open carbon dioxide system. Model simulation of the phase change of Hg^0 as a function of temperature was as shown in Figure 3.2a. Elemental liquid mercury was slowly transformed to Hg^0 gas until the temperature reached around 358.15 K, a temperature below the boiling point of water.

Table 3. 2 Thermodynamic phase transition reactions and decomposition of mercury solid and carbonate components in soil.

no.	Phase transition of mercury	log *K*	ΔH^0 (kcal mol^{-1})
1	$Hg_{(l)}$ = **$Hg_{(g)}$**	-5.585	14.670
2	$HgCl_{2(s)}$ = **$HgCl_{2(g)}$**	-6.835	20.036
3	$HgS_{(s)}$ = **$Hg_{(g)}$**	-13.636	27.570
	Decomposition of mercury solid		
4	$2HgO_{(s)} = 2$**$Hg_{(g)}$** $+ O_2$	-31.664	72.738
5	$HgO_{(s)}$ = **$HgO_{(g)}$**	-14.414	31.699
6	$2HgO_{(g)} = 2$**$Hg_{(g)}$** $+ O_2$	-2.836	9.340
7	$HgSO_{4(s)}$ = **$Hg_{(g)}$** $+ SO_{2(g)} + O_2$	-57.126	112.833
8	$2HgSO_{4(s)} = 2$**$HgO_{(g)}$** $+ 2SO_{2(g)} + O_2$	-111.413	216.326
	Decomposition of carbonate components		
9	$H_2CO_3 = H_2O +$ **CO_2**		
10	$Ag_2CO_{3(s)} = Ag_2O +$ **CO_2**	-5.480	19.492
11	$CdCO_{3(s)} = CdO +$ **CO_2**	-8.220	23.750
12	$CaCO_{3(s)} = CaO +$ **CO_2**	-5.490	42.622

In the model simulation of HgS, mercury sulfide precipitated at ambient temperature by reaction no. 22 in Table 3.1, when low Cl but high reduced sulfur concentrations ($[Cl^-] < 10^{-18}$ M, $[HS^-] = 10^{-3}$ M, and $[SO_4^{2-}] < 10^{-18}$ M in Table 3.3) exist in soil, typical of that for waterlogged conditions (pe = -5). The temperature history during the thermal process consists of heat-up, boiling water, and superheating (Stegemeier and Vinegar, 2001). All the pore water is evaporated during the heat-up stage and at the boiling point of water, but mercury sulfide remained as a solid form until the dry soil began to be superheated. It can be decomposed to Hg^0 and vaporized at

363.15 K. The complete phase change to Hg^0 gas was observed when the temperature reached around 410.15 K, as in Figure 3.2b.

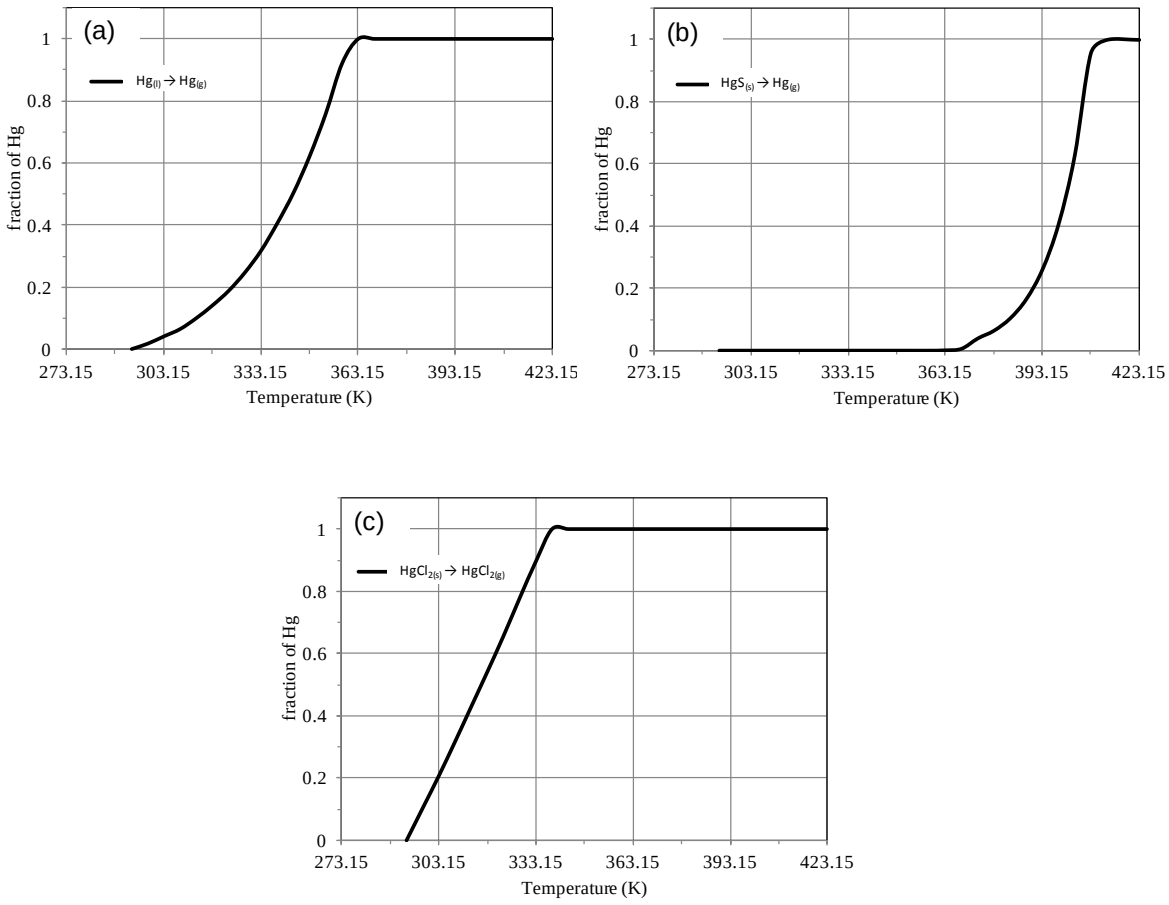

Figure 3. 2 Model simulation of phase transition of mercury, (a) Hg^0 (liquid), (b) HgS (solid), and (c) $HgCl_2$ (solid) as temperature increases.

Mercury chloride exists in the solid form at ambient temperature with a boiling point of 577.15 K and melting point of 550.15 K (Ho *et al.*, 1998). The model results showed that formation of mercury chloride solid (reaction no. 21 in Table 3.1) at 20°C was predicted in soil rich in Cl ($[Cl^-]$ = 8.9 M, $[HS^-] = 10^{-33}$ M, and $[SO_4^{2-}] < 10^{-18}$ M in

Table 3) at oxic conditions (pe > 15) where drainage is excellent in soil. The open system phase transition to $HgCl_2$ gas was simulated in Figure 3.2c according to reaction no. 2 in Table 3.2 without decomposition of mercury. Mercury chloride was stripped off at temperatures below the point of Hg^0 vaporization. The complete transition of $HgCl_{2(s)}$ occurred at temperature 335.15 K, which is consistent with the model results from Taube *et al.* (2008) that $HgCl_2$ gas was expected to release at around 363.15 K for a system of high oxygen availability.

Table 3. 3 Soil conditions used in model calculations for phase transition of mercury solid.

Model species	**Soil composition**					
	Mercury (M)		**Inorganic ligands (M)**			**Redox condition**
	Hg^{2+}	**Hg_2^{2+}**	**Cl^-**	**S as HS^-**	**S as SO_4^{2-}**	**pe**
$Hg_{(l)}$	2.4	9.0e-7	< 1.0e-1	< 1.0e-33	< 1.0e-18	< 4.4
$HgS_{(s)}$	2.4	1.0e-8	< 1.0e-18	1.0e-3	< 1.0e-18	-5
$HgCl_{2(s)}$	2.4	1.0e-8	8.9	< 1.0e-33	< 1.0e-18	> 15

3.3.3 Impact of Soil Components on Mercury Removal

In Situ Thermal Desorption (ISTD) processes should be designed with an understanding of several mechanisms including vaporization and chemical reactions that occur in the soil during application of heat. Mercury and soil compositions will vaporize by boiling or steam distillation in vapor streams under moderate heating. The fractions of individual gaseous components that are miscible can be described by Raoult's Law,

which states that the partial pressure of an ideal solution is dependent on the vapor pressure of each chemical component and its mole fraction in the liquid phase:

$$p_t = x_1 p_1^{\circ} + x_2 p_2^{\circ} \ldots x_n p_n^{\circ}$$

Each component present in soil vaporizes independently as single-component vapor pressure, which is only a function of the temperature. The vaporization mechanism of thermal treatment is highly influenced by the vapor pressure of the soil substances which normally increases with temperature. Therefore, vapor pressures of soil substances including inorganic mercury salts were quantified as a function of temperature at local redox conditions to better understand thermal remediation processes as summarized in Figure 3.3. Examination of Figure 3.3. shows clear differences in the temperatures at which particular gas phases form for different solid phases. For example, the vapor pressure of Hg(g) is higher at a given temperature if HgO(s) is present rather than $HgSO_4$(s). This implies that a higher temperature would be required if oxidizing conditions prevail and sulfate present in the soil matrix leads to the formation of $HgSO_4$(s).

Decomposition of carbon components in soil was taken into account for the displacement of gas phase mercury, where the solid carbonate decomposes to the solid oxide and carbon dioxide gas and organic matter releases carbon dioxide and further partially decomposes to $CO_{(g)}$ and $1/2O_{2(g)}$ during thermal treatment (CHERIC; Stern, 2001). This gas production can facilitate the transport of mercury gas to the vacuum

treatment system at elevated temperature. It was assumed that an average total carbonate concentration of 1-2 mM including organic carbon content (which is approximately 58% of organic matter present typically at 1 to 10 % of mineral soils) was present in the soil matrix. Partial pressure of total carbonate varies from 0.39 matm (atmospheric) to 10-50 matm due to plant respiration and microbial decomposition of natural organic matter in various aqueous settings (Bolt and Bruggenwert, 1978; Buyanovsky and Wagner, 1983; Sposito, 1989), within 0.1-0.2 atm in certain groundwater systems (Hem, 1970; Bulter, 1982, Langmuir, 1997), or between 0.002 and 130 atm in confined aquifers of sedimentary basins and 10^{-6} to 50 atm in geothermal fields with magmatic rocks at higher temperature (Coudrain-Ribstein *et al.*, 1998). Inorganic carbonate minerals are also predominantly present as sparingly soluble alkaline-earth carbonates on soils (Loeppert and Suarez, 1996). They decompose to the oxide or a basic carbonate (e.g., $PbO{\cdot}PbCO_3$) with evolution of carbon dioxide. The thermal stability of group 2 alkaline earth metal compounds tends to be higher than transition metal or d-block group compounds because of the smaller cationic charge and lower polarizing power. The decomposition order for these compounds with increasing temperature is $BaCO_2 > SrCO_3 > CaCO_3 > MgCO_3 > ZnCO_3 > CdCO_3 > Ag_2CO_3$ (L'vov, 2002). Calcite forms dominantly with concentration ranging from traces to greater than 80 % in active pedogenic environments. However, the initial temperature of decomposition (T_{in}) of calcite was reported to be 895 K (theoretical) and 934 K (experimental) in vacuum (Darroudl and Searcy, 1981; L'vov, 2002). Kaolinite is a clay mineral that can undergo the endothermic dehydration beginning at 550-600°C to form disordered metakaolin, $Al_2Si_2O_7$, as well as a series of further phase

transformations during the thermal processes (Bellotto *et al.*, 1995). In this study, only two inorganic carbonate minerals, $Ag_2CO_{3(s)}$ and $CdCO_{3(s)}$, which can decompose by reactions no. 10 and 11 in Table 3.2 at 371 and 442 °C, respectively, were included in the modeling summarized in Figure 3.3, since 99% of mercury can be removed at temperature below 500°C (Stern, 2001).

Table 3. 4 Thermodynamic equilibrium constants and Gibbs free energy of the reaction, $2HgO_{(g)} \rightarrow 2Hg_{(g)} + O_{2(g)}$ (Chase, 1998).

Temp (K)	**$2HgO_{(g)} \rightarrow 2Hg_{(g)} + O_{2(g)}$**	
	Log *K*	**G_f^0 (kcal mol^{-1})**
293.15	-2.953	4.026
298.15	-2.836	3.866
323.15	-2.304	3.141
348.15	-1.849	2.521
353.15	-1.766	2.407
358.15	-1.685	2.297
363.15	-1.606	2.189
368.15	-1.530	2.085
373.15	-1.455	1.983
398.15	-1.110	1.513
423.15	-0.806	1.099
448.15	-0.536	0.731
473.15	-0.295	0.402
498.15	-0.077	0.105
523.15	0.119	-0.162
548.15	0.298	-0.406
573.15	0.461	-0.628
598.15	0.610	-0.832
623.15	0.748	-1.019
648.15	0.874	-1.192
673.15	0.992	-1.352
698.15	1.101	-1.501
723.15	1.202	-1.639
748.15	1.297	-1.768

The gas pressures produced by the evaporation or decomposition of large masses of soil pore-water, natural organic materials, and inorganic carbonate minerals were high enough to displace gas phase mercury out of the soil at each redox condition. This can be seen in Figure 3.3 by examining the high vapor pressure associated with cadmium and silver carbonates, carbon dioxide and water relative to the Hg(II) species. Decomposition of mercury oxide formed under oxidizing conditions was expected to vaporize as Hg^0 or HgO gas to a minor extent at around 140°C and maximum extent at 230°C, and mercury sulfate decomposes to Hg^0 or HgO gas at around 270°C by thermodynamic reactions 4-8 presented in Table 3.2 (Chase, 1998; Cox *et al.*, 1989; NIST; Stumm and Morgan, 1996; Taube *et al.*, 2008; Wagman *et al.*, 1969). The decomposed mercury oxide gas can further decompose to Hg^0 gas and oxygen by spontaneous reaction at the temperature around 520.15 K as shown in Table 3.4. However, the vapor pressures of decomposed Hg^0 and HgO gas were relatively low compared to those of other substances, so that mercury gas can be easily removed with assistance from soil components with higher gas production during thermal remediation.

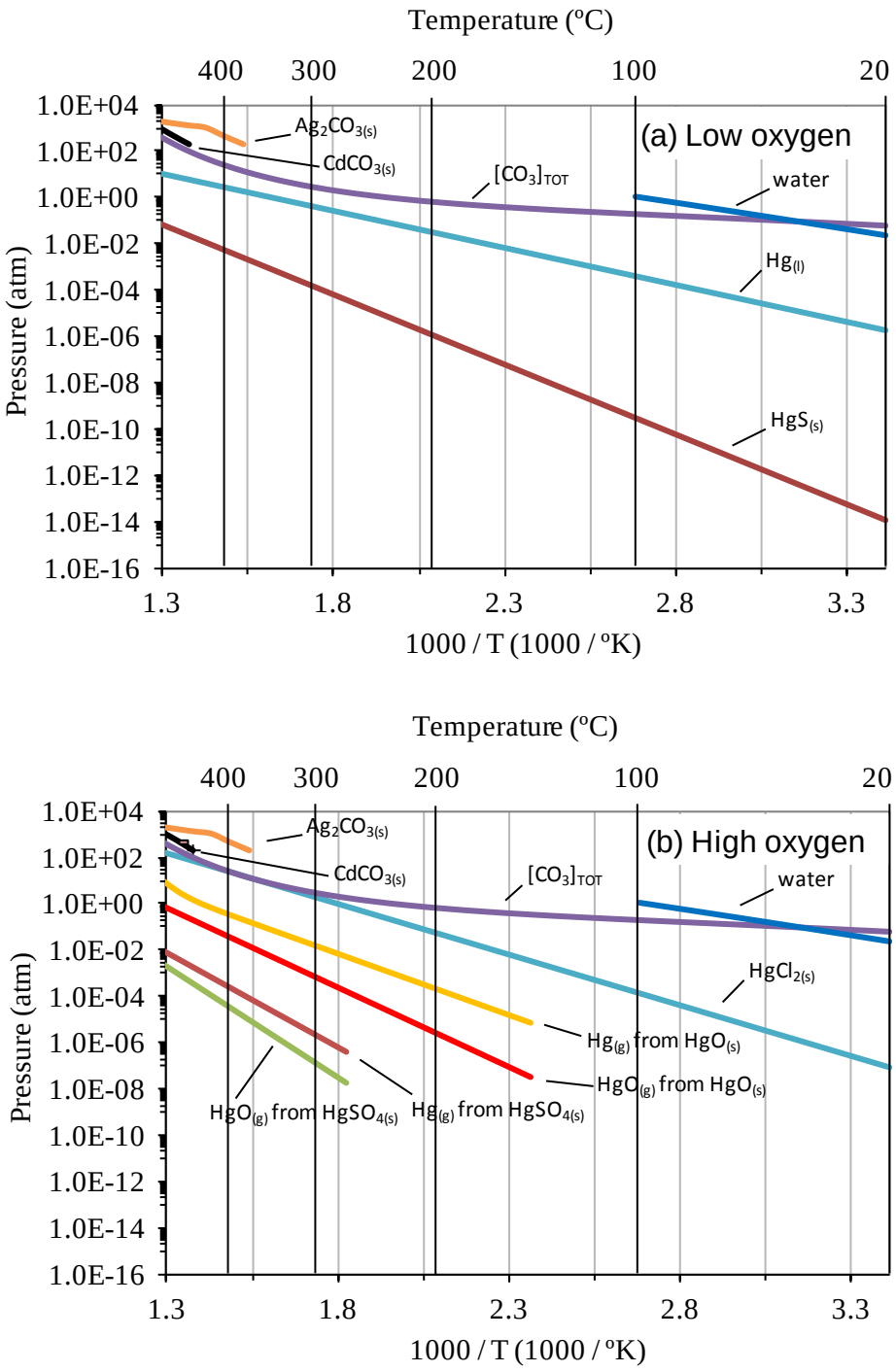

Figure 3. 3 Vaporization of mercury solid and soil components including soil pore water and carbonate at (a) reducing and (b) oxidizing conditions.

3.4 Summary

In this chapter, equilibrium calculations were conducted to identify mercury speciation and the impact of soil composition on Hg removal over a range of environmental conditions and temperatures for thermal remediation of mercury. Mercury equilibrium reactions and their enthalpy data were collected to study mercury speciation at elevated temperature. The distribution of mercury and the phase transitions of Hg were simulated in an open carbon dioxide system using MINEQL+ 4.5 due to complex reactions participating in the soil-solution.

Elemental mercury can form at ambient temperature when low concentrations of Cl and S exist in soil at suboxic conditions (pe < 4.4). It was slowly transformed to Hg^0 gas until the temperature reached around 358.15 K. The model simulation of HgS was performed for conditions of low Cl but high reduced sulfur concentrations. Mercury sulfide remained as a solid until the dry soil began to be superheated. The complete phase change to Hg^0 gas was observed at 410.15 K. The complete transition of $HgCl_{2(s)}$ without decomposition occurred at temperature 335.15 K which is below the point of Hg^0 vaporization.

Vapor pressures of mercury and soil substances were compared as a function of temperature to evaluate thermal processes in which the vaporization mechanism is highly influenced by those pressures. It was found that the mercury gas can be easily removed due to higher gas pressures produced by the evaporation or decomposition of soil pore-water, NOM, and inorganic carbonate that can displace Hg gas in soil.

Chapter 4: Mercury(II) Adsorption on Goethite (α-FeOOH)

4.1 Introduction

Adsorption of ions to mineral phases in solution is of great importance in the regulation of many trace metals in the environment. Unlike other trace metals such as Cd, Zn, and Cu, Hg(II) has unique physico-chemical properties especially with respect to its redox speciation and ability to form stronger complexes with carbonate and chloride. Mercury contamination has occurred extensively from a broad range of industries from historical uses for paper industry, cosmetic, and pharmaceutics to modern uses for chlor-alkali plants (45 percent of all domestic mercury emissions), writing devices and switches, lighting, and dental work (U.S. EPA, 2006). The fate of Hg (II) in the environment is often controlled by its adsorption behavior on fixed or mobile adsorbents (Schindler, 1967). Among the most common inorganic adsorbents including hydroxides, oxyhydroxides, and clay minerals; metal (hydr)oxides have the highest affinity for inorganic ions in solution due to their high specific surface area, charge, and reactive sites (Sarkar, 1999). While the adsorption behavior of Hg (II) on metal (hydr)oxides has not been extensively studied, it is understood that incorporation of both aqueous complexation and the potential for ternary complex formation can impact the extent of adsorption to mineral surfaces (Bargar *et al.*, 1997; Barrow and Cox, 1992; Bonnissel-Gissinger *et al.*, 1999; Davis and Leckie, 1978; Gunneriusson and Sjöberg, 1993).

Numerous experimental and modeling studies for metal ion adsorption have been performed and the data obtained have been fit to a variety of adsorption isotherm or surface complexation models (SCMs) (Barrow and Cox, 1992; Bonnissel-Gissinger *et al.*,

1999; Gunneriusson and Sjoberg, 1993; Kinniburgh and Jackson, 1978; Lockwood and Chen, 1974; MacNaughton and James, 1974; Sarkar and Misra, 2000; Sarkar *et al.*, 1999; Tiffreau *et al.,* 1995; Viraraghavan and Kapoor, 1994; Weerasooriya *et al.,* 2000, 2001, 2003, 2007; Yin *et al.,* 1996). Surface complexation models that allow formation of inner-/outersphere complexes between surface hydroxyl functional groups and the adsorbing free metal cations offer the greatest potential for describing Hg(II) adsorption because they have the potential to account for impacts of pH, ionic strength and ternary complex formation. There are a number of different surface complexation models that differ in their description of the interfacial region both with respect to the description of the relationship between surface charge and potential, and the location of sorbing species. The Non-Electrostatic Model (NEM) and the Diffuse Layer Model (DLM) offer simplistic descriptions of the double layer region that require minimal parameter estimation but only allow formation of inner-sphere complexes (Hayes *et al.,* 1991; Rojo *et al.,* 2009). Both the Triple Layer Model (TLM) and the Charge Distribution Multi-Site Complexation (CD-MUSIC) models provide a more complete description of the interfacial region and means to incorporate inner- and outer- sphere complexation and ligand exchange (Sverjensky and Fukushi, 2006) that is consistent with spectroscopic measurements. The CD-MUSIC model can be differentiated from the TLM by three major characteristics; representation of surface acidity, placement of ions and charge in electrostatic planes, and representation of reactive surface adsorptions sites (Hiemstra *et al.,* 1996; Lützenkirchen, 1998; Venema *et al.,* 1996, 1997). Both models have potential

for describing Hg(II) adsorption in complex systems that include complexing ligands such as chloride.

The majority of macroscopic Hg(II) adsorption studies were conducted by uptake measurements on numerous natural or synthetic substrates as a function of pH (Barrow and Cox, 1992; Bonnissel-Gissinger *et al.*, 1999; Forbes *et al.*, 1974; Farrah and Pickering, 1978; Jean and Bancroft, 1986; Kinniburgh and Jackson, 1978; MacNaughton and James, 1974; Newton *et al.*, 1976; Tiffreau, *et al.*, 1995). MacNaughton and James (1974) investigated the adsorption of Hg (II) on SiO_2 and showed a sharp increase in the extent of adsorption in the range of pH 3 to 4 with a maxima at pH 4. When chloride ions were present in solution, Hg(II) removal was still attributed to $Hg(OH)_2$ adsorption. Lockwood and Chen (1974) investigated Hg (II) adsorption on $Fe(OH)_3$ and also showed a sharp increase in adsorption in the range of pH 3 to 4 and chloride inhibition of Hg (II) adsorption at neutral pH. They also concluded that the hydrolysis products $HgOH^+$ and $Hg(OH)_2$ were the major species controlling Hg (II) adsorption. Several previous investigators have applied surface complexation/precipitation modeling to describe this adsorption behavior for Hg (II) onto silica and iron oxides as a function of pH and chloride concentrations. Tiffreau *et al.* (1995) employed the Diffuse Layer Model (DLM) to describe adsorption onto α-SiO_2 (quartz) and HFO (amorphous hydrous ferric oxide). While the DLM incorporated ternary surface complexes such as ≡S—OHgOH and ≡S—OHgCl and required fewer parameters to describe adsorption compared to the TLM or CD-MUSIC, the DLM overpredicted Hg(II) data in a number of their simulations of data from MacNaughton (1973) and Kinniburgh and Jackson (1978). All of these

modeling efforts were conducted in the absence of spectroscopic data to guide the selection of surface complexes.

In this study, a model describing Hg(II) adsorption and aqueous speciation has been developed over a range of experimental conditions to provide a tool for predicting the fate and transport of mercury down gradient of a spill or after residual Hg(II) remains at a remediated site. The competitive Hg(II) adsorption on ubiquitous soil minerals such as goethite has been evaluated over a range of experimental conditions. Previous research has shown that classic 2-p*K*, CCM and TLM modeling efforts did not predict Hg(II) adsorption adequately or did not employ surface species that are consistent with molecular scale analyses. These studies also did not incorporate the presence of carbonate even when it was apparent that carbonate was present in their experimental system (Barrow and Cox, 1992; Bonnissel-Gissinger *et al.*, 1999). Thus, the development of a more accurate surface complexation model that incorporates carbonate adsorption and utilizes spectroscopic data to guide the selection of surface species for Hg(II) adsorption onto goethite was the main goal of this research.

4.2 Materials and Methods

Several sets of adsorption data were obtained from the literature for this modeling study. Data for carbonate adsorption onto goethite in an open system at atmospheric CO_2 values were obtained from the literature (Villalobos and Leckie, 2000 and 2001) to account for the undesired carbonate contamination present in most of the published data for Hg(II) adsorption onto goethite. The reported specific surface area of this material

was 70 (±2) m^2/g determined by N_2 BET (Brunauer, Emmett and Teller) adsorption on the dry (105ºC) material. The influence of pH, mercury, and chloride concentration on Hg(II) adsorption on goethite was evaluated using data from Barrow and Cox (1992). In their research, equilibrium studies were conducted over a range of conditions: nitric acid or sodium hydroxide was used to vary pH; mercury(II) nitrate was used as the mercury source; and sodium nitrate was employed to maintain constant ionic strength. The mass of goethite was 4.01 g/L and the specific surface area was determined to be 76 m^2/g using ethylene glycol monoethyl ether. The experimental description did not indicate that carbonate was eliminated from the system.

Bonnissel-Gissinger *et al.* (1999) investigated the effect of the nature and/or the structure of the oxide on mercury sorption experimentally. Their research investigated adsorption onto a commercial goethite (Bayferrox 910, standard 86) from Bayer. The specific surface area of the goethite was obtained by N_2 BET. The pH_{pzc} of 7.85 and the surface site density of 5.5 OH nm^{-2} were determined and confirmed by potentiometric titrations (Muller and Sigg, 1992). The goethite was washed with degassed Milli-Q water and dried to minimize carbonate species formation prior to the sorption experiments. The sorption experiments were conducted in 40 mL Teflon FEP centrifuging tubes (Nalgene) to avoid mercury loss onto the tube walls. Sodium nitrate was used as the background electrolyte and the solid concentration was 10 g L^{-1} in all of the experiments. The pH of the solution was adjusted using nitric acid and decarbonated sodium hydroxide. The Hg(II) concentration of 12.4 µM was prepared from a $Hg(NO_3)_2$ standard solution. After 24 hours of equilibration, the concentration of supernatant was analyzed following

28,000 *g* centrifugation. The physico-chemical parameters and suspension properties are listed in Table 4.1.

4.3 Modeling Approach

The **c**harge distribution multi-site complexation (CD-MUSIC) developed by Hiemstra *et al.*, (1996) and Venema *et al.*, (1996) describes surface acidity using a 1-p*K* assumption following a scheme that includes two consecutive reactions

$$\equiv Me_nO^{-2+nv} + H^+ \rightarrow \equiv Me_nOH^{-1+nv} + H^+ \rightarrow \equiv Me_nOH_2^{nv}$$

where *n* and *v* are Pauling's bond valence and valence number. The Boltzmann factors related to the electrostatic energy change of the species are used for electrostatic 0-, 1-, and 2-planes. For those specifically adsorbed ions (SAIs, innersphere by ligand exchange), the change of charge (Δz) on the 0- and 1-planes can be obtained as

$$\Delta z_0 = \Delta n_H z_H + f z_{Me}$$

and

$$\Delta z_1 = (1 - f) z_{Me} + \sum m_j z_j$$

where Δn_H is the net change in protons on the 0-plane, z_{H} is the charge of the proton, f is is the charge distribution (CD) factor, z_{Me} is the charge of the central metal ions in the adsorbed species, m_{j} is the number of ligands adsorbed in the 1-plane, and z_{j} is the charge of adsorbed ligands m_{j} in the 1-plane. A certain fraction f of the central metal ions represents the charge neutralization of ligands placed in the 0-plane if symmetrically distributed. The remaining portion (1 - f) is attributed to ligands in the 1-plane. It is also possible that non symmetrical charge neutralization occurs in the 0-plane due to a shift in electron density in the adsorbed species. A larger neutralization (i.e. higher f value) on the solution side may take place in the process of adsorption, since former surface ligands can be buried and incorporated into the bulk solid, and vice versa (Hiemstra and Van Riemsdijk, 1996).

The apparent equilibrium constant of a reaction can be simplified with an intrinsic term and an electrostatic contribution which represents the Boltzmann factor that describes the effect of surface potential on ion adsorption at equilibrium. The intrinsic equilibrium constant can be written from the mass action equations taking into account a numerical scaling factor based on mole fraction standard states for adsorbed species.

$$K_{app} = K_{int} \exp^{-\frac{\Delta z_i F \Psi_i}{RT}}$$

$$K_{int} = \frac{\theta_{\mathrm{ads}}}{\theta_{\mathrm{ref}}^{\mathrm{m}} \Pi C_{\mathrm{sol}}^{n}} = \frac{\frac{S_{\mathrm{ads}}}{\rho A N_{\mathrm{S.j}}}}{\left(\frac{S_{\mathrm{ads}}}{\rho A N_{\mathrm{S.j}}}\right)^{\mathrm{m}} \Pi C_{\mathrm{sol}}^{n}}$$

where θ_{ads} is the mole fraction of an adsorbed species, θ_{ref} is the mole fraction of the reference surface component, m is the stoichiometric coefficient for the reference site component (e.g., 1 for monodentate and 2 for bidentate), C_{sol} is the concentration of solution components with stoichiometric coeffeicients *n*, S_{ads} is the adsorbed complex species concentration (mol L^{-1}), S_{ref} is the reference surface component concentration (mol L^{-1}), ρ is the solid-solution ratio (kg L^{-1}), *A* is the specific surface area (m^2 kg^{-1}), and $N_{s,j}$ is the site density (mol m^{-2}) of the reference surface component *j* (Hiemstra and Van Riemsdijk, 1996).

The change in the Gibbs free energy of adsorption on charged surfaces can be divided into a standard Gibbs free energy ΔG_r^o which can be connected to the intrinsic and electrostatic Gibbs free energy and a composition dependent Gibbs free energy change. The latter term can be expressed as *RT* ln *Q*, in which *Q* is the reaction quotient that is analogous to the reaction quotient for aqueous reactions.

$$\Delta G_{adsorption} = \Delta G_{intrinsic} + \Delta G_{electrostatic} + RT \ln Q$$

where

$$\Delta G_{intrinsic} = -RT \ln K_{int}^{s}$$

and

$$\Delta G_{elec} = \sum \Delta z_i F \Psi_i$$

in which Δz_i is the net change of charge on the surface, Ψ_i is the surface potential at position *i*, and *F* is the Faraday's constant. The intrinsic component reflects the energy change due to adsorption to surface functional groups, while the electrostatic energy term (determined by the electrostatic potential) represents the energy required to move ions from bulk solution to the surface (Tadanier and Eick, 2002).

Literature data from molecular scale analyses that provide an important basis for more precise adsorptive mechanisms/processes of metal ions adsorption and definition of the mode of adsorption were reviewed to select the predominant adsorptive surface species for Hg(II), Hg-Cl ternary complexes, carbonate and Hg-CO_3 ternary complexes. Extended X-ray absorption fine structure (EXAFS) spectroscopy fittings combined with the molecular modeling programs (e.g., Cerius^2 from Accelrys, Inc. and PC Spartan Pro from Wavefunction, Inc.) provides a nondestructive *in situ* analytical methods uniquely suited to determine the identity, number of nearest neighbors, interatomic distances, and degree of structural order. In addition, Kim *et al.*, (2004a) used bond valence analysis that allowed assessment of the stability of different potential sorption complexes at the surface by placing basic bonding constraints on various modes of sorption.

The adsorption behavior of Hg (II) on goethite was formulated for the CD-MUSIC model to depict the underlying physicochemical processes in the equilibrium adsorption computer code FITEQLC (Gustafsson, 2003). The surface and aqueous

complexation reactions were formulated in the pre-processor of the existing framework of FITEQL 4.0 (Herbelin and Westall, 1999). FITEQL4.BAS and FQMOD1.BAS modules in FITEQL 4.0 were modified in order to incorporate CD-MUSIC into the TLM routine in FITEQLC. The solution obtained from FITEQLC requires description of the mass-action expressions formulated in the system (Gibbs, 1957; Westall and Hohl, 1980). In the CD-MUSIC formulation, a set of species are defined as the product of thermodynamic reactions with a set of components and an iterative strategy is used to obtain solutions to the chemical equilibrium problems. The entire modeling approach applied in this Chapter was based on a sequential optimization approach; (1) simulation of carbonate adsorption on goethite with surface species proposed by Villalobos and Leckie (2001) to account for the low pH_{pzc} of the surface charge data from Barrow and Cox (1992); (2) calibration of the three potentiometric titration data obtained from Barrow and Cox (1992) assuming an open system with fixed pCO_2 and the fixed affinity constants and parameters previously determined; (3) simulation of Hg(II) adsorption on goethite incorporating carbonate species with the same parameters used in previous steps; and (4) simulation of Hg(II) adsorption on a goethite with a different surface area to verify the model used.

The 1-p*K* CD-MUSIC model requires the determination of six parameters (acidity constants (K_a), electrolyte binding constants (K_{anion} and K_{cation}), surface site density (N_s), and Helmholtz capacitance (C_1 and C_2)), while both 2-p*K* TLM and SLM require (maximum) seven parameters. Intrinsic equilibrium constants are determined by numerical optimization approach using FITEQLC when the calibration to proton

adsorption is conducted. For the crystal structure of goethite, the Fe^{3+} ions are surrounded by 6 O(H) ligands (coordination number = 6) in Figure 4.1. Thus, the charge applied per one bond, ν, in CD-MUSIC is ½, while the classic 2-p*K* model assumes one unit charge per a bond. According to electron microscopy studies, goethite exhibits a needle-like shape elongated in the *c*-axis with {110} planes (longitudinal faces) and {210} planes (the crystal ends) (Cornell and Schwertmann, 1996; Schwertmann and Cornell, 1991; Torrent *et al.,* 1990). On the basis of Fe—O and H—O distances, the oxide ligands can be considered a protonated oxygen with a high proton affinity (O_I) and an unprotonated oxygen with a hydrogen bridge and a low proton affinity (O_{II}) (Venema *et al.*, 1998).

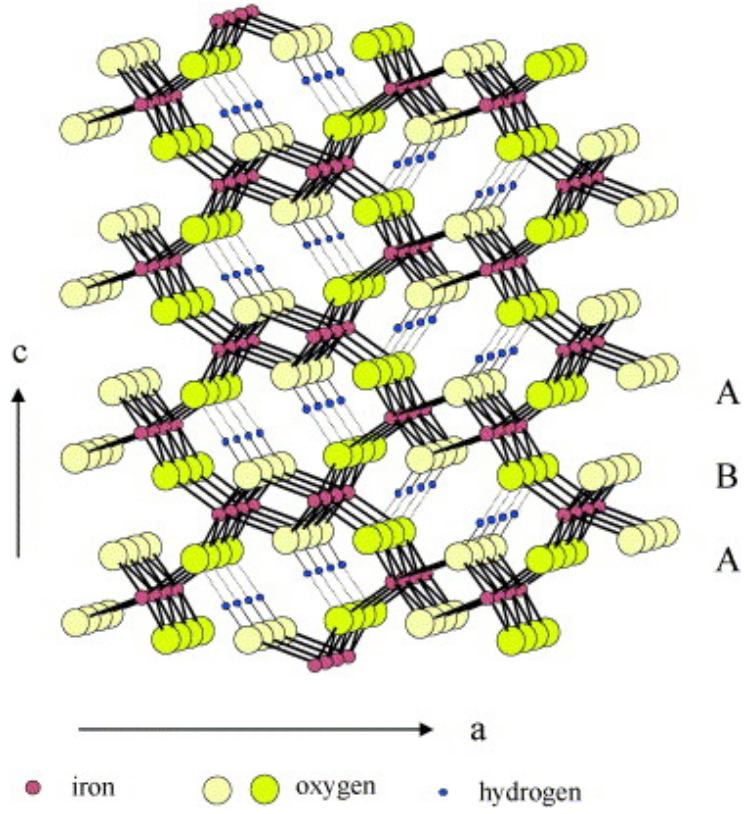

Figure 4. 1 Crystal structure of goethite. Source: Cudennec and Lecerf, 2005.

The theoretical analysis of crystallographic data provides surface site densities for each type of surface group with different proton affinity at each crystal face. The reactive surface site density of singly (≡FeOH), doubly (≡Fe_2OH), and triply coordinated surface group (≡Fe_3OH) for Hg(II) adsorption on goethite was determined using the proton charging congruency exercises developed by Villalobos and co-workers (Salazar-Camacho and Villalobos, 2010; Villalobos and Pérez-Gallegos, 2008; Villalobos *et al.*, 2009). The basis for this approach stems from observed differences in surface reactivity for goethites with different surface areas. For systems where no ideal reference titration

data are available, site densities for each type of surface group (≡FeOH, ≡Fe_2OH, ≡Fe_3OH) were obtained by adjusting the proton reactive site density (≡FeOH + ≡Fe_3OH) to the maximum proton adsorption value for the working goethite systems based on the documented crystallography data from Barron and Torrent (1996), Boily *et al.* (2001), Gaboriaud and Ehrhardt (2003), and Venema *et al.* (1996). However, the following assumptions are employed during the analysis.

- The singly coordinated surface groups with a low proton affinity (O_{II}) are assumed to be nonreactive due to the high affinity constant of ≡$FeO^{3/2-}$ (Venema *et al.*, 1998).
- The doubly coordinated surface groups on the (101) and (001) faces and half of the doubly coordinated surface groups on the (210) and (010) faces are assumed to be nonreactive (Gaboriaud and Ehrhardt, 2003; Venema *et al.*, 1996).
- The triply coordinated surface groups are absent on the (210) and (010) faces (Villalobos and Pérez-Gallegos, 2008).

Electrical Stern layer capacitance values are dependent on the solution properties and the thickness of the interfacial region.

$$C = \frac{\varepsilon_0 \varepsilon}{d}$$

where ε_0 is the permittivity of free space, ε is the solution dielectric constant, and *d* is the thickness of the molecular capacitor. The Helmholtz inner- (C_1) and outer-layer (C_2) capacitance of the electrostatic three plane model in Figure 2.8 can be determined for molecular capacitor at the mineral-water interface. In this study, 0.97 and 4.1 F/m^2 for C_1

and C_2 was used respectively (overall stern layer capacitance 0.78 F/m^2) corresponding to dielectric constants of approximately 30 and 80 and layer thickness of 2.8 and 1.7 Å (Tadanier and Eick, 2002; Villalobos *et al.,* 2003). The overall stern layer capacitance can be calculated from

$$\frac{1}{C} = \frac{1}{C_1} + \frac{1}{C_2}$$

The electro-neutrality condition, $\sigma_H + \sigma_{IS} + \sigma_{OS/IP} + \sigma_D = 0$ where σ_i represents the surface charge derived by H, protons; IS innersphere complexes; OS, outersphere or IP, ion-pair complexes; and D, diffuse swarm ions, must be fulfilled for the particles in aquatic suspension (Sposito, 1998). The surface charge derived by proton binding, σ_H can be calculated as

$$\sigma_H = \left(\Delta C_A^{sample} - \Delta C_B^{sample}\right)\frac{F}{a}S_i F \ \ m^{-2}$$

where C_A^i and C_B^i represent the concentration of acid and base added. The *a* and *S* are the solid content (g L^{-1}) and specific surface area (g m^{-2}) respectively. *F* is Faraday's constant, 96500 C mol^{-1}.

Table 4. 1 The physico-chemical parameters and suspension properties used in model simulations with the 1-p*K* CD-MUSIC approach.

Parameter	**System label**		
	VIL70[a]	**BAR76**[b]	**BON15**[c]
Specific surface area, $m^2\ g^{-1}$	70	76	15
Suspension density, $g\ L^{-1}$	13.8[d] and 9.4[e]	4.01	10
pH_{pzc}	8.9	7.7	7.85
Proton reactive site density, sites nm^{-2}	4.6	6.02	5.5
Stern layer capacitance		0.78	
C_1, Helmholtz inner layer, $F\ m^{-2}$		0.97[f]	
C_2, Helmholtz outer layer, $F\ m^{-2}$		4.1[g]	

a. Villalobos and Leckie (2000 and 2001)

b. Barrow and Cox (1992)

c. Bonnissel-Gissinger *et al.* (1999)

d. used in acid-base titration in 0.1 and 0.015M $NaNO_3$ (Villalobos and Leckie, 2000 and 2001)

e. used in carbonate adsorption on goethite (Villalobos and Leckie, 2000 and 2001)

f. Villalobos *et al.* (2003)

g. Tadanier and Eick (2002)

Molecular scale studies provide an important basis for more precise adsorptive mechanisms/processes of metal ions adsorption and definition of the mode of adsorption (e.g., bidentate corner-sharing complexes). Extended X-ray absorption fine structure (EXAFS) spectroscopy fittings combined with the molecular modeling programs (e.g., Cerius[2] from Accelrys, Inc. and PC Spartan Pro from Wavefunction, Inc.) is a nondestructive *in situ* analytical method uniquely suited to determine the identity, number of nearest neighbors, interatomic distances, and degree of structural order. The bond valence analysis gives useful information for coordinative stability of sorption complexes at the surface by placing basic bonding constraints on potential modes of sorption (Kim *et al.*, 2004a). The analysis results for various modes of Hg(II) sorption on the surface of Fe (hydr)oxides are presented in Table 4.2.

Table 4. 2 Bond valence analysis of various Hg(II) sorption complexes on the surface of Fe (hydr)oxides (Kim *et al.*, 2004a).

Surface species/bonds	$\sum s_{M\text{-}O}$ at oxygen (vu)		Oxygen coordination state	$r_{Fe/Al\text{-}O,\ bv}$ (Å)	Prediction
	No H-bonds	With H-bonds			
Fe—O—Hg	**1.16—1.48**	**1.42—1.97**	**Saturated**	**1.66—1.96**[c]	**Stable**
Fe—OH—Hg	**1.84—2.36**	**1.97—2.61**	**Saturated**	**1.94—2.94**[c]	**Stable**
Fe—OH_2—Hg	2.52—3.24	2.52—3.24	Oversaturated	>2.32[b]	Doesn't occur
Fe_2—O—Hg	**1.56—2.07**	**1.70—2.32**	**Saturated**	**1.92—2.09**	**Stable**
Fe_2—OH—Hg	2.25—2.95	2.25—2.95	Oversaturated	2.19—2.63	Doesn't occur
Fe_3—O—Hg	**1.97—2.67**	**1.97—2.67**	**Saturated**	**2.07—2.14**[c]	**Stable**

[a] Rows in bold indicate conditions suitable for Hg(II) binding

[b] Limit imposed by the maximum range of Fe-O bond lengths observed in mineral structures

[c] Distance range overlaps that of Fe (hydr)oxides (Fe-O = 1.95-2.09 Å)

4.4 Results and Discussion

4.4.1 Dissolved Mercury Speciation

The dissolved aqueous Hg(II) speciation was calculated as a function of pH using the equilibrium software, MINEQL+ 4.5, with the thermochemical reaction constants listed in Table 4.3 (Schecher, 2001).

Table 4. 3 The intrinsic solution equilibrium constants of various Hg(II) species used in the 1-p*K* CD-MUSIC model calculation (Schecher, 2001).

Reactions	**log *K***
$Hg^{2+} + H_2O = HgOH^+ + H^+$	-3.40 ± 0.08
$Hg^{2+} + 2H_2O = Hg(OH)_2 + 2H^+$	-6.17
$Hg^{2+} + 3H_2O = Hg(OH)_3^- + 3H^+$	-21.1
$Hg^{2+} + Cl^- = HgCl^+$	6.72
$Hg^{2+} + 2Cl^- = HgCl_2$	13.23
$Hg^{2+} + 3Cl^- = HgCl_3^-$	14.2
$Hg^{2+} + 4Cl^- = HgCl_4^{2-}$	15.3
$Hg^{2+} + H^+ + CO_3^{2-} = HgHCO_3^+$	16.372
$Hg^{2+} + CO_3^{2-} = HgCO_{3(aq)}$	12.102
$Hg^{2+} + H_2O + Cl^- \leftrightarrow Hg(OH)Cl + H^+$	4.27 ± 0.35

The distribution of aqueous species provides a better understanding of model simulations for goethite, since the adsorptive behavior of Hg(II) is highly dependent on pH and the presence of adsorbable species. A total Hg(II) concentration of 5 µM was used to calculate aqueous Hg(II) speciation in the absence and presence of chloride at 20°C in Figure 4.2. In the absence of chloride and at low pH (< 3), the hexaqua ion, $Hg(H_2O)_6^{2+}$, dominates the speciation. As pH increases, contributions from $HgOH^+$ and $Hg(OH)_2$

species increase. In the presence of 5000 μM total chloride added to the system, $HgCl_2$ and HgClOH are dominant at low to mid pH range, while the region of $Hg(OH)_2$ dominance shifts to higher pH.

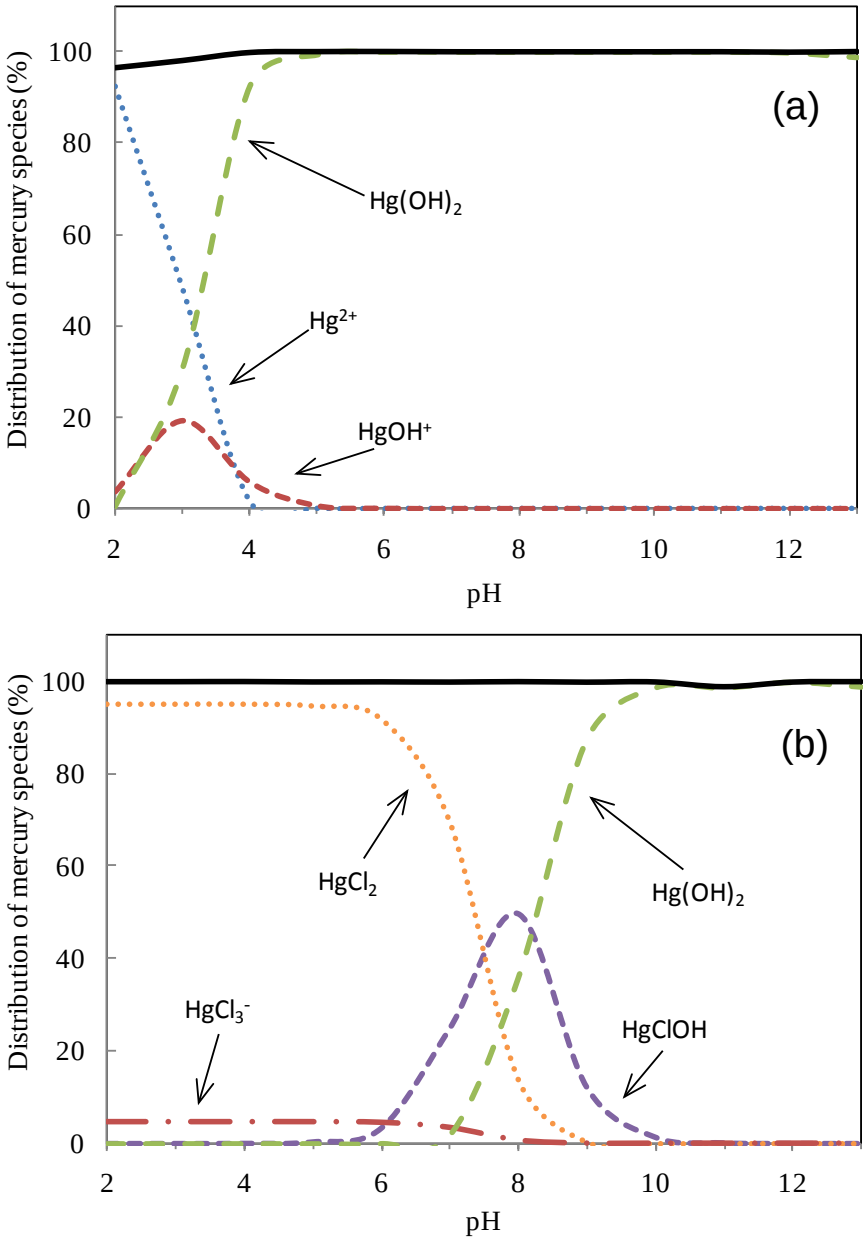

Figure 4. 2 Distribution of aqueous mercury species as a function of pH, (a) $[Hg_{TOT}] = 5$ μM and (b) $[Hg_{TOT}] = 5$ μM and $[Cl_{TOT}] = 5000$ μM. The model lines were calculated using MINEQL+ 4.5 (Schecher and McAvoy, 2003). Solid line indicates the total dissolved mercury concentration.

4.4.2 Carbonate Species on Goethite

Potentiometric acid-base titration data collected at several different ionic strengths give rise to a typical surface charge profile such as that shown in Figure 4.3.

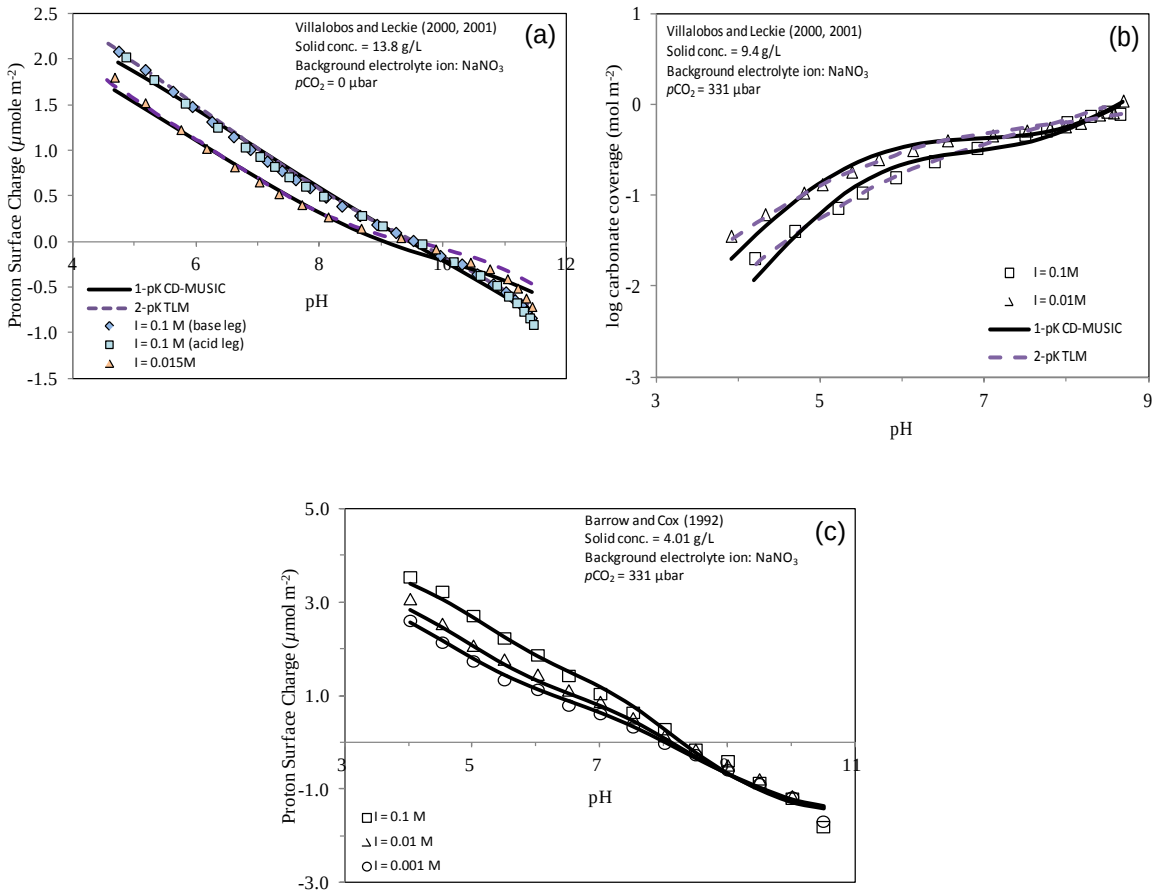

Figure 4. 3 Optimization of surface acidity constants, ion-pair formation, and carbonate surface reactions. (a) Proton surface charge profile of carbonate-free goethite (closed system) in 0.1 M (closed squares) and 0.015 M (closed triangles) $NaNO_3$. (b) Calibration of carbonate species with the adsorption of carbonate on goethite in open CO_2 system in 0.1 M (open squares) and 0.01 M (open triangles) $NaNO_3$. (c) Surface charge profile of goethite in open system in 0.1 M (open squares), 0.01 M (open triangles), and 0.001 M (open circles) of $NaNO_3$.

The crossover point or intersection of the data collected at different ionic strengths is termed the point of zero salt effect and is an estimate of the pH_{pzc} (Sposito, 1998). Previous research has suggested that the titration data and pH_{pzc} is a function of the solid synthesis method and the nature of electrolyte used (Weerasooriya *et al.,* 2000). However, a number of carefully controlled potentiometric titration experiments conducted for goethite have obtained similar estimates of the pH_{pzc}. For example, the pH_{pzc} for goethite has been determined to be 9.2 in NaCl, 9.0 in $NaNO_3$ (Villalobos and Leckie, 2000), 9.1 in NaCl (Lumsdon and Evans, 1994), 8.9 (Geen *et al.,* 1994), 9.0 $\pm$ 0.3 (Zeltner and Anderson, 1988) in suspensions of $NaClO_4$, and 9.2—9.3 in $NaNO_3$ (Filius *et al.,* 1997). In contrast, the surface charge data obtained from Barrow and Cox (1992) exhibited a low pH_{pzc} estimate of 7.7. Low estimates of the pH_{pzc} are often attributed to adsorption of carbonate on the goethite or the contamination of the suspension with carbonate (Bargar *et al.,* 2005; Gaboriaud and Ehrhardt, 2003; Naveau *et al.,* 2005; Villalobos and Leckie, 2000; Zeltner and Anderson, 1988). Given the low estimate of the pH_{pzc} for the Barrow and Cox data and the fact that the experimental plan did not indicate that precautions were used to minimize carbonate in the system, the low pH_{pzc} determined by Barrow and Cox (1992) was attributed to adsorption of dissolved carbonate species to the goethite surface which reduced the net positive surface charge (Lumsdon and Evans, 1994). Thus, it was necessary to incorporate carbonate adsorption to the goethite surface. Fortunately, data for carbonate adsorption was available from Villalobos and Leckie (2001). These data were used to identify relevant surface

equilibria and the intrinsic constants for modeling carbonate adsorption to goethite. The surface reactions investigated included:

$$\equiv FeOH^{1/2-} + CO_3^{2-} + H^+ = FeOCOO^{3/2-} + H_2O \ (\Delta z_0 = -1 \text{ and } \Delta z_1 = -2)$$

$$\equiv FeOH^{1/2-} + CO_3^{2-} + 2H^+ = \equiv FeOCOOH^{1/2-} + H_2O \ (\Delta z_0 = 1 \text{ and } \Delta z_1 = 0)$$

$$\equiv FeOH^{1/2-} + CO_3^{2-} + Na^+ + H^+ = \equiv FeOCOONa^{1/2-} + H_2O \ (\Delta z_0 = 0 \text{ and } \Delta z_1 = -1)$$

The change of charge (Δz) on the 0- and 1-planes were obtained from $\Delta z_0 = z_0 + \Delta n_H$ and $\Delta z_1 = z_1$, where n_H is the net change in protons on the 0-plane and z is the charge of oxygen adsorbed at each innersphere plane.

Of potential surface groups for acidity ($\equiv Me_nO^{-2+nv}$, $\equiv Me_nOH^{-1+nv}$, and $\equiv Me_nOH_2^{nv}$, where v and n is Pauling's bond valence and valence number, respectively), singly coordinated surface groups have two consecutive protonation steps in the 1-p*K* CD-MUSIC approach. The dominant species for the singly coordinated surface groups are $\equiv FeOH^{1/2-}$ and $\equiv FeOH_2^{1/2+}$ due to a very high protonation constant for $\equiv FeO^{3/2-}$. The doubly coordinated surface group, $\equiv Fe_2OH^0$, is assumed to be nonreactive over a wide range of pH values. Only the first protonation step for the triply coordinated groups, $\equiv Fe_3O^{1/2-}$, is incorporated in the model, since all four oxygen orbitals are occupied after uptake of a proton on the 0-plane. The charge developed on the surface plane provides a

mechanism for interaction of the surface with the background electrolyte via ion-pair formation.

The intrinsic constants for the protonation and ion-pair formation reactions shown in Table 4.4 for the singly and triply coordinated surface groups were optimized using FITEQLC using the data from a carbonate-free goethite (13.8 g/L) in 0.1 and 0.01 M $NaNO_3$ (Villalobos and Leckie, 2000, 2001) as shown in Figure 4.3a. The adjustment of proton reactive site density to the maximum proton adsorption value yielded a surface site density of 4.6 sites/nm^2 in proportions of (101)/(210) faces of 16/84 which exhibits greater site predominance on the (210) face compared to the (101) face than other goethites (43/57 and 32.8/67.2 for BAR76 and BON15 goethites, respectively). The protonation constants optimized in this work are in agreement with those of goethite preparation in Hiemstra and Van Riemsdijk (1996). The calculated data resulted in the symmetric binding of electrolyte ions on goethite describing $K_{Na} = K_{NO3} = -1$. The quality of the model fits to the data appears to be similar to those reported by Villalobos and Leckie (2001) for the 2-pK TLM. In both cases, the models slightly overpredicted the surface charge at high pH and low ionic strength; however, the 1 p*K*-CD MUSIC fit appears to provide a better fit to the data in this range.

The adsorption of carbonate on the same goethite (9.4 g L^{-1}) was simulated using the 1-p*K* CD-MUSIC model and is shown in Figure 4.3b. The model calibration for carbonate adsorption employed three innersphere surface species, ≡FeOCOO, ≡FeOCOOH, and ≡FeOCOONa in conjunction with the protonation and ion-pair reactions constants obtained from the calibration of the carbonate free data. The intrinsic

constants for carbonate surface complex were simultaneously optimized in FITEQLC (Table 4.4). Comparison of the TLM modeled with parameters presented in Table 4.1 and the same carbonate complexes in this study to the 1-p*K* CD-MUSIC fits indicate that both models adequately described the carbonate adsorption data.

The three potentiometric titration data sets obtained from Barrow and Cox (1992) were simulated at each ionic strength, assuming that H^+ is a specifically adsorbing ion in an open system (pCO_2 = 331 µbar). The only required step for translating the parameters from the data from Villalobos and Leckie to the data from Barrow and Cox was to account for differences in the surface area and reactivity of the two goethites. The face distribution of 43 % for the (101) plane and 57 % for the (210) face resulted from the adjustment of the proton reactive site densities (≡FeOH + ≡Fe_3OH) to the maximum adsorption of protons and hydroxyl ions of 10 µmol m^{-2} (Barrow and Cox, 1992). The predictions of the surface charge data shown in Figure 4.3c verified the previously optimized affinity constants for protonation, ion-pair formation, and carbonate surface species.

4.4.3 Calibration of Mercury(II) Adsorption on Goethite

The adsorption modeling for Hg(II) incorporated competition with carbonate species, since it was assumed that atmospheric CO_2 was present in the headspace of the reactors for the data collected by Barrow and Cox (1992). Hg(II) surface complexation was initially calibrated using data collected for Hg(II) adsorption in the absence of Cl, and a subsequent model calibration was then performed in the presence of Cl in a

background of 0.1 M $NaNO_3$. All parameters and constants optimized from the previous simulations (modeling titration and carbonate adsorption data) were integrated into the model as fixed parameters including aqueous complexation equilibrium constants and the Stern layer capacitances (Helmholtz inner- and outerlayer capacitances, C_1 and C_2) listed in Table 4.1 and 4.4.

Several surface species were used to describe Hg(II) sorption to the goethite. The selection of potential surface species was based on analysis of previous literature. Extended X-ray absorption fine structure (EXAFS) spectroscopy analysis for Hg(II) adsorption to goethite in the absence of chloride suggested a bidentate corner-sharing (binuclear) Hg surface complex to singly coordinated oxygens of two surface $Fe(O,OH)_6$ octahedra (Kim *et al.,* 2004a). Collins *et al.* (1999) also determined the same mode of Hg(II) sorption based on EXAFS analysis and DFT calculations. From the bond valence approach (Pauling, 1929) that serves as a complement to EXAFS analysis, the bidentate corner-sharing complex requires either ≡FeOHg or ≡FeOHHg species in consideration of both the coordinative saturation state of the surface oxygen site and Fe—O bond length. Additionally, the minor species, $\equiv Fe_2OHg$ and $\equiv Fe_3OHg$ were also reported to be stable based on bond valence constraints, but EXAFS fitting does not support these sorption arrangements (Kim *et al.,* 2004a). In the presence of chloride, the possible formation of ternary surface species ≡FeOHgCl was also proposed at high ligand concentration in a monodentate fashion (Bargar *et al.,* 1997; Barrow and Cox, 1992; Bonnissel-Gissinger, 1999; Davis and Leckie, 1978; Gunneriusson and Sjöberg, 1993). The formation of Hg-chloro ternary complexes coordinated to goethite was consistent with the microscopic

analysis for the interatomic distances and coordination numbers (Kim *et al.*, 2004b). Other ternary complexes for iron-oxide surfaces have also been postulated for co-adsorption of the carbonate species with dissolved metals (Ho and Miller, 1986; Bargar *et al.*, 2000). Thus, inclusion of a surface complex such as $\equiv FeOHgOCOO^{3/2-}$ may be reasonable to account for strong Hg(II)-CO_3^{2-} aqueous interactions.

Table 4. 4 Surface complexation reactions, and intrinsic equilibrium constants used in the 1-p*K* CD-MUSIC modeling of Hg(II) adsorption on goethite.

Surface reactions	**Spectroscopic prediction**	**log K_{int}**
Surface acidity		
$\equiv FeOH^{1/2-} + H^+ = \equiv FeOH_2^{1/2}$		9.5
$\equiv Fe_3O^{1/2-} + H^+ = \equiv Fe_3OH^{1/2}$		9.5
Ion-pair formation		
$\equiv FeOH^{1/2-} + H^+ + NO_3^{2-} = \equiv FeOH_2NO_3^{1/2-}$		9.4
$\equiv FeOH^{1/2-} + Na^+ = \equiv FeOHNa^{1/2}$		-0.1
$\equiv Fe_3O^{1/2-} + H^+ + NO_3^{2-} = \equiv Fe_3OHNO_3^{1/2-}$		9.4
$\equiv Fe_3O^{1/2-} + Na^+ = \equiv Fe_3ONa^{1/2}$		-0.1
Carbonate surface complexation		
$\equiv FeOH^{1/2-} + CO_3^{2-} + H^+ = \equiv FeOCOO^{3/2-} + H_2O$		9.46
$\equiv FeOH^{1/2-} + CO_3^{2-} + 2H^+ = \equiv FeOCOOH^{1/2-} + H_2O$		21.22
$\equiv FeOH^{1/2-} + CO_3^{2-} + Na^+ + H^+ = \equiv FeOCOONa^{1/2-} + H_2O$		13.65
Hg(II) surface complexation		
$\equiv FeOH^{1/2-} + Hg^{2+} = \equiv FeOHg^{1/2} + H^+$	Stable[a]	4.83
$2\equiv FeOH^{1/2-} + Hg^{2+} = \equiv Fe_2OHg^+ + H_2O$	Stable[a]	2.00
$\equiv FeOH^{1/2-} + Hg^{2+} + Cl^- = \equiv FeOHgCl^{1/2-} + H^+$	Stable[b,c]	4.94
$\equiv FeOH^{1/2-} + Hg^{2+} + CO_3^{2-} = \equiv FeOHgOCOO^{3/2-} + H^+$	–	3.83
Other Hg(II) surface complexation		
$\equiv FeOH^{1/2-} + Hg^{2+} = \equiv FeOHHg^{3/2}$	Stable[a]	–
$2\equiv FeOH^{1/2-} + Hg^{2+} = \equiv Fe_2O_2Hg^- + 2H^+$	Stable[a]	–
$\equiv Fe_3O^{1/2-} + Hg^{2+} = \equiv Fe_3OHg^{3/2} + H_2O$	Stable[a]	–

a. Kim *et al.* (2004a)

b. Kim *et al.* (2004b)

c. Bargar *et al.* (1997)

Based on the spectroscopic and bond valence data, the surface species incorporated into the model calibration for Hg(II) sorption to goethite included a non-protonated, doubly coordinated, ternary complex, and carbonate-binding species in Table 4.4. Adsorption pH-edges for nine different total loadings of [Hg_{TOT}] = 5 to 50 µM in the absence of Cl and [Hg_{TOT}] = 10 µM and [Cl^-_{TOT}] = 0 to 5000 µM on 76 m^2/g goethite were successfully simulated using the 1-p*K* CD-MUSIC model in Figure 4.4-4.7. The adsorption edges with [Hg_{TOT}] = 25 µM in the absence of Cl and [Hg_{TOT}] = 10 µM and [Cl_{TOT}^-] = 500 µM were calibrated initially to determine which species among those observed in the microscopic analysis would provide the best fits and to optimize the intrinsic equilibrium constants for those proposed species. The surface speciation of Hg(II) on goethite are presented in Figures 4.5 and 4.7.

The following adsorption edges were simulated in the same model simply by changing the total loading to the system without any adjustment to the constants. All model calculations were equally good and showed an obvious trend for the surface species. A symmetric distribution of charge change for surface reactions associated with Hg(II) on goethite was used in the adsorption modeling. The optimized intrinsic constants of the surface reactions are represented in Table 4.4. The affinity constant for the formation of ≡FeOHg groups (log $K^{int}_{S\text{-}OHg}$ = 4.83) was close to the values reported in other studies. Bonnissel-Gissinger *et al.* (1999) and Gunneriusson and Sjöberg (1993) proposed affinity constants of log $K^{int}_{S\text{-}OHg^+}$ = 4.9 ± 0.1 and 4.4 ± 0.04 respectively in the simulation of a constant capacitance model (CCM). The optimal affinity constant of

ternary surface species, ≡FeOHgCl used was somewhat lower than the constants found in those studies.

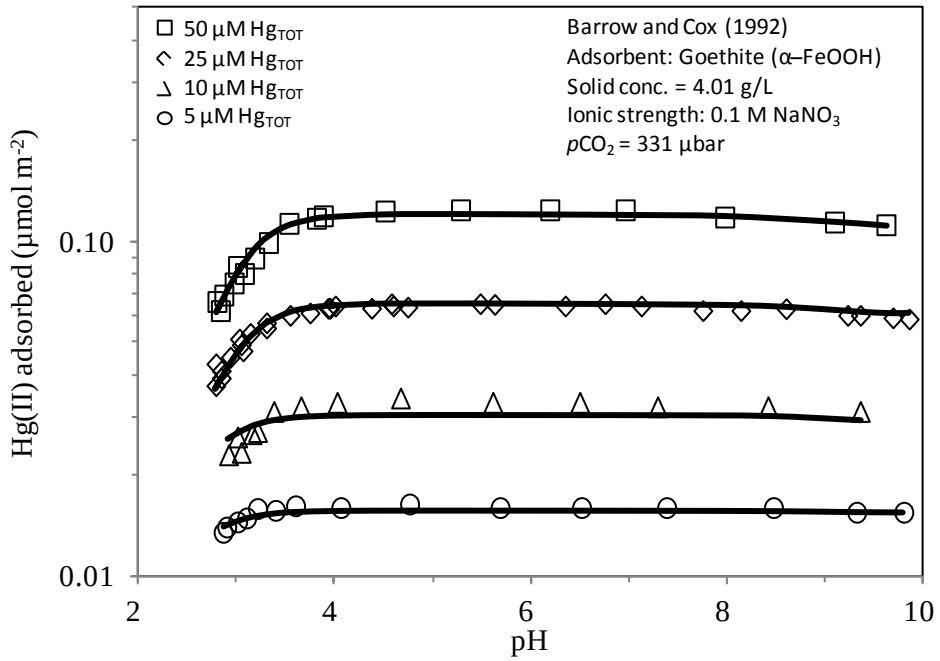

Figure 4. 4 CD-MUSIC modeling of adsorption pH-edge data collected for total Hg(II) loadings of 5, 10, 25, and 50 μM on goethite (76 m^2/g) in the absence of Cl. The model lines were calculated using innersphere surface species described by reactions in Table 4.4 and assuming an open CO_2 system.

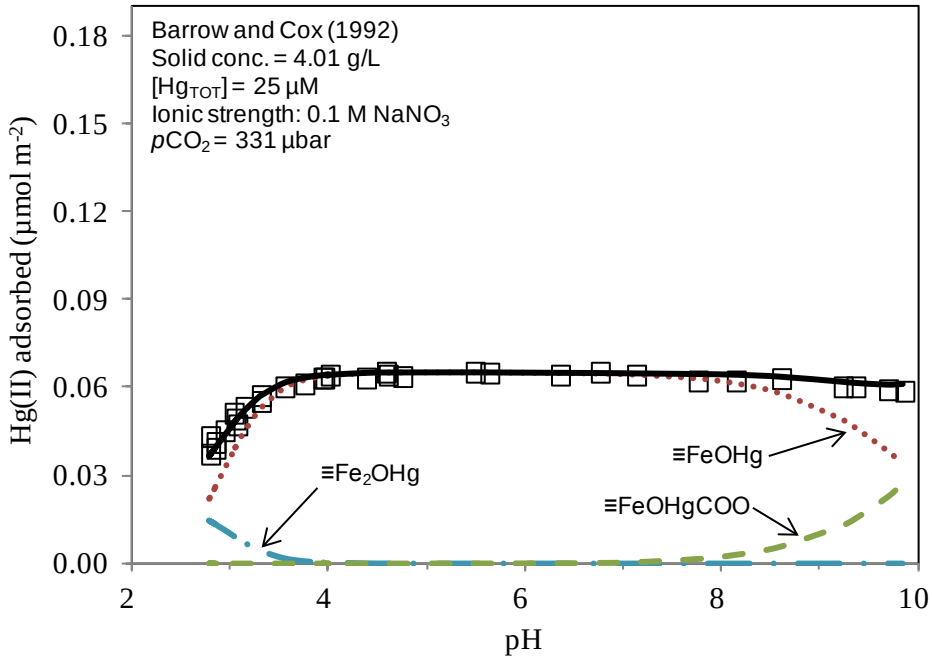

Figure 4. 5 The surface speciation of Hg(II) on goethite (76 m^2/g) for the model simulation of the adsorption pH edge data collected at a total Hg(II) loading of 25 µM in the absence of Cl. The solid line represents the total Hg(II) adsorbed and the dashed and dotted lines represent the surface species used in the 1-p*K* CD-MUSIC model.

In the absence of Cl, the concentration of monodentate surface species, ≡FeOHg by a ligand exchange mechanism is predominant in the adsorption pH-edge and plateau due to the formation of non-sorbing aqueous $Hg(OH)_2$ species at higher pH in Figure 4.8. The decreasing capacity of the dominant singly coordinated surface groups in the absence of Cl can be adequately described by the formation of the ternary surface complex with carbonate that can incorporate the increasing amount of carbonate as pH increases in an open system. The presence of Cl resulted in inhibition of Hg(II) ion adsorption which is evident because the adsorption pH-edges shift to higher values that are consistent with many studies performed for various types of adsorbents (Dzomback and Morel, 1990;

MacNaughton and James, 1974; Thanabalasingam and Pickering, 1985; Yin *et al.,* 1996). The dissolved Hg(II) species as shown in Figure 4.7 exhibited broad adsorption edges over several pH units. The aqueous Hg(II) speciation after equilibrium in the goethite-water system in Figure 4.8 indicated that a large proportion of non-sorbing $HgCl_2$ species suppressed the formation of surface species of ≡FeOHg and ≡FeOHgCl on goethite. The ternary surface Hg-chloro complex is dominant at low pH with similar affinity constants (log $K^{int}_{S\text{-}OHgCl}$ = 4.94) to ≡FeOHg species. The carbonate species did not impact the adsorption behavior in the working pH range in terms of competitive Hg(II) adsorption with Cl.

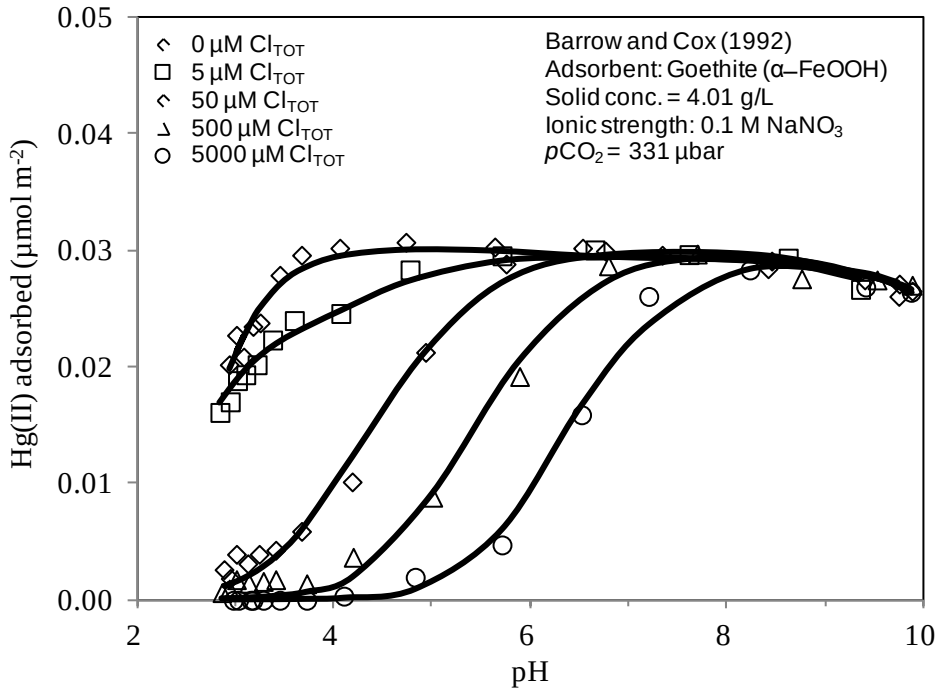

Figure 4. 6 CD-MUSIC modeling for adsorption pH-edges for experiments conducted at a total Hg(II) loading of 10 μM and [Cl_{TOT}] = 0, 5, 50, 500, and 5000 μM on goethite (76 m^2/g). The model lines were calculated assuming innersphere surface species and an open system.

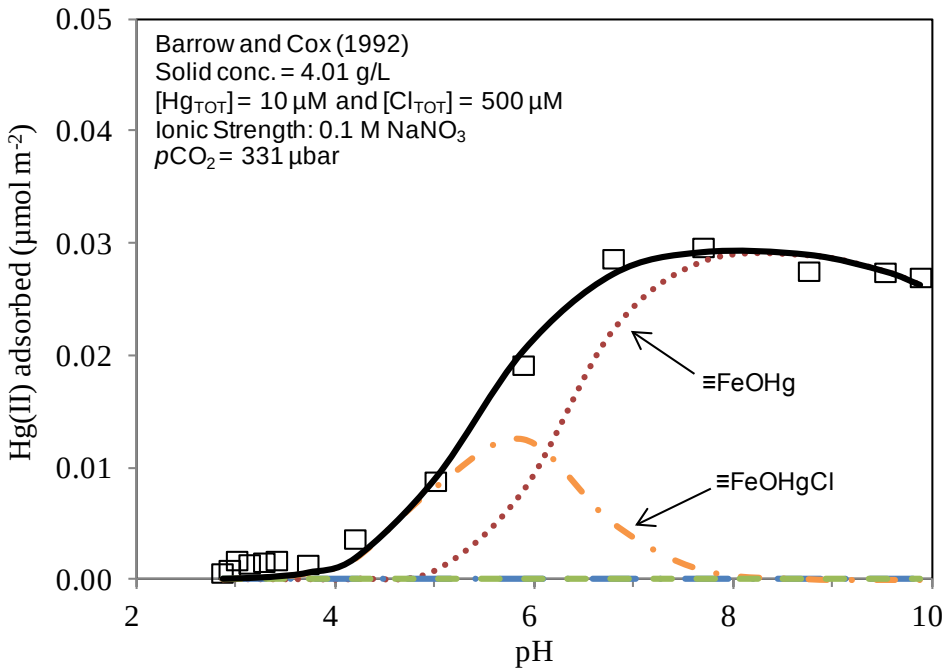

Figure 4. 7 Surface speciation of Hg(II) on goethite (76 m^2/g) in a model simulation of adsorption pH edge for a total Hg(II) loading of 10 µM and total Cl^- loading of 500 µM. The solid model line indicates the total Hg(II) adsorbed and the dashed and dotted lines represent the surface species used in the 1-p*K* CD-MUSIC model.

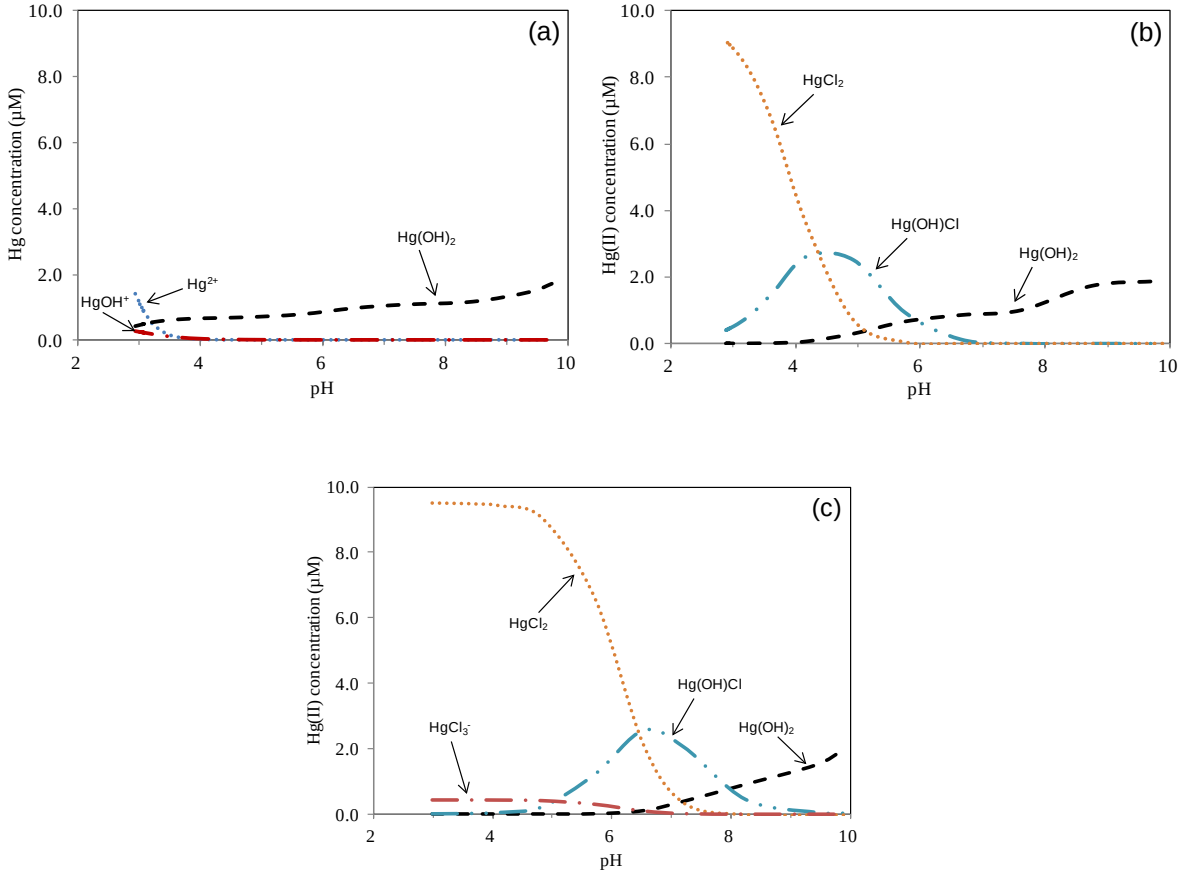

Figure 4. 8 The dissolved Hg(II) speciation in model simulation of adsorption pH edges on goethite (76 m^2/g). The total Hg(II) loading for these simulations was 10 μM and total Cl loading was (a) 0 μM, (b) 50 μM, and (c) 5000 μM. The model lines were calculated using the 1-p*K* CD-MUSIC model.

4.4.4 Model Verification

An entirely separate set of data was used to verify the surface complexation model. The experimental data set was abstracted from Bonnissel-Gissinger *et al.* (1999) in which Bayferrox goethite (Bayer, Germany) was used to examine Hg(II) adsorption in the presence of chloride. The total Hg(II) loading in their experiments was 12.4 μM, and the total chloride loadings were 20 μM and 100 mM. Even though these researchers took care to prevent carbonate contamination on the goethite surface, carbonate was detected

by X-ray diffraction, Mössbauer spectroscopy, and XPS (Bonnissel-Gissinger *et al.*, 1999). These researchers employed the constant capacitance model to describe their Hg(II) sorption experiments on goethite. However, the presence of carbonate was not accounted for in their model calculations, and not surprisingly their potentiometric titration data exhibited a crossover point at a low pH of 7.85. In this study, the 1-p*K* CD-MUSIC model approach was used to simulate adsorption edges for their goethite experiments, which had a reported surface area of 15 m^2/g. Model simulations were conducted using the constants reported in Table 4.4, but the face distribution was adjusted to account for the change in surface area. A face distribution of 32.8% was assigned to the (101) face and 67.2 % to the (210) face by adjustment of the proton reactive site to a total site density of 5.5 OH^- nm^{-2} determined from Muller and Sigg (1992). The model results are shown in Figure 4.9. The model simulations demonstrate that the 1-p*K* CD-MUSIC model was capable of providing excellent predictions for Hg(II) adsorption in the goethite-water system and determining the proportions of (101)/(210) face distributions with the reported proton reactive site densities. Not only was the overall removal of Hg(II) consistent with the previous data, but the speciation of Hg(II) in the aqueous phase helped to explain the impacts of pH, chloride concentration, and carbonate concentration on Hg(II) adsorption.

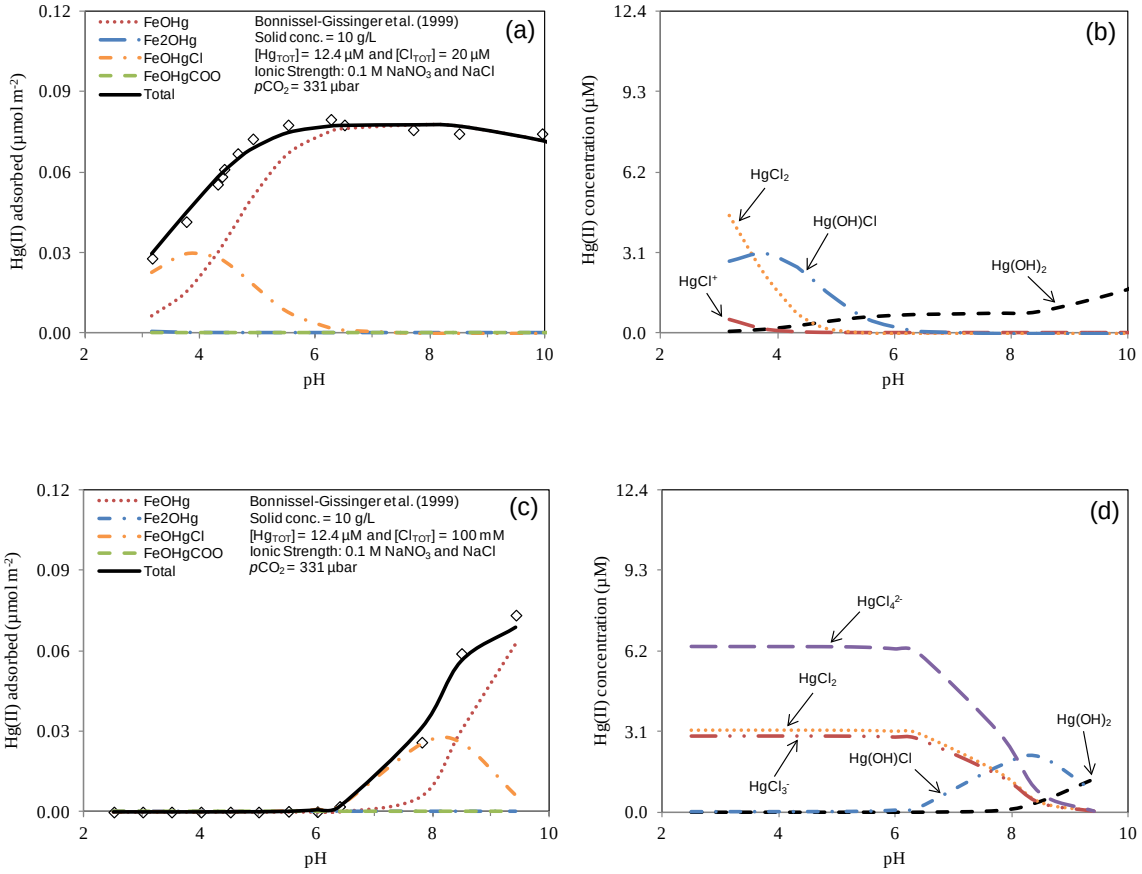

Figure 4. 9 Model verification of Hg(II) adsorption on goethite with data from Bonnissel-Gissinger *et al.*, (1999). The estimated parameters (i.e. the consistent innersphere surface species and the intrinsic affinity constants previously determined) were used and an open system was assumed. The solid model lines indicate the total Hg(II) adsorbed and the dashed and dotted lines represent individual surface or dissolved species of Hg(II) used in the 1-p*K* CD-MUSIC model. (a, b) $[Hg_{TOT}]$ = 12.4 μM and $[Cl_{TOT}]$ = 20 μM; (c, d) $[Hg_{TOT}]$ = 12.4 μM and $[Cl_{TOT}]$ = 100 mM.

4.5 Summary

The macroscopic adsorption experiments conducted by Hg(II) uptake measurements on goethite were simulated as a function of pH using the 1-p*K* CD-MUSIC model. The model was employed to describe the adsorption behavior on goethite and aqueous speciation in systems that included carbonate species and Cl over a range of

experimental conditions. The unique modeling effort in this study includes simulation of Hg(II) adsorption on goethite in an open carbonate system by incorporating spectroscopically supported mercury-chloride ternary surface complexes and surface complexation reactions for carbonate directly with the surface as a ternary mercury-carbonate complex. Thus, the decreasing capacity of monodentate surface species in the absence of chloride was adequately described by the formation of the ternary carbonate surface complex incorporating the increasing amount of carbonate expected as pH increases in an open system.

The surface complexes used in the model were based on molecular scale analyses reported in the literature. All of the affinity constants were determined by a sequential optimization approach. The modeling studies determined that a mononuclear Hg(II) surface species was the dominant surface complex in the absence of Cl at pH values below 8. At higher pH values and in the absence of chloride, ternary Hg(II)-carbonte species dominated. In the presence of Cl, ternary surface complexes became significant, and competition with carbonate and aqueous Hg-Cl species inhibited adsorption.

Chapter 5. Mercury(II) Adsorption on Gibbsite (α-$Al(OH)_3$)

5.1 Introduction

Mercury (Hg), which is known as a quicksilver or hydragyrum, is a common metal that can be found in the environment in various forms, including inorganic, and organic mercury. Elemental mercury can be extremely detrimental to human health and to the environment despite its usefulness in a broad range of industries. Moreover, transformation of mercury to ionic forms can lead to greater mobility in aqueous environments, and increases the potential for transport to environments in which methylation may occur. The divalent form of mercury (Hg(II)) is more stable than monovalent mercury (Hg(I)) in the environments, and has strong complexing ability towards S-derived ligands and halides (Stein *et al.*, 1996; Stumm and Morgan, 1996).

Several studies have documented the influence of pH, and the presence of chloride and sulfate on Hg(II) adsorption by various mineral surfaces. The formation of nonsorbing aqueous complexes with inorganic ligands or competitive ligand sorption can lower Hg(II) sorption to soil minerals by competing with the surface or blocking reactive surface sites, respectively. For example, the shift of adsorption edges to higher pH levels has been observed when chloride ion is present in the system due to inhibition of Hg(II) adsorption (Barrow and Cox, 1992a, b; Farrah and Pickering, 1978; Kinniburgh and Jackson, 1978; Newton *et al.*, 1976; Thanabalasingam and Pickering, 1985; Yin *et al.*, 1996). In contrast, direct sorption or accumulation of anions such as sulfate can reduce the electrostatic repulsion of metal cations towards the positive surface charge of minerals, thereby enhancing Hg(II) uptake to soil substrates (Kim et al., 2004b).

Surface Complexation Models (SCMs) can be used to describe the adsorptive behaviors of metal ions on the electrostatic planes of mineral surfaces. These models can successfully incorporate the surface charge and ionic strength dependency as a function of pH, reactive surface area, and adsorbate loadings. Description of the surface sites as proton reactive functional groups follows either the 1-p*K* or 2-p*K* approach on the surface planes of the mineral (Piasecki, 2006). The sorption of metal ions to soil minerals can be defined by surface complexation reactions on the surface functional groups at various distances from the surface based on surface affinity and electrostatic interactions.

The main goal of this research was to develop a model for Hg(II) adsorption on gibbsite using a self-consistent set of surface species and parameters. The model incorporates carbonate adsorption that can be expected in most aqueous systems. Gibbsite was selected in this study because of its abundance in soils (Dissanayake and Vitanage, 1977). A number of macroscopic investigations for Hg(II) adsorption conducted for different gibbsite preparations provided the data for this modeling study (Sarkar *et al.*, 1999; Weerasooriya *et al.*, 2007). Previous modeling efforts with these data described Hg(II) sorption by gibbsite (α–$Al(OH)_3$), and speciation of aqueous and surface species in the presence of inorganic ligands using the TLM and CD-MUSIC surface complexation models. However, neither of these prior efforts adequately described the adsorption behavior over the range of conditions investigated.

5.2 Materials and Methods

Several sets of experimental data for Hg(II) adsorption on gibbsite were extracted from the literature for the model development. Sarkar *et al.* (1999) investigated macroscopic Hg(II) adsorption on gibbsite using the triple layer model (TLM) in the presence of Cl^-, SO_4^{2-}, or PO_4^{3-}. They used superfine 4 gibbsite [Alcan Chemicals, $Al(OH)_2$] treated with 0.01 M NaOH for 30 min for Hg(II) removal. The Hg(II) stock solution was prepared by dissolving $Hg(NO_3)_2 \cdot H_2O$ in a matrix of 10 % HNO_3. The solutions of 0.1 M $NaNO_3$ and 0.01 M NaCl were used as background electrolytes. A 0.1 g of gibbsite was added to 24 mL of background electrolyte solution with 6 mL of Hg(II) working solution (3.3 g L^{-1} with 0.6 µM Hg(II)). The solution was equilibrated for 48 hours in capped 50-mL Teflon centrifuge tubes. The pH of solution was adjusted with 0.02 M HNO_3 or 0.02 M NaOH. The concentration of adsorbed Hg(II) on gibbsite was calculated by the difference between the concentration of Hg in the supernatant after centrifugation of equilibrated samples and the initial concentration of Hg added.

The protonation of gibbsite and Hg(II)-gibbsite interactions were also quantified using the 1-p*K* CD-MUSIC model (Weerasooriya *et al.*, 2000, 2001, 2007). The gibbsite used was obtained from Alcoa (Australia). They controlled the atmospheric CO_2 more rigorously using a glove box for equilibration and distilled water that was boiled for two hours to remove carbonate. These attempts to remove carbonate were based on the assumption that carbonate species can strongly bind to mineral surfaces. The surface charge profile of gibbsite was obtained from three titration experiments performed in 0.1, 0.01, and 0.001 M $NaNO_3$ and NaCl. The pH of the solution was adjusted with NaOH

and HNO_3. The 10 mL of well-equilibrated gibbsite suspension (2 g L^{-1} in $NaNO_3$ and 8 g L^{-1} in NaCl) was placed in tightly capped 25 mL polypropylene centrifuge tubes. The supernatant was analyzed after centrifugation at 14,000 rpm for 30 min. The pH_{pzc} for gibbsite has been determined to be 8.7 ± 0.2 (Weerasooriya *et al.*, 2000), 9.9 (Hiemstra *et al.*, 1999) in $NaNO_3$, and 8.35 ± 0.2 in NaCl (Weerasooriya *et al.*, 2001). The surface parameters and suspension properties used in model simulations are listed in Table 5.1.

Table 5. 1 The physico-chemical parameters and suspension properties used in model simulations with the 1-p*K* CD-MUSIC approach.

Parameter	**System label**		
	WEE1[a]	**WEE2**[b]	**SAR**[c]
Specific surface area, m^2 g^{-1}	13		3.5
Suspension density, g L^{-1}	2 ($NaNO_3$) and 8 (NaCl)	2	3.3
Proton reactive site density, sites n m^{-2}	8.15	3.5	8.15
Stern layer capacitance	0.17		
C_1, Helmholtz inner layer, F m^{-2}	1.3[d]		
C_2, Helmholtz outer layer, F m^{-2}	0.2[d]		

a. Weerasooriya *et al.* (2000, 2001)

b. Weerasooriya *et al.* (2007)

c. Sarkar *et al.* (1999)

d. Meng and Letterman (1993)

5.3 Modeling Approach

The modeling approach in this research used the Charge Distribution and Multi-SIte Complexation (CD-MUSIC) that was developed to incorporate the finite size of adsorbing ions and multisite heterogeneities based on the documented crystallography

data (Hiemstra *et al.*, 1996; Venema *et al.*, 1996). The symmetric charge distribution of bonds surrounding metal cations can be defined by the bond valence (ν) as

$$\nu = \frac{z}{\mathrm{CN}}$$

where *z* is charge of a cation and CN represents coordination number. In the crystal structure of gibbsite, the Al^{3+} ions (*z* = +3) are surrounded by 6 O(H) ligands (CN = 6) leading the charge per bond is ½ by Pauling's principle, while the classic 2-p*K* models assume one unit charge per bond. The Boltzmann factors for electrostatic 0-, 1-, and 2-planes are used for the electrostatic energy change of the species.

The 1-p*K* CD-MUSIC model for Hg(II) adsorption on gibbsite can be formulated in equilibrium adsorption computer codes such as ECOSAT (Keizer and Van Riemsdijk, 1996) or FITEQLC (an equilibrium computer code that combines a nonlinear least squares fitting routine with a chemical model that describes aqueous and surface equilibria) (Gustafsson, 2003) for optimum fitting to adsorption data. In the pre-processor of FITEQL 4.0 (Herbelin and Westall, 1999), a series of mass-action constraints can be included, and an iterative strategy is used for the solution to the equilibrium problems using a Newton-Raphson approximation. The intrinsic constants are regarded as non-adjustable parameters (once the model has been calibrated to the potentiometric titration and a limited set data for metal ion adsorption) over a range of pH, ionic strengths, and competing metal ions and ligands. Then, the extensibility of the model was evaluated

using other data sets that represent different experimental conditions for single and multi-solute adsorption.

The six parameters required in the 1-p*K* CD-MUSIC model include acidity constants (K_a), electrolyte binding constants (K_{anion} and K_{cation}), surface site density (N_s), and Helmholtz capacitances (C_1 and C_2)). Gibbsite is a thin flat hexagonal crystal composed of stacked sheets of linked octahedrons in which Al^{3+} is coordinated to six OH^- ions. Gibbsite particles develop well in x and y directions but are limited in the z direction.

It has two crystal faces including a planar (001) face with only doubly coordinated surface groups ($\equiv Al_2OH^0$) and the edge (100) face with singly ($\equiv AlOH^{1/2-}$) and doubly ($\equiv Al_2OH^0$) coordinated surface groups. The surface site density N_s of singly coordinated surface groups at the edge face is calculated to be 8.15 nm^{-2} and of doubly coordinated surface groups is 13.8 nm^{-2} at the planar face (Hiemstra *et al.*, 1999). In the 1-p*K* CD-MUSIC approach, the singly coordinated surface groups of $\equiv AlOH^{1/2-}$ and $\equiv AlOH_2^{1/2}$ (higher proton affinity constant of log K = ~22 for $\equiv AlO^{3/2-}$ in comparison with log K = ~10 for $\equiv AlOH^{1/2-}$) are dominant when 4 < pH < 10 among the potential surface groups for acidity, $\equiv Me_nO^{-2+nv}$, $\equiv Me_nOH^{-1+nv}$, and $\equiv Me_nOH_2^{nv}$, where v and n is Pauling's bond valence and valence number, respectively (Hiemstra and Van Riemsdijk, 1991, 1999). The doubly coordinated groups ($\equiv Al_2OH$) are considered inert due to low protonation/deprotonation constants. In the 1-p*K* CD-MUSIC model, estimation of both inner-layer (C_1) and outer-layer (C_2) capacitance of the electrostatic three plane model are required (Davis and Leckie, 1978). In this study, the overall Stern layer capacitance of

0.17 F/m^2 was used with inner-layer capacitance, C_1 = 1.3 and outer-layer capacitance, C_2 = 0.2 F/m^2 suggested by Meng and Letterman (1993) and Venema *et al.* (1996).

Table 5. 2 Bond valence analysis of various Hg(II) sorption complexes on the surface of Al (hydr)oxides (Kim *et al.*, 2004a).

Surface species/bonds	$\sum_{sM\text{-}O}$ at oxygen (vu)		Oxygen coordination state	$r_{Fe/Al\text{-}O,\ bv}$ (Å)	Prediction
	No H-bonds	With H-bonds			
Al—O—Hg	**1.20—1.45**	**1.47—1.94**	**Undersaturated**	**1.66—1.96**[d]	**Plausible**
Al—OH—Hg	**1.89—2.33**	**2.02—2.58**	**Saturated**	**1.94—2.94**[d]	**Stable**
Al—OH_2—Hg	2.57—3.21	2.57—3.21	Oversaturated	>1.98[b]	Doesn't occur
Al_2—O—Hg	**1.66—2.02**	**1.79—2.26**	**Saturated**	**1.92—2.09**[d]	**Stable**
Al_2—OH—Hg	2.35—2.90	2.35—2.90	Oversaturated	2.19—2.63	Doesn't occur
Al_3—O—Hg	2.12—2.58	2.12—2.58	Oversaturated	2.07—2.14	Doesn’t occur

[a] Rows in bold indicate conditions suitable for Hg(II) binding

[b] Limit imposed by the maximum range of Fe-O bond lengths observed in mineral structures

[c] Distance range overlaps that of Al (hydr)oxides (Al-O = 1.86-1.94 Å)

Molecular scale analyses were reviewed to provide accurate descriptions of the surface species used in the modeling effort (Table 5.2). Extended X-ray absorption fine structure (EXAFS) spectroscopy in conjunction with molecular modeling programs (e.g., Cerius^2 from Accelrys, Inc. and PC Spartan Pro from Wavefunction, Inc.) and bond valence analysis were used to predict coordinative stability of sorption complexes at the surface by bonding constraints (Kim *et al.*, 2004a). The stable species presented in Table 5.2 were considered for incorporation in the model.

5.4 Results and Discussion

5.4.1 Aqueous Mercury Speciation

The distribution of dissolved Hg(II) species were predicted using the equilibrium geochemical model MINEQL+ 4.5 (Schecher and McAvoy, 2003). Total concentrations of 0.1 μM Hg(II) in the absence of Cl, and 0.1 μM Hg(II) and 100 mM Cl were used to calculate the dissolved Hg(II) speciation to better understand the adsorption model simulation. The mass action equations for aqueous Hg(II) species defined in Table 5.3 were also formulated in the pre-processor of FITEQL to examine aqueous speciation after adsorption equilibrium as well.

Table 5. 3 The intrinsic solution equilibrium constants of various Hg(II) species used in the 1-p*K* CD-MUSIC model calculation (Schecher, 2001).

Reactions	**log *K***
$Hg^{2+} + H_2O = HgOH^+ + H^+$	-3.40 ± 0.08
$Hg^{2+} + 2H_2O = Hg(OH)_2 + 2H^+$	-6.17
$Hg^{2+} + 3H_2O = Hg(OH)_3^- + 3H^+$	-21.1
$Hg^{2+} + Cl^- = HgCl^+$	6.72
$Hg^{2+} + 2Cl^- = HgCl_2$	13.23
$Hg^{2+} + 3Cl^- = HgCl_3^-$	14.2
$Hg^{2+} + 4Cl^- = HgCl_4^{2-}$	15.3
$Hg^{2+} + H^+ + CO_3^{2-} = HgHCO_3^+$	16.372
$Hg^{2+} + CO_3^{2-} = HgCO_{3(aq)}$	12.102
$Hg^{2+} + H_2O + Cl^- \leftrightarrow Hg(OH)Cl + H^+$	4.27 ± 0.35

The Hg^{2+} ion octahedrally coordinated by water molecules was the predominant aqueous species at pH less than 3, as shown in Figure 5.1a. The contributions of the $HgOH^{+}$ and $Hg(OH)_2$ species increased through hydrolysis as pH increased. In the presence of Cl (added at a concentration six orders of magnitude higher than the total Hg(II) concentration), the $HgCl_{2(aq)}$ and $HgCl_3^{-}$ species were dominant at pH values up to pH 8.7; non-sorbing aqueous species $Hg(OH)_2$ and HgClOH became important at higher pH range.

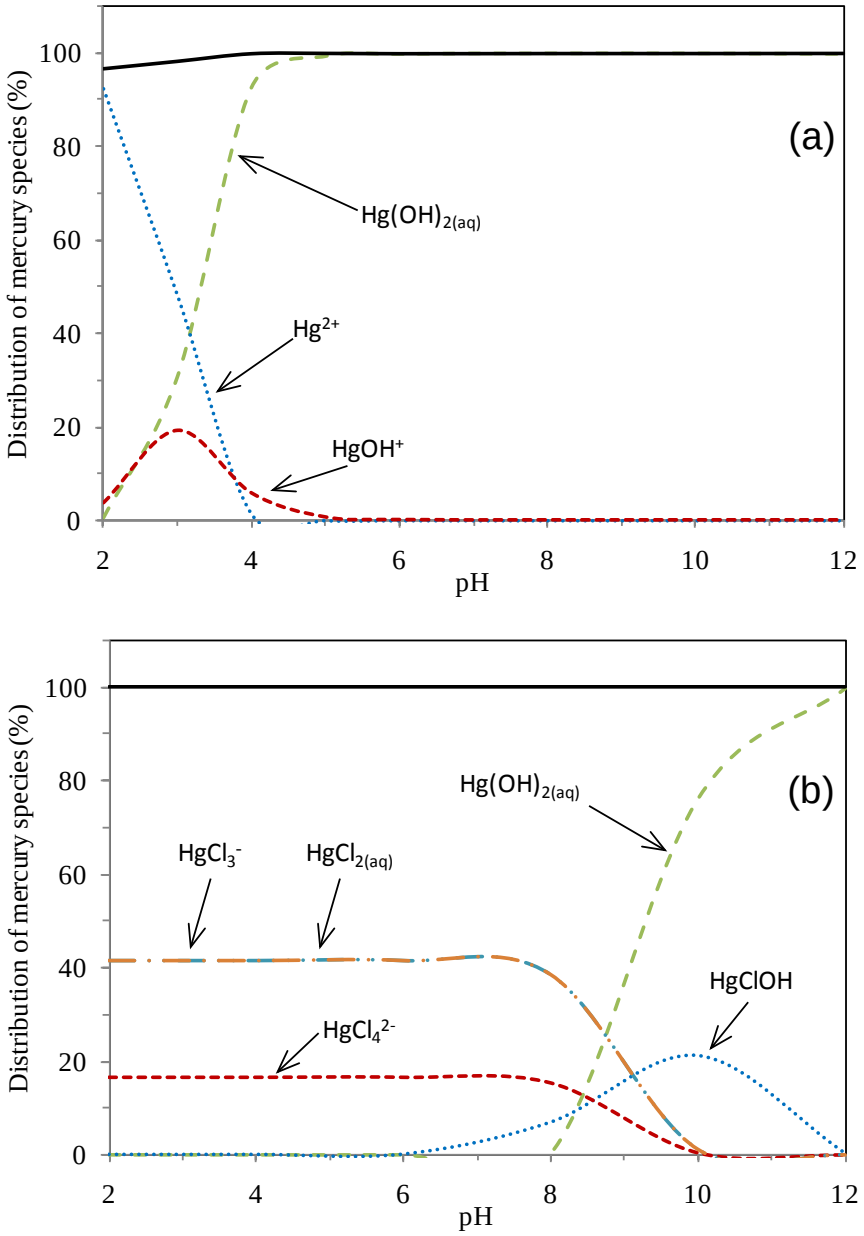

Figure 5. 1 Distribution of aqueous mercury species as a function of pH, (a) $[Hg_{TOT}]$ = 0.1 µM and (b) $[Hg_{TOT}]$ = 0.1 µM and $[Cl_{TOT}]$ = 0.1 M. The model lines were calculated using MINEQL+ 4.5 (Schecher and McAvoy, 2003). Solid line indicates the total dissolved mercury concentration.

5.4.2 Potentiometric Titration of Gibbsite

Potentiometric acid-base titration data from Weerasooriya *et al.* (2000, 2001) were used to calibrate the 1-p*K* CD-MUSIC model at three different ionic strengths of $NaNO_3$ and NaCl, and the results are shown in Figure 5.2. Only H^+ is assumed as a specifically adsorbing ion on the gibbsite surface in these titrations. The intersection of the three titration curves is termed the pH of the point of zero salt effect (pHpzse) and is an estimate of the pH_{pzc}. The data yielded an estimate of the pHpzc of 8.7 in $NaNO_3$ and 8.35 in NaCl considering $\equiv AlOH^{1/2-}$ at the edge (100) face (8.15 sites nm^{-2}) as the only proton binding site. In this model protonated/nonprotonated surface groups are allowed to interact with the background electrolyte ions on the electrostatic 1-plane in the gibbsite-water system. The change of proton charge, $\Delta n_H = 1$ on the 0-plane and change in charge on the 1-plane, $\Delta z = 1$ for Na^+ and -1 for NO_3^- and Cl^-, were incorporated into the model formulation in FITEQL. The intrinsic affinity constants for protonation and ion-pair formation reactions were optimized in the model simulation of the titration curves for carbonate-free gibbsite (2 g/L in $NaNO_3$ and 8 g/L in NaCl) and are provided in Table 5.4. The asymmetric binding constants for the two electrolyte ions on gibbsite (K_{Na} = 0.70, K_{NO3} = -1.37, and K_{Cl} = -0.13) were also estimated. A previous study demonstrated that the asymmetric binding of electrolyte on gibbsite resulted from a shift to a higher pH in the pH_{IEP} in the zeta potential data profile (Hiemstra *et al.*, 1999).

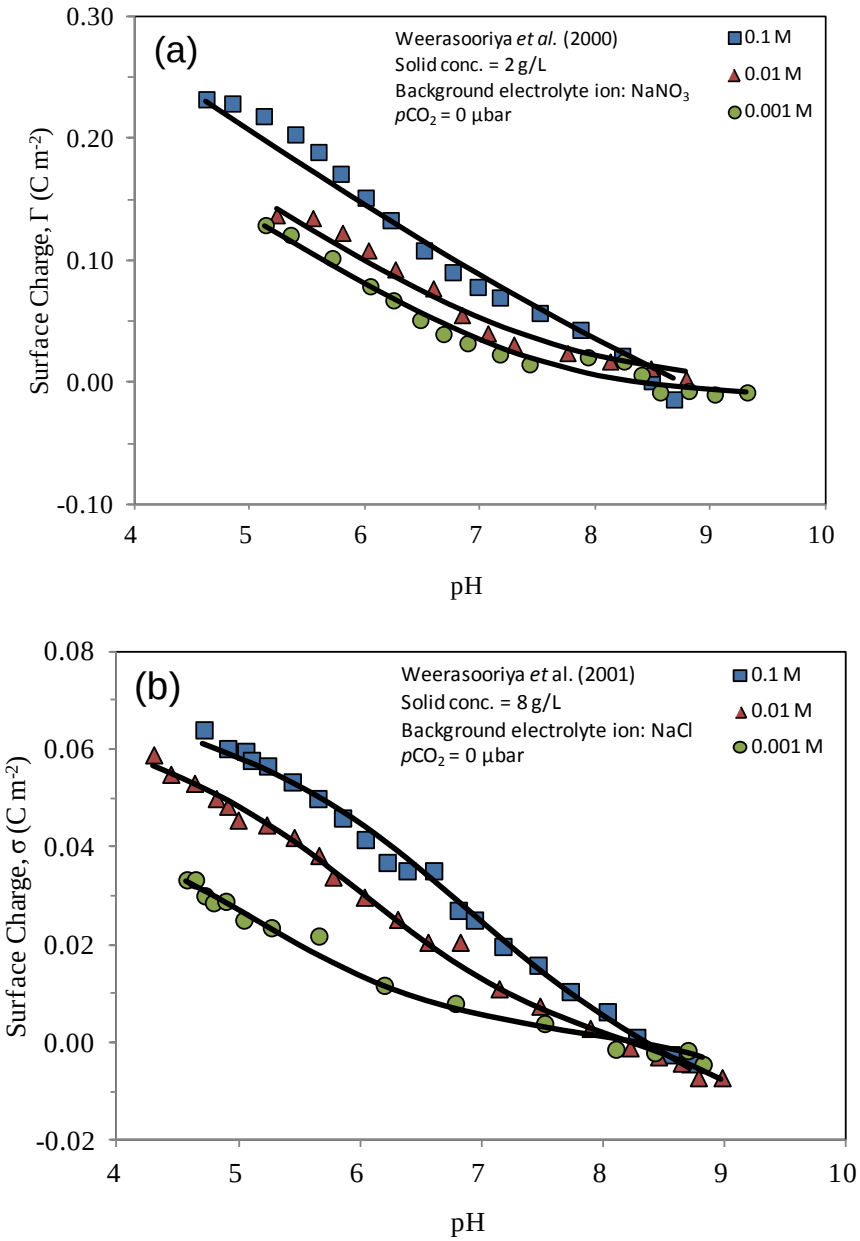

Figure 5. 2 Proton surface charge profile of carbonate-free gibbsite in 0.1 M (closed squares), 0.01 M (closed triangles), and 0.001 M (closed circles) of (a) $NaNO_3$ and (b) NaCl. The solid lines were calculated using the 1-p*K* CD-MUSIC model.

5.4.3 Calibration of Hg(II) Adsorption on Gibbsite

The 1-p*K* CD-MUSIC model was applied to simulate adsorption of Hg(II) on gibbsite (2 g/L) with data obtained from Weerasooriya *et al.* (2007). A proton reactive site density of 3.5 sites nm^{-2}, employed by Weerasooriya *et al*., (2007) was also employed in this work. The several surface species selected from the molecular scale analysis were used to describe Hg(II) adsorption on gibbsite.

Table 5. 4 Surface complexation reactions, and intrinsic equilibrium constants used in the 1-p*K* CD-MUSIC modeling of Hg(II) adsorption on gibbsite.

Surface reactions	**Spectroscopic prediction**	**log K_{int}**
Surface acidity		
$\equiv AlOH^{1/2-} + H^+ = \equiv AlOH_2^{1/2}$		9.87
Ion-pair formation		
$\equiv AlOH^{1/2-} + H^+ + NO_3^{2-} = \equiv AlOH_2NO_3^{1/2-}$		8.40
$\equiv AlOH^{1/2-} + H^+ + Cl^- = \equiv AlOH_2Cl^{1/2-}$		9.74
$\equiv AlOH^{1/2-} + Na^+ = \equiv AlOHNa^{1/2}$		0.70
Carbonate surface complexation		
$\equiv AlOH^{1/2-} + CO_3^{2-} + H^+ = \equiv AlOCOO^{3/2-} + H_2O$	Stable[a]	-0.30
Hg(II) surface complexation		
$\equiv AlOH^{1/2-} + Hg^{2+} = \equiv AlOHg^{1/2} + H^+$	Plausible[b]	9.29
$\equiv AlOH^{1/2-} + Hg^{2+} + H_2O = \equiv AlOHgOH^{1/2-} + 2H^+$	–	1.80
Other Hg(II) surface complexation		
$\equiv AlOH^{1/2-} + Hg^{2+} + H^+ = \equiv AlOHHg^{3/2} + H^+$	Stable[b]	–
$2\equiv AlOH^{1/2-} + Hg^{2+} = \equiv Al_2OHg^+ + H_2O$	Stable[b]	–

a. Wijnja and Schulthess (1999)

b. Kim *et al.* (2004a)

Previous research that utilized a combination of macroscopic Hg(II) uptake measurements, EXAFS spectroscopy (modeled with Cerius[2] and Spartan Pro), and bond valence analysis for Hg(II) adsorption to γ–alumina (γ–Al_2O_3) and bayerite (β–$Al(OH)_3$), a polymorph of gibbsite was used to identify appropriate surface species (Kim *et al.*, 2004a, b). The results of their analysis yielded monodentate, and corner-/edge-sharing

bidentate complexes to the $Al(O,OH)_6$ octahedra involving Al-O-Hg, Al-OH-Hg, and Al_2-O-Hg species to the bayerite (001) surface over pH 4 to 8 (Kim *et al.*, 2004a). The spectra also showed that the dominant sorbed complexes in the presence of chloride are similar to those in the absence of chloride, and the ternary surface complex is in minor proportions (Kim *et al.,* 2004b). Thus, the monodentate surface complex without a ligand exchange and bidentate corner-/edge-sharing complex were assumed to be non-reactive in the system. However, a ternary surface species, $\equiv AlOHgOH^{1/2-}$, formed by retention of the positively charged aqueous species $HgOH^+$ to the singly coordinated surface groups was included in model simulations (Barrow and Cox, 1992a; Bonnissel-Gissinger, *et al.*, 1999; Davis *et al.*, 1978; Gunneriusson and Sjoberg, 1993; Sarkar *et al.*, 1999).

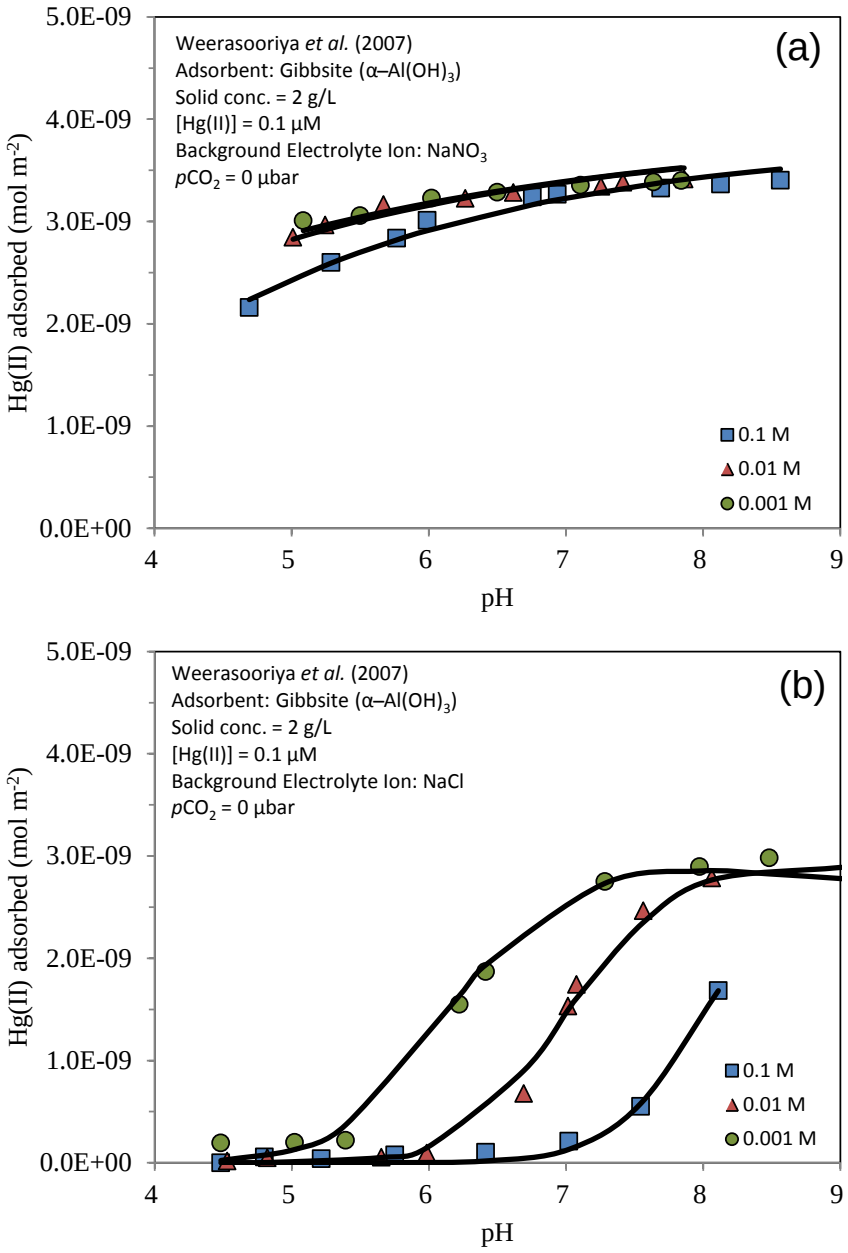

Figure 5. 3 CD-MUSIC modeling for adsorption pH-edges for experiments conducted at a total Hg(II) loading of 0.1 μM on gibbsite (13 m^2/g) in closed system. The model lines were calculated using innersphere surface species described by reactions in Table 5.4 in 0.1 M (closed squares), 0.01 M (closed triangles), and 0.001 M of (a) $NaNO_3$ and (b) NaCl.

Model calibrations were initially conducted in 0.1 M $NaNO_3$ in the absence of Cl and 0.1 M NaCl in FITEQLC with the optimized parameters (acidity constants). Reactions involving surface species (non-protonated and ternary complex with hydroxide) that were observed by molecular scale analysis were optimized in the model calibration. All the surface binding reactions were assumed to be innersphere complexes due to the high polarizability of Hg(II). The optimized constants are listed in Table 5.4.

Subsequent modeling of systems containing a total Hg(II) loading of 0.1 μM on 13 m^2/g gibbsite in 0.01, and 0.001 M $NaNO_3$ and NaCl were successfully simulated with the proposed surface species in Figure 5.3. Asymmetric distribution of charge for the ternary surface species ($\equiv AlOHgOH^{1/2-}$) was used in the adsorption modeling. The CD factor *f* that is the fraction of surface charge neutralizing ligands located in the 0-plane was set to 0.55 ($\Delta z_0 = 0.1$ and $\Delta z_1 = 0.1$) in the absence of Cl and 0 ($\Delta z_0 = -1$ and $\Delta z_1 = 1$) in the presence of Cl during the calibration process. Further evaluation of this distribution should be conducted using molecular orbital/density functional theory (Hiemstra *et al.*, 2007).

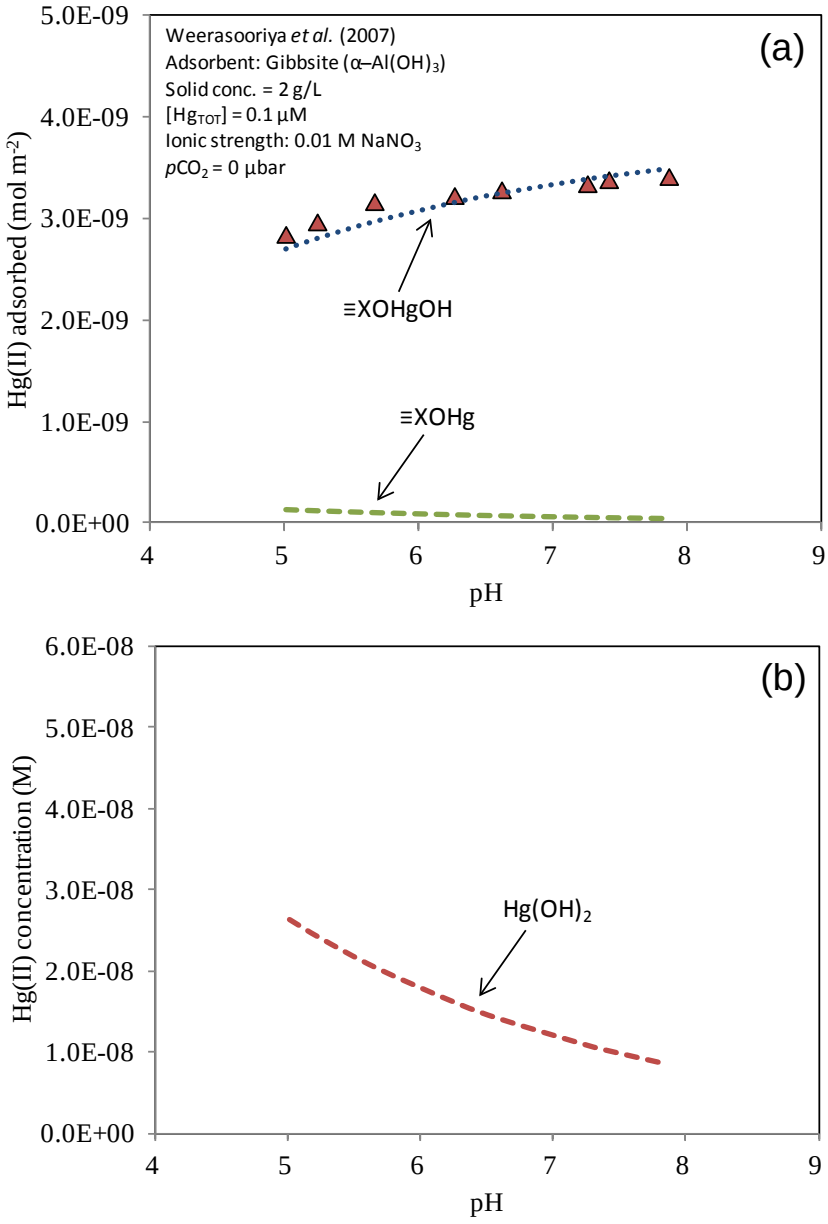

Figure 5. 4 Speciation of (a) Hg(II) adsorbed on gibbsite (13 m^2/g) in 0.01 M of $NaNO_3$ and (b) dissolved Hg(II) species in 0.01 M of $NaNO_3$ for the model simulation of the adsorption pH-edge data collected at a total Hg(II) loading of 0.1 μM. The model lines were calculated using the 1-p*K* CD-MUSIC model.

The speciation of Hg(II) adsorbed on gibbsite and dissolved Hg(II) species presented in Figures 5.4 and 5.5 exhibited broad adsorption edges as the adsorption profile extended over several pH units. The ionic strength of $NaNO_3$ had a minor impact on adsorption pH-edges, since the aqueous ions associated with the background electrolyte, Na and NO_3^-, interact insignificantly with oxide surfaces (Mac Naughton and James, 1974; Sposito, 1984). The adsorption of Hg(II) was adequately described by the two innersphere surface species proposed (i.e. a non-protonated surface complex and ternary complex with hydroxide). The ternary surface species, $\equiv AlOHgOH^{1/2-}$ was dominant but exhibited a relatively low formation constant (log $K^{int}_{S\text{-}OHgOH}$ = 1.80). In comparison to the predominant surface species on goethite, ≡FeOHg which had a log $K^{int}_{S\text{-}OHg}$ = 4.83 (Chapter 4), Hg adsorbs less on gibbsite than goethite. The monodentate surface species resulting from ligand exchange ($\equiv AlOHg^{1/2+}$) was present as minor species at equilibrium for adsorption pH-edges both in the presence and absence of Cl. The predominance of aqueous Cl species inhibited the extent of adsorption by ≡AlOHgOH at low pH as shown in in Figures 5.5b and 5.5c. The ternary Hg-chloro species (≡FeOHgCl) was included in model simulations to examine the impact of the species on Hg(II) adsorption on gibbsite. However, it was not found to be significant over the range of pH values examined in Figure 5.5a. This observation contrasts similar modeling efforts conducted for Hg(II) adsorption on goethite in the presence of Cl in which the ternary species with Cl was evident, but the modeling results are consistent with differences in EXAFS spectroscopy studies on the two adsorbents.

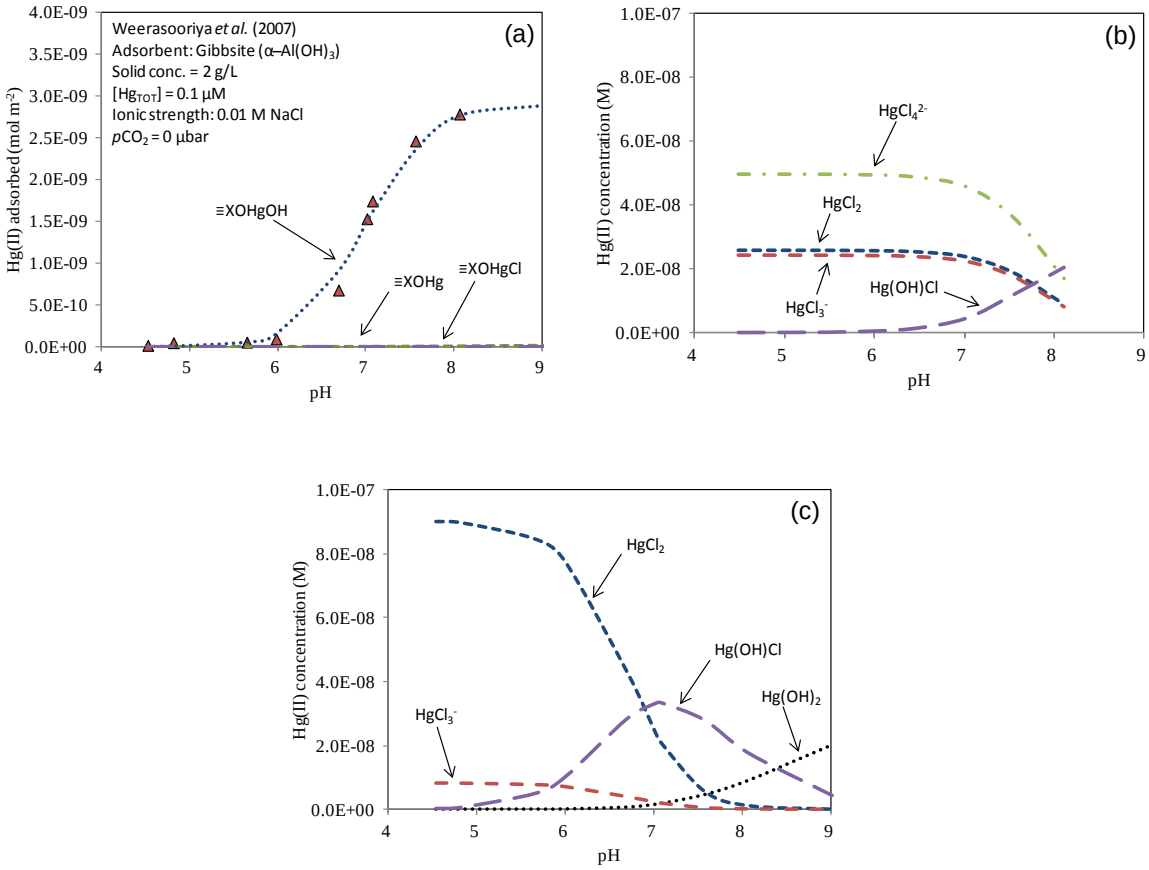

Figure 5. 5 Speciation of (a) Hg(II) adsorbed on gibbsite (13 m^2/g) in 0.01 M NaCl and dissolved Hg(II) species in (b) 0.01 M and (c) 0.001 M of NaCl for the model simulation of the adsorption pH-edges data collected at a total Hg(II) loading of 0.1 μM. The model lines were calculated using the 1-p*K* CD-MUSIC model.

5.4.4 Model Verification

The 1-p*K* CD-MUSIC surface complexation model was verified by simulating data from a completely different gibbsite preparation (superfine 4 gibbsite, Alcan Chemicals) as shown in Figure 5.6. Sarkar *et al.* (1999) investigated the sorption behavior of Hg onto gibbsite in a system with a total Hg(II) loading of 0.6 µM (3.3 g/L) using the classic 2-p*K* TLM. They simulated the experimental data by introducing different surface

complexes than used in this work. They incorporated the surface species of ≡AlOHgOH (innersphere complex), ≡AlO-HgOH (outersphere complex), ≡$AlOHg(OH)_2$ and ≡AlOHgOHCl. Those species used in their modeling are not consistent with the spectroscopy analysis provided in Table 5.4. However, the discrepancy between adsorption pH-edge data and corresponding model simulations suggest that either the model or the surface species were not adequate. In addition, the data indicated that adsorption of Hg(II) onto gibbsite decreased at higher pH in the absence of Cl. This observation is consistent with previous data for adsorption onto goethite and suggested the presence of carbonate in the system. The experimental plan given by Sarkar *et al.* (1999) did not indicate that precautions were taken to control atmospheric contamination by CO_2. Thus, the approach used in Chapter 4 was employed to incorporate carbonate species on gibbsite. He included a carbonate species in the goethite system to simulate Hg(II) adsorption in an open goethite-water system using data from Barrow and Cox (1992a). Previous research provided ATR-FTIR and DRIFT spectroscopic evidence that carbonate species adsorb at the aluminum oxide/water interfaces as a result of chemisorptions of CO_2 (Wijnja and Schulthess, 1999). Thus, the formation of innersphere carbonate complexes by a ligand exchange mechanism was included in the matrix to describe the decreasing capacity of Hg(II) adsorption on gibbsite.

$$\equiv AlOH^{1/2-} + CO_3^{2-} + H^+ = \equiv AlOCOO^{3/2-} + H_2O \quad (\Delta z_0 = -1 \text{ and } \Delta z_1 = 0)$$

The same surface site density of 8.15 nm^{-2} as one used in the potentiometric acid-base titration data calibration was used in this model verification. The symmetric charge distribution, which is a default setting for the ternary species was used ($\Delta z_0 = 0$ and $\Delta z_1 = -1$, CD factor $f = 0.5$) for the surface species $\equiv AlOHgOH^{1/2-}$ in the absence of Cl. The model confirmed surface reactions and their constants that were previously determined in the model calibration of adsorption pH-edges with data from Weerasooriya *et al.* (2007).

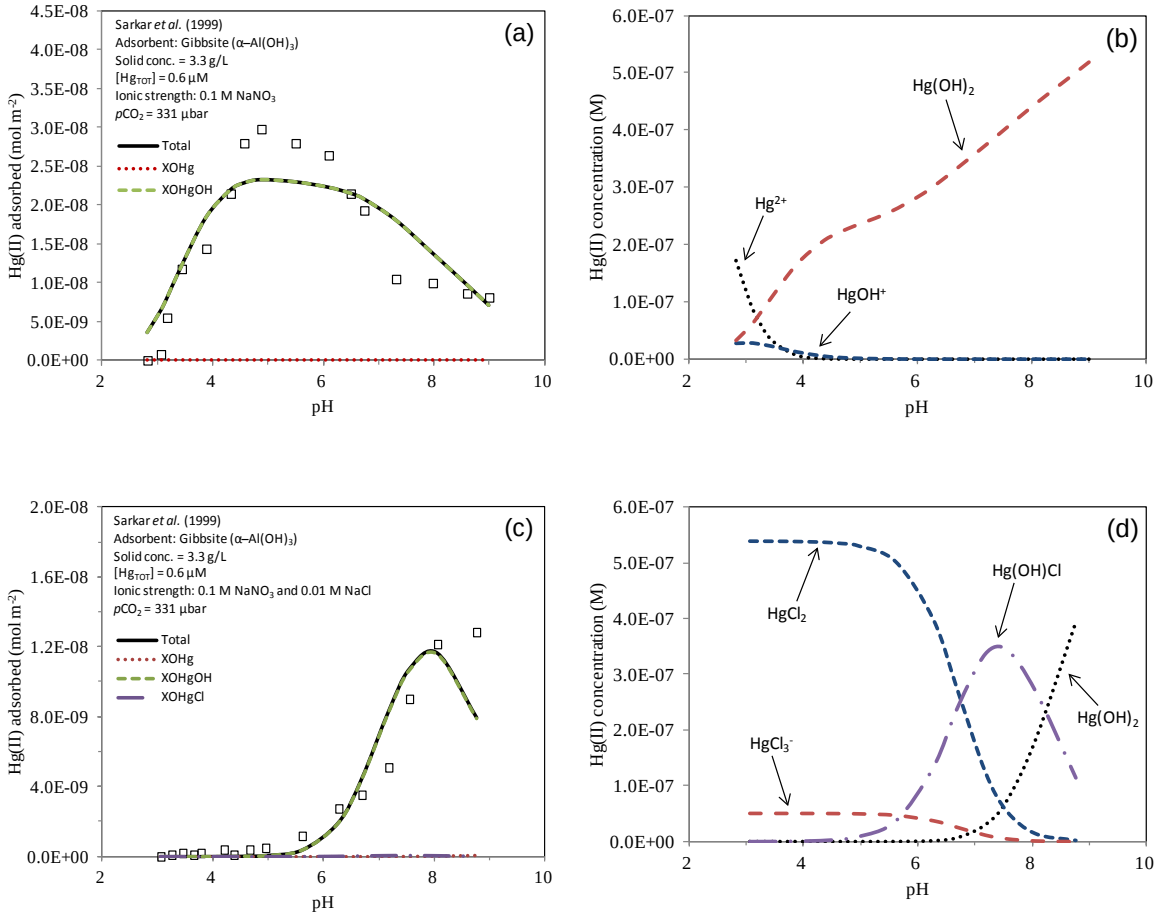

Figure 5. 6 Model verification of Hg(II) adsorption on gibbsite with other data set from Sarkar *et al.* (1999). The estimated parameters (i.e. the consistent innersphere surface species and the intrinsic affinity constants previously determined) were used and an open system was assumed. The solid model lines indicate the total Hg(II) adsorbed and the dotted and dashed lines represent individual surface or dissolved species of Hg(II) used in the 1-p*K* CD-MUSIC model. The total loadings of Hg(II) was 0.6 μM in (a) 0.1 M $NaNO_3$ and (b) 0.1 M $NaNO_3$ and 0.01 M NaCl.

The refined model provided reasonable predictions of the data. Hg(II) adsorption was predominantly controlled by the ternary complex $\equiv AlOHgOH^{1/2-}$ over the pH range for this data. In the absence of Cl, the carbonate species did not competitively bind to the gibbsite surface. The decrease in Hg(II) adsorption with increasing pH can be accounted

for by the formation of a stable $Hg(OH)_{2(aq)}$ species as pH increased in Figure 5.6b. The aqueous speciation of Hg(II) after equilibration with the solid phase in Figure 5.6d showed that the ternary complex $\equiv AlOHgOH^{1/2-}$ was inhibited due to formation of non-sorbing aqueous species of $HgCl_2$ and $HgCl_3^-$ at low pH in the presence of Cl (Barrow and Cox, 1992a; Bonnissel-Gissinger *et al.*, 1999; Dzombak and Morel, 1990; Mac Naughton and James, 1974; Thanabalasingam and Pickering, 1985; Weerasooriya *et al.*, 2007; Yin *et al.*, 1996).

5.5 Summary

The macroscopic Hg(II) sorption experiments by gibbsite (α-$Al(OH)_3$), a representative aluminum (hydr)oxide mineral, were simulated using the 1-p*K* CD-MUSIC approach. The model successfully incorporated both the presence of inorganic ligands at the dominant edge (100) face of gibbsite with the consistent surface species which were consistent with molecular scale analysis. The sequential optimization approach was used to determine the affinity constants of the surface species. The asymmetric binding constants for electrolyte ions (K_{Na} = 0.70, K_{NO3} = -1.37, and K_{Cl} = -0.13) were obtained in model simulations of potentiometric titrations using FITEQLC where the change in charge of the proton and adsorbing ions were formulated on 0- and 1-plane. The ternary Hg-chloro surface species were predicted as non-reactive species in the gibbsite-water system, while the ternary surface species, $\equiv AlOHgOH^{1/2-}$ was dominant with log $K^{int}_{S\text{-}OHgOH}$ = 1.80 in the presence of Cl. These results contrast those obtained from the model simulations in the goethite-water system. The model was

verified with an independent set of Hg(II) adsorption data incorporating carbonate binding (≡AlOCOO) to describe the decreasing capacity of Hg(II) adsorption as pH increased.

The surface complexes used in this chapter were based on molecular scale analyses reported in the literature, and a sequential optimization approach was used to determine their affinity constants. The modeling results determined that the ternary surface species, $\equiv AlOHgOH^{1/2-}$ was dominant both in the absence and presence of Cl, but the ternary Hg-chloro species (≡AlOHgCl) was not significant over the range of pH values. In addition, a ternary Hg-carbonate species (≡AlOHgOCOO) was neither supported in the literature nor required to describe Hg(II) adsorption in the open system examined in this work. Differences between Hg(II) adsorption on goethite and gibbsite have significant implications for understanding fate and transport of Hg(II) in natural and engineered systems.

Chapter 6. Conclusions and Recommendations

6.1 Summary and Conclusions

6.1.1 Thermodynamic Speciation Modeling

Elemental mercury and its compounds can cause hazardous impacts to human health and the environment. *In Situ* Thermal Desorption (ISTD) is a potential method to remediate mercury contaminated sites. ISTD applies both heat and vacuum simultaneously within the target treatment zone using electrical resistance elements. Knowledge of mercury speciation is of significance in order to understand the fate and transport of mercury and to operate treatment processes such as ISTD in a cost-effective manner. In this research, models for thermodynamic mercury speciation both at ambient and higher temperatures were developed to investigate potential transformations of mercury at near source conditions as well as the distribution of dissolved mercury at near source environments.

The volatilization of $Hg^0_{(liq)}$ and $HgS_{(s)}$ was simulated as a function of temperature. The thermodynamically stable form in each case was determined to be elemental liquid mercury at 20°C in reducing soil environments with limited availability of organic matter and limited reduction of sulfate to sulfide. Mercury sulfide was predicted to be the stable solid species at ambient temperature at decreased redox potential. $Hg_{(liq)}$ was slowly transformed to $Hg_{(g)}$ as its vapor pressure increased below the boiling point of water in an open system. HgS was completely converted to $Hg_{(g)}$ at a temperature around 410.15 K in an open system. Mercury chloride solid was predicted to

be the stable form in soil rich in Cl at oxidizing conditions. It can be volatilized to $HgCl_{2(g)}$ at around 335.15 K or much lower temperatures than for $Hg_{(liq)}$ or $HgS_{(s)}$.

The effect of soil carbon and soil carbonate compositions on mercury removal was also investigated to better understand the mechanism of thermal treatment at each redox condition. Vaporization from soil natural organic matter and inorganic carbonate minerals in soil was quantified as a function of temperature. The partial pressures of carbon dioxide from natural organic carbon, solid inorganic carbonates, and soil pore-water were predicted to be high enough to displace mercury gases in soil. Decomposition of solid forms of mercury HgO and $HgSO_4$ was also expected at temperatures above 140°C.

6.1.2 CD-MUSIC Modeling for Hg(II) Adsorption

The charge distribution and multi-site complexation (CD-MUSIC) model was used to simulate macroscopic adsorption experiments conducted by Hg(II) uptake measurements as a function of pH. The model was employed in this research to describe the adsorption behavior on soil minerals and aqueous speciation in systems that included carbonate species and Cl over a range of experimental conditions. Thus, the modeling effort included: calibration of carbonate surface complexation constants on goethite and gibbsite; calibration of surface complexation reactions in the absence and presence of chloride; and model verification of Hg(II) adsorption data sets not used to calibrate the model. The model simulation of Hg(II) adsorption on soil mineral phases in an open carbonate system is one of the unique components of this study in which

spectroscopically supported mercury-chloride ternary surface complexes and surface complexation reactions for carbonate directly with the surface as a ternary mercury-carbonate complex were incorporated. The decreasing capacity of monodentate surface species in the absence of chloride was adequately described by the formation of a carbonate surface complex that became more dominant with increasing pH. The surface species used in this study were based on molecular scale analyses reported in the literature. All of the affinity constants were determined by a sequential optimization approach. A binuclear surface configuration to two singly coordinated oxygen atoms was the dominant surface complex for Hg(II) adsorption on goethite in the absence of Cl. Ternary surface complexes with hydroxyl, chloride and carbonate ligands were also evident; however, the presence of Cl inhibited Hg(II) adsorption due to the formation of non-sorbing $HgCl_2$ species at low pH.

The macroscopic Hg(II) sorption experiments by gibbsite were simulated using the 1-p*K* CD-MUSIC approach. The asymmetric binding constants for electrolyte ions (K_{Na} = 0.70, K_{NO3} = -1.37, and K_{Cl} = -0.13) were obtained in model calibration using FITEQLC. The model successfully incorporated both the presence of chloride and carbonate species using surface complexes on the dominant edge (100) face of gibbsite that are consistent with molecular spectroscopy. The ternary Hg-chloro surface species were predicted to be non-reactive in the system, while the species $\equiv AlOHgOH^{1/2-}$ was dominant with a log $K^{int}_{S\text{-}OHgOH}$ = 1.80 in the presence of Cl. These results contrast those obtained from the goethite-water system in which the chloride containing ternary species (≡FeOHgCl) was evident in similar Hg(II) adsorption modeling. The model verification

for an independent Hg(II) adsorption data set took into account an innersphere complex with carbonate as ≡Al-OCOO to describe the decreasing adsorption capacity of Hg(II). The discrepancy between data and simulation results was significantly reduced in the open gibbsite-water system compared to previous modeling efforts. The ternary Hg-carbonate species (≡AlOHgOCOO) was neither supported in the literature nor required to describe Hg(II) adsorption in the open system examined in this work. The ternary surface species, $\equiv AlOHgOH^{1/2-}$ was dominant both in the absence and presence of Cl, while ≡AlOHgCl was not significant over a range of pH. Differences between Hg(II) adsorption on goethite and gibbsite have significant implications for understanding fate and transport of Hg(II) in natural and engineered systems.

6.2 Engineering Implications

ISTD is typically applied at sites where high concentrations of contaminants exist in the vadose zone. Both mercury speciation during thermal remediation and the fate and transport of residual mercury were investigated to predict the impact of thermal treatment on the environment. The model results provide valuable data to predict the removal of mercury based on knowledge of mercury speciation that incorporates pure component volatilization to the gas phase. The results also provide an assessment of the composition of the vapor phase that must be captured and treated as part of the ISTD process and the residual mercury remaining in the soil that must be monitored following treatment.

Several batch experiments for Hg(II) adsorption performed in many literature showed the difference in Hg(II) affinity on the geological substrates, goethite, gibbsite,

and silica that are the most abundant oxide minerals in soil. Hg(II) has a higher affinity for iron and aluminum surfaces. Thus, adsorption modeling in complex systems will require characterization of the soil composition with respect to aluminum and iron oxides. Once the soil is characterized, the calibrated models developed in this work can be applied to the discrete mineral phases. The successful model developed in this research for Hg(II) adsorption onto those discrete mineral phases not only establishes the model parameters required to quantify Hg(II) adsorption in more complex soil systems, but also provides guidance for selecting the most appropriate surface complexes for any simpler model for ion adsorption on soil minerals.

6.3 Recommendations for Future Work

The research presented here combined the study of both (1) the thermochemical mercury speciation during thermal treatment of near source environments in various soil conditions and (2) Hg(II) adsorption on minerals that are ubiquitous in soil. Future work outlined below that could further develop the current state of knowledge is highly recommended.

6.3.1 Experimental Approach for Thermodynamic Mercury Speciation

The research presented here focused on thermochemical mercury speciation modeling including potential transformations to account for the fate and transport of mercury in contaminated-soil. Kunkel *et al.* (2006) investigated the feasibility of ISTD for elemental mercury removal from soils by a laboratory soil column test. However, an investigation

of other mercury speciation should be verified with laboratory and field-scale experiments to validate the modeling prediction in various soil conditions.

Treatability tests can be devised to determine the temperature as well as the heating time required for removal of mercury species that are stable in the ambient temperature. A simple heating test by placing known amount of mercury in a soil bath can be used to simulate ISTD in the field projects. The heating temperatures are chosen based on the model simulation over a period of treatment time. The sample can then be held constant at the desired temperature for the treatment time. The remediation strategies that accounts for the high temperature for a short period of heating time or low temperature for a longer period of heating time can be determined to optimize ISTD processes for mercury removal in soil.

The identification of individual mercury species (gaseous divalent mercury, Hg^{2+} and gaseous elemental mercury, Hg^{0}) as well as quantification of the total mercury is essential to account for mercury toxicity, emission control, and atmospheric fate and transport due to the distinctive physicochemical properties of each species. Moreover, Hg capture from the off-gas associated with thermal processes such as ISTD rely on an understanding of Hg speciation. This is evident in analytical methods for measurement of gaseous mercury. In EPA Method 29, the Hg^{2+} and Hg^{0} can be collected by preferential adsorption of Hg(II) species in impingers of hydrogen peroxide–nitric acid (H_2O_2–HNO_3) and Hg^{0} in potassium permanganate–sulfuric acid ($KMNO_4$–H_2SO_4) impingers (Laudal *et al.*, 2000). The Ontario Hydro method (Devito and Rosenhoover, 1998), which is a modification of EPA method 29 (ASTM; EPPR, 1994; Radian, 1994;

SRI, 1994; Tumati and DeVito, 1993; Weston, 1994) substitutes the first impinger containing H_2O_2–HNO_3 by three KCl impingers because they believe that this is the most promising approach for selective separation of mercury gases in the Hg(II) and Hg(0) oxidation states. Processes used for capturing different forms of gaseous products from *In Situ* Thermal Desorption as a function of temperature need to be confirmed and the ability of the model developed in this research could then be used to guide the capture process.

6.3.2 Temperature Effects on Hg(II) Sorption

The model results presented in Chapters 4 and 5 described Hg(II) adsorption over a range of experimental conditions to predict the fate and transport of mercury down gradient of a spill or residual Hg(II) remaining at a remediated site. Weerasooriya et al. (2006) quantified with isotherms for Hg(II) adsorption on gibbsite as a function of temperature, pH, and the type of background electrolytes. The thermodynamic parameters including enthalpy data were calculated using the equilibrium constants that were obtained in adsorption isotherms. To date, no attempts to describe the temperature dependence and the chemical kinetics of Hg(II) adsorption on goethite have been conducted. Experimental data collected as a function of temperature can be used to obtain enthalpy and heat capacities which could be used to identify the temperature dependence of the pristine point of zero charge (p.p.z.c.) and adsorption edges or envelopes (Sposito, 2004).

References

Alshawabkeh, A. N., Yeung, A. T., and Bricka, M. R. (1999). Practical aspects of *in situ* electrokinetic extraction. *J. Environ. Eng.* 125:16362.

ASTM, D6784-02 Standard Test Method for Elemental, Oxidized, Particle-Bound and Total Mercury in Flue Gas Generated for Coal-Fired Stationary Sources (Ontario Hydro Method).

Babiarz, C. L., Hurley, J. P., Hoffmann, S. R., Andren, A. W., Shafer, M. M., and Armstrong, D. E. (2001). Partitioning of total mercury and methylmercury to the colloidal phase in freshwaters. *Environ. Sci. Technol.* 35:4773-4782.

Bale, C. W., Chartrand, P., Degterov, S. A., Eriksson, G., Hack, K., Ben Mahfoud, R., Melancon, J., Pelton, A. D. and Petersen, S. (2002). FactSage thermochemical software and databases. *Calphad* 26:189-228.

Bargar, J. R., Kubicki, J. D., Reitmeyer, R. and Davis, J. A. (2005). ATR-FTIR spectroscopic characterization of coexisting carbonate surface complexes on hematite. *Geochim. Cosmochim. Acta* 69:1527-1542.

Bargar, J. R., Reitmeyer, R., Lenhart, J. J. and Davis, J. A. (2000). Characterization of U(VI)-carbonate ternary complexes on hematite: EXAFS and electrophoretic mobility measurements. *Geochim. Cosmochim. Acta* 64:2737-2749.

Bargar, J., Persson, P. and Brown, G. (1997). XAFS studies of Pb (II)-chloro and Hg (II)-chloro ternary complexes on goethite. *J. Phys. IV* C2:825.

Barnett, M. O., Harris, L. A., Turner, R. R., Stevenson, R. J., Henson, T. J., Melton, R. C. and Hoffman, D. P. (1997). Formation of mercuric sulfide in soil. *Environ. Sci.*

Technol. 31:3037-3043.

Barron, V. and Torrent, J. (1996). Surface hydroxyl configuration of various crystal faces of hematite and goethite. *J. Colloid Interface Sci.* 177:407-410.

Barrow, N. J. and Cox, V. C. (1992a). The effects of pH and chloride concentration on mercury sorption. I. By goethite. *J. Soil Sci.* 43:295-304.

Barrow, N. J. and Cox, V. C. (1992b). The effects of pH and chloride concentration on mercury sorption. II. By a soil. *Eur. J. Soil Sci.* 43:305-312.

Bellotto, M., Gualtieri, A., Artioli, G. and Clark, S. M. (1995). Kinetic study of the kaolinite-mullite reaction sequence. Part I: kaolinite dehydroxylation. *Phys. Chem. Miner.* 22:207-217.

Benes, P. and Havlik, B. (1979). Speciation of mercury in natural waters. *The biogeochemistry of mercury in the environment*:175-202.

Boening, D. W. (2000). Ecological effects, transport, and fate of mercury: a general. *Chemosphere* 40:1351.

Boily, J. F., Lutzenkirchen, J., Balm, O., Beattie, J. and Sjoerg, S. (2001). Modeling proton binding at the goethite ([alpha]-FeOOH)-water interface. *Colloids Surf., A* 179:11-27.

Bolt, G. H. and Bruggenwert, M. G. M. (1976). *Soil chemistry*. Elsevier Publishing Company.

Bonnissel-Gissinger, P., Alnot, M., Lickes, J. P., Ehrhardt, J. J. and Behra, P. (1999). Modeling the Adsorption of Mercury (II) on (Hydr) oxides II:[alpha]-FeOOH (Goethite) and Amorphous Silica. *J. Colloid Interface Sci.* 215:313-322.

Butler, J. N. (1982). *Carbon dioxide equilibria and their applications*. Addison-Wesley.

Buyanovsky, G. A. (1983). Annual Cycles of Carbon Dioxide Level in Soil Air1. *Soil Sci. Soc. Am. J.* 47:1139.

Carpi, A. (1997). Mercury from Combustion Sources: A Review of the Chemical Species Emitted and Their Transport in the Atmosphere. *Water, Air, Soil Pollut.* 98:241-254.

Chase, M. W. (1998). NIST-JANAF Thermochemical Tables. *J. Physical and Chemical Reference Data, 4th Ed. (Monograph No. 9).*

Chemfinder.Com (2004). Database, CambridgeSoft Corporation.

CHERIC Pure component properties (Queriable database), Chemical Engineering Research Information Center.

Cloutier-Hurteau, B., Sauv, S. and Courchesne, F. (2007). Comparing WHAM 6 and MINEQL+ 4.5 for the Chemical Speciation of Cu2+ in the Rhizosphere of Forest Soils. *Environ. Sci. Technol.* 41:8104-8110.

Collins, C. R., Sherman, D. M. and Ragnarsdottir, K. V. (1999). Surface complexation of Hg2+ on goethite: Mechanism from EXAFS spectroscopy and density functional calculations. *J. Colloid Interface Sci.* 219:345-350.

Conner, J. R. (1990). Chemical Fixation and Solidification of Hazardous Wastes, Van Nostrand Reinhold, New York.

Cornell, R. M. and Schwertmann, U. (1996). The Iron Oxides: Structure, Properties; Reactions, Occurrence and Uses. *VCH, Weinheim, Germany*.

Coudrain-Ribstein, A., Gouze, P. and de Marsily, G. (1998). Temperature-carbon dioxide

partial pressure trends in confined aquifers. *Chem. Geol.* 145:73-89.

Cox, J. D., Wagman, D. D. and Medvedev, V. A. (1989). *CODATA key values for thermodynamics*. Hemisphere New York.

Darroudl, T. and Searcy, A. W. (1981). Effect of CO_2 pressure on the rate of decomposition of calcite. *J. Phys. Chem.* 85:3971-3974.

Davis, J. A. and Leckie, J. O. (1978). Effect of adsorbed complexing ligands on trace metal uptake by hydrous oxides. *Environ. Sci. Technol.* 12:1309-1315.

Davis, J. A. and Leckie, J. O. (1978). Surface ionization and complexation at the oxide/water interface: I. Computation of electrical double layer properties in simple electrolytes. *J. Colloid Interface Sci.* 63:480-499.

Davis, J. A. and Leckie, J. O. (1980). Surface ionization and complexation at the oxide/water interface. 3. Adsorption of anions. *J. Colloid Interface Sci.* 74:32-43.

DeVito, M. S. and Rosenhoover, W. A. (1998). Flue Gas Mercury and Speciation Studies at Coal-Fired Utilities Equipped with Wet Scrubbers, in *15th International Pittsburgh Coal Conference*, Pittsburgh, PA.

Dissanayake, C. B. and Vitanage, P. W. (1977). Exploration for bauxite in Sri Lanka: preliminary investigation. *J. Geol. Soc. India* 18:338-343.

DOE (2002). Department of Energy News: Cleanup begins of Y-12 mercury in creek, http://www.oakridge.doe.gov/media_releases/2002/r-2002-2040.htm.

Doner, H. E. and Lynn, W. C. (1977). Carbonate, halide, sulfate, and sulfide minerals. *Miner. Soil Environ.*:75-98.

Dyrssen, D. and Wedborg, M. (1991). The sulphur-mercury (II) system in natural waters.

Water, Air, Soil Pollut. 56:507-519.

Dzombak, D. A. and Morel, F. (1990). *Surface complexation modeling: Hydrous ferric oxide*. Wiley-InterScience, New York.

Electrical Power Research Institute (1994). Electric Utility Trace Substances Synthesis Report.

EPA (1997). Recent Developments for *In Situ* Treatment of Metal Contaminated Soils, United States Environmental Protection Agency.

EPA (2006). Binational Toxics Strategy Mercury Progress Report. .

EPA (2007). Treatment Technologies for Mercury in Soil, Waste, and Water, U.S. Environmental Protection Agency Washington, DC 20460

Evanko, C. R. and Dzomback, D. A. (1997). Remediation of Metals-Contaminated Soils and Groundwater. *Technology Evaluation Report TE-97-01. GWRTAC (Ground-Water Remediation Technologies Analysis Center).*

Evanko, C. R. and Dzombak, D. A. (1997). Remediation of metals-contaminated soils and groundwater, Ground-water remediation technologies analysis center (GWRTAC), Pittsburgh, PA.

Farrah, H. and Pickering, W. F. (1978). The sorption of mercury species by clay minerals. *Water, Air, Soil Pollut.* 9:23-31.

Filius, J. D., Hiemstra, T. and Van Riemsdijk, W. H. (1997). Adsorption of small weak organic acids on goethite: Modeling of mechanisms. *J. Colloid Interface Sci.* 195:368-380.

Forbes, E. A., Posner, A. M. and Quirk, J. P. (1974). The Specific Adsorption of

Inorganic Hg(II) Species and Co(III) Complex Ions on Goethite. *J. Colloid Interface Sci.* 49:403-409.

Gaboriaud, F. and Ehrhardt, J. J. (2003). Effects of different crystal faces on the surface charge of colloidal goethite ([alpha]-FeOOH) particles: an experimental and modeling study. *Geochim. Cosmochim. Acta* 67:967-983.

Gabriel, M. C. and Williamson, D. G. (2004). Principal biogeochemical factors affecting the speciation and transport of mercury through the terrestrial environment. *Environ. Geochem. Health.* 26:421-434.

Galbreath, K. C. and Zygarlicke, C. J. (1996). Mercury speciation in coal combustion and gasification flue gases. *Environ. Sci. Technol.* 30:2421-2426.

Gibbs, J. W. (1957). *The Collected Works of J.W. Gibbs*. Yale University Press, New Haven, CT

Gunneriusson, L. and Sjoberg, S. (1993). Surface Complexation in the H+-Goethite ([alpha]-FeOOH)-Hg (II)-Chloride System. *J. Colloid Interface Sci.* 156:121-128.

Gustafsson, J. P. (2003). FITEQLC: Implementation of CD-MUSIC in FITEQL 4.0, Land and Water Resources Engineering. Royal Institute of Technology (KTH).

Hayes, K. F. and Leckie, J. O. (1987). Modeling ionic strength effects on cation adsorption at hydrous oxide/solution interfaces. *J. Colloid Interface Sci.* 115:564-572.

Hayes, K. F., Redden, G., Ela, W. and Leckie, J. O. (1991). Surface complexation models: An evaluation of model parameter estimation using FITEQL and oxide mineral titration data. *J. Colloid Interface Sci.* 142:448-469.

Hem, J. D. (1970). Study and interpretation of the chemical characteristics of natural water (2nd ed.). *U.S. Geol. Surv. Water-Supply Pap.* 1473:363.

Hempel, M. and Thoeming, J. (1999). Remediation techniques for Hg-contaminated sites.

Herbelin, A. L. and Westall, J. C. (1999). FITEQL 4.0: A Computer Program for Determination of Chemical Equilibrium Constants from Experimental Data, Corvallis: Department of Chemistry, Oregon State University.

Hesterberg, D., Chou, J. W., Hutchison, K. J. and Sayers, D. E. (2001). Bonding of Hg (II) to reduced organic sulfur in humic acid as affected by S/Hg ratio. *Environ. Sci. Technol.* 35:2741-2745.

Hiemstra, T. and Van Riemsdijk, W. H. (1991). Physical chemical interpretation of primary charging behaviour of metal (hydr) oxides. *Colloids Surf.* 59:7-25.

Hiemstra, T. and Van Riemsdijk, W. H. (1996). A surface structural approach to ion adsorption: The charge distribution (CD) model. *J. Colloid Interface Sci.* 179:488-508.

Hiemstra, T. and Van Riemsdijk, W. H. (1999). Surface Structural Ion Adsorption Modeling of Competitive Binding of Oxyanions by Metal (Hydr) oxides* 1. *J. Colloid Interface Sci.* 210:182-193.

Hiemstra, T., Rietra, R. P. J. J., and van Riemsdijk, W. H. (2007). Surface complexation of selenite on goethite: MO/DFT geometry and charge distribution. *Croat. Chem. Acta* 80:3-4 Studeni.

Hiemstra, T., Venema, P. and Riemsdijk, W. H. V. (1996). Intrinsic proton affinity of reactive surface groups of metal (hydr) oxides: The bond valence principle. *J.*

Colloid Interface Sci. 184:680-692.

Hiemstra, T., Young, H. and Van Riemsdijk, W. H. (1999). Interfacial charging phenomena of aluminum (hydr) oxides. *Langmuir* 15:5942-5955.

Ho, C. H. and Miller, N. H. (1986). Adsorption of uranyl species from bicarbonate solution onto hematite particles. *J. Colloid Interface Sci.* 110:165-171.

Ho, T. C., Yang, P., Kuo, T. H. and Hopper, J. R. (1998). Characteristics of mercury desorption from sorbents at elevated temperatures. *Waste Manage.* 18:445-452.

Hudson, R. J. M., Gherini, S. A., Watras, C. J. and Porcella, D. B. (1994). Modeling the biogeochemical cycle of mercury in lakes: The Mercury Cycling Model (MCM) and its application to the MTL Study lakes, in *Mercury as a global pollutant: Toward integration and synthesis*, C. J. a. H. Watras, J.W. (eds.), ed., Lewis Publishers, Boca Raton, FL, 473-523.

Jean, G. E. and Bancroft, G. M. (1986). Heavy metal adsorption by sulphide mineral surfaces. *Geochim. Cosmochim. Acta* 50:1455-1463.

Keizer, M. G. and Van Riemsdijk, W. H. (1996). ECOSAT. A computer program for the calculation of speciation and transport in soil-water systems. Version 4.3., Dept. Soil Science and Plant Nutrition, Wageningen Agricultural Univ. Wageningen, The Netherlands.

Kernorff, H. and Schnitzer, M. (1980). Sorption of metals on humic acids. *Geochim. Cosmochim. Acta.* 44:1701-1708.

Khodadoust, A. P., Reddy, K. R., and Maturi, K. (2005). Effect of different extraction agents on metal and organic contaminant removal from a field soil. *J. Hazard.*

Mater. 117:15-24.

Kim, C. S., Rytuba, J. J. and Brown, G. E. (2004a). EXAFS study of mercury (II) sorption to Fe-and Al-(hydr) oxides: II. Effects of chloride and sulfate. *J. Colloid Interface Sci.* 270:9-20.

Kim, C. S., Rytuba, J. J. and Brown, G. E. (2004b). EXAFS study of mercury (II) sorption to Fe-and Al-(hydr) oxides: I. Effects of pH. *J. Colloid Interface Sci.* 271:1-15.

Kinniburgh, D. G. and Jackson, M. L. (1978). Adsorption of mercury (II) by iron hydrous oxide gel. *Soil Sci. Soc. Am. J.* 42.

Kloke, A., Sauerbeck, D. R. and Vetter, H. (1994). Changing metal cycles and human health. *Heavy Metals in Soils; Alloway, BJ (ed.), Blackie Academic and Professional: Glasgow, UK*.

Koopal, L. K., Van Riemsdijk, W. H. and Roffey, M. G. (1987). Surface ionization and complexation models: a comparison of methods for determining model parameters. *J. Colloid Interface Sci.* 118:117-136.

Kunkel, A. M. (2004). Remediation of Elemental Mercury Using *In Situ* Thermal Desorption (ISTD), in *Civil, Architectural and Environmental Engineering*, The University of Texas at Austin, Austin.

Langmuir, D. (1997). *Aqueous environmental geochemistry*. Prentice-Hall, Upper Saddle River, New Jersey.

Laudal, D. L., Brown, T. D. and Nott, B. R. (2000). Effects of flue gas constituents on mercury speciation. *Fuel Processing Technology* 65-66:157-165.

Lazaridis, N. K. and Charalambous, C. (2005). Sorptive removal of trivalent and hexavalent chromium from binary aqueous solutions by composite alginate-goethite beads. *Water Res.* 39:4385-4396.

Liao, L., Selim, H. M., and DeLaune, R. D. (2009). Mercury Adsorption-Desorption and Transport in Soils. *J. Environ. Qual.* 38:1608-1616.

Lide, D. R. e. (2007). *CRC Handbook of Chemistry and Physics, 88th ed.* CRC Press, Boca Raton, FL.

Lindberg, S. E. and Stratton, W. J. (1998). Atmospheric Mercury Speciation: Concentrations and Behavior of Reactive Gaseous Mercury in Ambient Air. *Environ. Sci. Technol.* 32:49-57.

Lockwood, R. A. and Chen, K. Y. (1973). Adsorption of Hg(II) by hydrous manganese oxides. *Environ. Sci. Technol.* 7:1028-1034.

Lockwood, R. A. and Chen, K. Y. (1974). Adsorption of Hg (II) by ferric hydroxide. *Environ. Lett.* 6:151-166.

Loeppert, R. H. and Suarez, D. L. (1996). Carbonate and gypsum, USDA Agricultural Research Service, Lincoln, Nebraska.

Lovley, D. R. (1993). Dissimilatory Metal Reduction. *Annu. Rev. Microbiol.* 47:263-290.

Lumsdon, D. O. and Evans, L. J. (1994). Surface Complexation Model Parameters for Goethite ([alpha]-FeOOH). *J. Colloid Interface Sci.* 164:119-125.

Lutzenkirchen, J. (1998). Comparison of 1-p*K* and 2-p*K* Versions of Surface Complexation Theory by the Goodness of Fit in Describing Surface Charge Data of (Hydr)oxides. *Environ. Sci. Technol.* 32:3149-3154.

L'Vov, B. V. (2002). Mechanism and kinetics of thermal decomposition of carbonates. *Thermochim. Acta* 386:1-16.

Macalady, D. L., Langmuir, D., Grundl, T. and Elzerman, A. (1990). Use of model-generated Fe3+ ion activities to compute Eh and ferric oxyhydroxide solubilities in anaerobic systems, in *Chemical Modeling of Aqueous Systems II*, ACS Publications, 350-367.

MacNaughton, M. G. (1973). Adsorption of Mercury (II) at the Solid-water Interface, in *Dept. of Civil Engineering*, Stanford University, Palo Alto, CA.

MacNaughton, M. G. and James, R. O. (1974). Adsorption of aqueous mercury (II) complexes at the oxide/water interface. *J. Colloid Interface Sci.* 47:431-440.

Manning, B. A., Fendorf, S. E. and Goldberg, S. (1998). Surface structures and stability of arsenic (III) on goethite: Spectroscopic evidence for inner-sphere complexes. *Environ. Sci. Technol.* 32:2383-2388.

Mason, R. P., Reinfelder, J. R. and Morel, F. M. M. (1996). Uptake, toxicity, and trophic transfer of mercury in a coastal diatom. *Environ. Sci. Technol.* 30:1835-1845.

MassDEP (1996). An Evaluation of Sources, Emissions, Impacts and Controls, Massachusetts Department of Environmental Protection, Massachusetts.

Meng, X. and Letterman, R. D. (1993). Modeling ion adsorption on aluminum hydroxide modified silica. *Environ. Sci. Technol.* 27:1924-1929.

Muller, B. and Sigg, L. (1992). Adsorption of lead (II) on the goethite surface: voltammetric evaluation of surface complexation parameters. *J. Colloid Interface Sci.* 148:517-532.

Naveau, A., Monteil-Rivera, F., Dumonceau, J. and Boudesocque, S. h. (2005). Sorption of europium on a goethite surface: influence of background electrolyte. *J. Contam. Hydrol.* 77:1-16.

Nelson, R. E. (1982). *Carbonate and Gypsum. Methods of soil analysis. Part 2. Chemical and microbiological properties*. Agronomy, Madison, WI.

Newton, D. W., Ellis, J., R. and Paulsen, G. M. (1976). Effect of pH and Complex Formation on Mercury(II) Adsorption by Bentonite. *J. Environ. Qual.* 5:251-254.

NIST Chemistry WebBook, National Institute of Standards and Technology.

Park, C. M. (2011). Mercury Speciation during Thermal Remediation and Post-Treatment Environments, in *Civil, Architectural and Environmental Engineering*, The University of Texas at Austin, Austin.

Pauling, L. (1929). The principles determining the structure of complex ionic crystals. *J. Am. Chem. Soc.* 51:1010-1026.

Piasecki, W. (2006). Determination of the parameters for the 1-pK triple-layer model of ion adsorption onto oxides from known parameter values for the 2-pK TLM. *J. Colloid Interface Sci.* 302:389-395.

Radian (1994). A Study of Toxic Emissions from a Coal-Fired Power Plant Utilizing and ESP While Demonstrating the ICCT CT-121 FGD Project, in *Final Report on Contract DE-AC22-93PC93253*.

Ramamoorthy, S. and Rust, B. R. (1978). Heavy-metal exchange processes in sediment-wter systems. *Environ. Geol.* 2:165-172.

Reddy, K. R., Xu, C. Y., and Chinthamreddy, S. (2001). Assessment of electrokinetic

removal of heavy metals from soils by sequential extraction analysis. *J. Hazard. Mater*. 84:279-296.

Revis, N. W., Osborne, T. R., Holdsworth, G. and Hadden, C. (1989). Distribution of mercury species in soil from a mercury-contaminated site. *Water, Air, Soil Pollut.* 45:105-113.

Rojo, I., Seco, F., Rovira, M., Giménez, J., Cervantes, G., Martí, V. and de Pablo, J. (2009). Thorium sorption onto magnetite and ferrihydrite in acidic conditions. *J. Nucl. Mater.* 385:474-478.

Salazar-Camacho, C. and Villalobos, M. (2010). Goethite surface reactivity: III. Unifying arsenate adsorption behavior through a variable crystal face-site density model. *Geochim. Cosmochim. Acta* 74:2257-2280.

Sarkar, D. and Misra, M. E. (2000). Adsorption of mercury (II) by kaolinite. *Soil Science Society of America Journal* 64:1968.

Sarkar, D., Essington, M. E. and Misra, K. C. (1999). Adsorption of mercury (II) by variable charge surfaces of quartz and gibbsite. *Soil Sci. Soc. Am. J.* 63:1626-1636.

Schecher, W. (2001). Thermochemical Data Used in MINEQL+ version 4.5 With Comparions to Versions 4.07 and Earlier, Hallowell, ME: Environmental Research Software.

Schecher, W. D. and McAvoy, D. C. (2003). MINEQL+: A Chemical Equilibrium Modeling System, Version 4.5 for Windows, User's Manual. *Environmental Research Software, Hallowell, Maine.*

Schindler, P. W. (1967). Heterogeneous equilibria involving oxides, hydroxides, carbonates, and hydroxide carbonates. *Equilibrium Concepts in Natural Water Systems*:196-221.

Schuster, E. (1991). The behavior of mercury in the soil with special emphasis on complexation and adsorption processes - A review of the literature. *Water, Air, Soil Pollut.* 56:667-680.

Schwertmann, U. and Cornell, R. M. (1991). Iron Oxides in the Laboratory: Preparation and Characterization. *VCH: Weinheim*.

Schwertmann, U. and Taylor, R. M. (1977). Iron oxides. In'Minerals in Soil Environments'.(Eds JB Dixon and SB Weed.) pp. 145-80. *Soil Sci. Soc. Am.: Madison, Wisc.*

Skyllberg, U., Qian, J., Frech, W., Xia, K. and Bleam, W. F. (2003). Distribution of mercury, methyl mercury and organic sulphur species in soil, soil solution and stream of a boreal forest catchment. *Biogeochemistry* 64:53-76.

Southern Research Institute (1994). Characterizing Toxic Emissions from a Coal-Fired Power Plant Demonstrating the AFGD ICCT Project and a Plant Utilizing a Dry Scrubber/Baghouse System, in *Final Report on Contract DE-AC22-93PC93254*.

Sparks, D. L. (2003). Environmental Soil Chemistry. *Academic Press. San Diego, CA.*

Sposito, G. (1984). *The Surface Chemistry of Soils*. Oxford University Press, New York.

Sposito, G. (1989). *The chemistry of soils*. Oxford Univ. Press, New York.

Sposito, G. (1998). On points of zero charge. *Environ. Sci. Technol.* 32:2815-2819.

Sposito, G. (2004). *The surface chemistry of natural particles*. Oxford University Press,

USA.

Stegemeier, G. L. and Vinegar, H. J. (2001). *Thermal conduction heating for in situ thermal desorption of soils*. CRC Press, Boca Raton, FL.

Stein, E. D., Cohen, Y. and Winer, A. M. (1996). Environmental distribution and transformation of mercury compounds. *Crit. Rev. Environ. Sci. Technol.* 26:1-43.

Stepan, D. J., Fraley, R. H. and Charlton, D. S. (1995). Remediation of mercury-contaminated soils: development and testing of technologies, in *Gas Research Institute Topical Report*.

Stern, K. H. (2001). *High temperature properties and thermal decomposition of inorganic salts with oxyanions.* CRC Press, Boca Raton, Fl.

Stumm, W. and Morgan, J. J. (1996). *Aquatic Chemistry: Chemical Equilibria and Rates in Natural Waters.* John Wiley and Sons, Inc, New York.

Sverjensky, D. A. and Fukushi, K. (2006). Anion adsorption on oxide surfaces: Inclusion of the water dipole in modeling the electrostatics of ligand exchange. *Environ. Sci. Technol.* 40:263-271.

Tadanier, C. J. and Matthew, J. (2002). Formulating the charge-distribution multisite surface complexation model using FITEQL. *Soil Sci. Soc. Am. J.* 66:1505.

Taube, F., Pommer, L., Larsson, T., Shchukarev, A. and Nordin, A. (2008). Soil Remediation-Mercury Speciation in Soil and Vapor Phase During Thermal Treatment. *Water, Air, Soil Pollut.* 193:155-163.

TerraTherm (2002). Remediating Subsurface Mercury Contamination using TerraThem's ISTD Technology, TerraTherm, Inc, Fitchburg, MA.

TerraTherm (2004). TerraTherm website. <www.terratherm.com> (7 Apr 2004).

Thanabalasingam, P. and Pickering, W. F. (1985). Sorption of mercury (II) by manganese (IV) oxide. *Environ. Pollut., Ser. B* 10:115-128.

Tiffreau, C., Lutzenkirchen, J. and Behra, P. (1995). Modeling the adsorption of mercury (II) on (hydr) oxides I. Amorphous iron oxide and -quartz. *J. Colloid Interface Sci.* 172:82-93.

Torrent, J., Barron, V. and Schwertmann, U. (1990). Phosphate adsorption and desorption by goethites differing in crystal morphology. *Soil Sci. Soc. Am. J* 54:1007-1012.

Tumati, P. R. and DeVito, M. S. (1993). Partitioning Behavior of Mercury During Coal Combustion, in *Joint ASME/IEEE Power Generation Conference*, ASME Paper 93-JPGC-EC-8, Kansas City.

Van Geen, A., Robertson, A. P. and Leckie, J. O. (1994). Complexation of carbonate species at the goethite surface: Implications for adsorption of metal ions in natural waters. *Geochim. Cosmochim. Acta* 58:2073-2086.

Venema, P., Hiemstra, T. and van Riemsdijk, W. H. (1996). Multisite adsorption of cadmium on goethite. *J. Colloid Interface Sci.* 183:515-527.

Venema, P., Hiemstra, T. and van Riemsdijk, W. H. (1997). Interaction of Cadmium with Phosphate on Goethite. *J. Colloid Interface Sci.* 192:94-103.

Venema, P., Hiemstra, T., Weidler, P. G. and van Riemsdijk, W. H. (1998). Intrinsic Proton Affinity of Reactive Surface Groups of Metal (Hydr) oxides: Application to Iron (Hydr) oxides* 1. *J. Colloid Interface Sci.* 198:282-295.

Villalobos, M. and Leckie, J. O. (2000). Carbonate adsorption on goethite under closed

and open CO2 conditions. *Geochim. Cosmochim. Acta* 64:3787-3802.

Villalobos, M. and Leckie, J. O. (2001). Surface complexation modeling and FTIR study of carbonate adsorption to goethite. *J. Colloid Interface Sci.* 235:15-32.

Villalobos, M. and Pérez-Gallegos, A. (2008). Goethite surface reactivity: A macroscopic investigation unifying proton, chromate, carbonate, and lead (II) adsorption. *J. Colloid Interface Sci.* 326:307-323.

Villalobos, M., Cheney, M. A. and Alcaraz-Cienfuegos, J. (2009). Goethite surface reactivity: II. A microscopic site-density model that describes its surface area-normalized variability. *J. Colloid Interface Sci.* 336:412-422.

Villalobos, M., Trotz, M. A. and Leckie, J. O. (2003). Variability in goethite surface site density: evidence from proton and carbonate sorption. *J. Colloid Interface Sci.* 268:273-287.

Viraraghavan, T. and Kapoor, A. (1994). Adsorption of mercury from wastewater by bentonite. *Applied Clay Science* 9:31-49.

Wagman, D. D., Evans, W. H., Parker, V. B., Halow, H., Bailey, S. M. and Schumm, R. H. (1969). Selected Values of chemical Thermodynamic Properties, U.S. Government Printing Office, Washington, D.C.

Weerasooriya, R., Aluthpatabendi, D. and Tobschall, H. J. (2001). Charge distribution multi-site complexation (CD-MUSIC) modeling of Pb(II) adsorption on gibbsite. *Colloids Surf., A* 189:131-144.

Weerasooriya, R., Dharmasena, B. and Aluthpatabendi, D. (2000). Copper-gibbsite interactions: an application of 1-pK surface complexation model. *Colloids Surf., A*

170:65-77.

Weerasooriya, R., Seneviratne, W., Kathriarachchi, H. A. and Tobschall, H. J. (2006). Thermodynamic assessment of Hg(II)-gibbsite interactions. *J. Colloid Interface Sci.* 301:452-460.

Weerasooriya, R., Tobschall, H. J. and Bandara, A. (2007). Modeling interactions of Hg(II) and bauxitic soils. *Chemosphere* 69:1525-1532.

Weerasooriya, R., Tobschall, H. J., Wijesekara, H. K. D. K., Arachchige, E. K. I. A. U. K. and Pathirathne, K. A. S. (2003). On the mechanistic modeling of As(III) adsorption on gibbsite. *Chemosphere* 51:1001-1013.

Westall, J. C. and Hohl, H. (1980). A comparison of electrostatic models for the oxide/solution interface. *Adv. Colloid Interface Sci.* 12:265-294.

Weston, R. F. (1994). Toxic Assessment Report Illinois Power Company Baldwin Power Station, Unit 2, in *Final Report on Contract DE-AC22-93PC93255*.

WHO (1990). environmental health criteria 101. *Geneva: World Health Organization*.

Wijnja, H. and Schulthess, C. P. (1999). ATR-FTIR and DRIFT spectroscopy of carbonate species at the aged [gamma]-Al2O3/water interface. *Spectrochim. Acta, Part A* 55:861-872.

Wuana, R.A. and Okieimen, F.E. (2011) Heavy Metals in Contaminated Soils: A Review of Sources, Chemistry, Risks and Best Available Strategies for Remediation. *ISRN Ecology*, vol. 2011, Article ID 402647. doi:10.5402/2011/402647.

Yin, Y., Allen, H. E., and Huang, C. P. (1997b). Adsorption/desorption isotherms of Hg(II) by soil. *Soil Sci.* 162:35-45.

Yin, Y., Allen, H. E., Li, Y., Huang, C. P. and Sanders, P. F. (1996). Adsorption of mercury (II) by soil: Effects of pH, chloride, and organic matter. *J. Environ. Qual.* 25:837-844.

Zeltner, W. A. and Anderson, M. A. (1988). Surface charge development at the goethite/aqueous solution interface: effects of CO2 adsorption. *Langmuir* 4:469-474.

VITA

Chang Min Park attended Gwangmoon High School, Seoul, South Korea. In 1998 he enrolled at Hanyang University in Seoul, South Korea. He received the degree of Bachelor of Science in civil engineering in Feb, 2006. In August, 2006, he entered the Graduate School at Virginia Tech in the Environmental and Water Resources program. He received the degree of Masters of Science in June, 2008 and chose to transfer school to pursue a Ph.D. After graduating from Virginia Tech, he attended the University of Texas at Austin in the Environmental and Water Resources Engineering program. Chang Min Park is a certified Engineer In Training.

Permanent Address: 102-204 Hanshin Apt. Jeonpo-dong Busanjin-gu Busan

This manuscript was typed by the author.